Copyright Warning & Restrictions

The copyright law of the United States (Title 17, United States Code) governs the making of photocopies or other reproductions of copyrighted material.

Under certain conditions specified in the law, libraries and archives are authorized to furnish a photocopy or other reproduction. One of these specified conditions is that the photocopy or reproduction is not to be "used for any purpose other than private study, scholarship, or research." If a, user makes a request for, or later uses, a photocopy or reproduction for purposes in excess of "fair use" that user may be liable for copyright infringement,

This institution reserves the right to refuse to accept a copying order if, in its judgment, fulfillment of the order would involve violation of copyright law.

Please Note: The author retains the copyright while the New Jersey Institute of Technology reserves the right to distribute this thesis or dissertation

Printing note: If you do not wish to print this page, then select "Pages from: first page # to: last page #" on the print dialog screen

The Van Houten library has removed some of the personal information and all signatures from the approval page and biographical sketches of theses and dissertations in order to protect the identity of NJIT graduates and faculty.

ABSTRACT

A MICROMACHINED THERMO-OPTICAL LIGHT MODULATOR BASED ON SEMICONDUCTOR-TO-METAL PHASE TRANSITION

by
Lijun Jiang

In this research, a micromachined thermo-optical light modulator was realized based on the semiconductor-to-metal phase transition of vanadium dioxide (VO_2) thin film. VO_2 undergoes a reversible phase transition at approximately 68 ^{o}C, which is accompanied with drastic changes in its electrical and optical properties. The sharp electrical resistivity change can be as great as five orders. Optically, VO_2 film will switch from a transparent semiconductor phase to a reflective metal phase upon the phase transition. The light modulator in this research exploits this phase transition related optical switching by using surface micromachined low-thermal-mass pixels to achieve good thermal isolations, which ensures that each pixel can be individually switched without cross talking. In operation, the pixel temperature was controlled by integrated resistor on each pixel or spatially addressed thermal radiation sources.

Active VO_2 thin film was synthesized by thermal oxidation of e-beam evaporated vanadium metal film. The oxidized film exhibits a phase transition at ~65 ^{o}C with a hysteresis of about 15 ^{o}C. A transmittance switching from ~90% to ~30% in the near infrared and a reflectance switching from ~50% to ~15% in the visible have been achieved. The surface microstructure was studied and correlated to its optical properties. A study on the hysteresis loop reveals that the VO_2 can be repetitively switched between the "on" and "off" states.

The micromachined thermal isolation pixel was a bridge-like silicon dioxide platform suspended with narrow supporting legs. The pixel design was optimized with both thermal and optical simulations. The VO_2 light modulator was fabricated by surface micromachining based on dry processing. Silicon dioxide was deposited on a polyimide sacrificial layer by PECVD and patterned to form the structural pixel. Vanadium film was e-beam evaporated and patterned with lift-off process. It was thermally oxidized into VO_2 at 390 ^{o}C. The thermal isolation pixel was anchored on substrate by aluminum pedestals. Finally, the structure was released in an oxygen plasma barrel asher. The VO_2 array was experimentally tested and its light switching and modulation ability were demonstrated. Further study shows that the surface micromachining process has no degrading effect on the optical property of VO_2 thin film.

A MICROMACHINED THERMO-OPTICAL LIGHT MODULATOR BASED ON SEMICONDUCTOR-TO-METAL PHASE TRANSITION

by

Lijun Jiang

A Dissertation
Submitted to the Faculty of
New Jersey Institute of Technology
In Partial Fulfillment of the Requirements for the Degree of
Doctor of Philosophy in Materials Science and Engineering

Interdisciplinary Program of Materials Science and Engineering

January 2004

Copyright © 2004 by Lijun Jiang
ALL RIGHTS RESERVED

APPROVAL PAGE

A MICROMACHINED THERMO-OPTICAL LIGHT MODULATOR BASED ON SEMICONDUCTOR-TO-METAL PHASE TRANSITION

Lijun Jiang

Dr. William N. Carr, Dissertation Advisor Date
Professor of Electrical and Computer Engineering, Professor of Physics, NJIT

Dr. Ken K. Chin, Committee Member Date
Professor of Physics, NJIT

Dr. Nuggehalli. M. Ravindra, Committee Member Date
Professor of Physics, NJIT

Dr. Onofrio L. Russo, Committee Member Date
Associate Professor of Physics, NJIT

Dr. Dadi Setiadi, Committee Member Date
Chief Technology Officer, New Jersey Microsystems, Inc.

BIOGRAPHICAL SKETCH

Author: Lijun Jiang

Degree: Doctor of Philosophy

Date: January, 2004

Undergraduate and Graduate Education:

- Doctor of Philosophy in Materials Science and Engineering,
  New Jersey Institute of Technology, Newark, NJ, USA, 2004

- Master of Engineering in Materials Physics and Chemistry,
  Shanghai Institute of Metallurgy (Now Institute of Microsystem and Information Technology), Chinese Academy of Sciences, Shanghai, P. R. China, 1999

- Bachelor of Science in Chemistry,
  Fudan University, Shanghai, P. R. China, 1996

Major: Materials Science and Engineering

Presentations and Publications:

Lijun Jiang and William N. Carr,
"A Surface Micromachined Light Modulator Based on Vanadium Dioxide Array," To be Presented at 17th IEEE International Conference on Micro Electro Mechanical Systems (MEMS 2004), Maastricht, The Netherlands, January 2004

Lijun Jiang and William N. Carr,
"A Micromachined Thermo-Optical Light Modulator Based on the VO_2 Phase Transition," To be Presented at SPIE Micromachining and Microfabrication Conference (Jointed with Photonics West 2004), San Jose, CA, January 2004

Lijun Jiang and William N. Carr,
"Vanadium Dioxide Thin Films for Thermo-Optical Switching," Presented at MRS Fall Meeting, Boston, MA, December 2003

Lijun Jiang and William N. Carr,
"Vanadium Dioxide Thin Films for Thermo-Optical Switching Applications," Presented at CNF Annual Meeting, Ithaca, NY, September 2003

Lijun Jiang and William N. Carr,

"Modeling and Simulation of A Surface Micromachined Capacitive Triaxial Accelerometer," Presented at International Conference on Modeling and Simulation of Microsystems, San Francisco CA, February 2003. Published in Proceedings of the NanoTech 2003, Vol.1

Lijun Jiang and William N. Carr,

"FEA Study and Applications of Bi-Material Structures in MEMS Devices," 2nd AIMS Materials Research Symposium, Newark NJ, May 2002

Lijun Jiang and William N. Carr,

"A Micromachined Thermo-Optical Light Modulator Based on Vanadium Dioxide Array," Submitted to Journal of Micromechanics and Microengineering

To my mother, for her love, dream and belief in us

ACKNOWLEDGMENT

I wish to express my deepest gratitude to my advisor, Professor William N. Carr, for his great guidance and support during the whole research.

Many thanks to the other members of the committee: Prof. Ken K. Chin, Prof. N. M. Ravindra, Prof. O. L. Russo and Dr. D. Setiadi for their careful review of the dissertation and many very helpful comments.

I want to extend my special thanks to Dr. D. E. Booth for his help in the cleanroom, and Mr. T. Yan for his help on device testing.

This work was performed in part at the Cornell Nano-Scale Science & Technology Facility (a member of the National Nanofabrication Users Network) which is supported by the National Science Foundation under Grant ECS-9731293, its users, Cornell University and Industrial Affiliates.

Mrs. Clarisa González-Lenahan of graduate studies office has carefully reviewed the format of this dissertation. I appreciate her great comments and help.

Last but not least, I am grateful to all my families for their love and encouragement. Specially, I am in debt to my wife, Wenwen, for her love, accompaniment and sacrifice during my study.

TABLE OF CONTENTS

Chapter | Page

1 INTRODUCTION 1

1.1 Micromachined Light Modulator 1

1.2 Principles of VO_2 Thermo-Optical Light Modulator 7

1.3 Dissertation Organization 12

2 LITERATURE REVIEW ON VO_2 THIN FILM 14

2.1 Semiconductor-to-Metal Phase Transition 14

2.2 Review of VO_2 Deposition Methods 18

2.2.1 Reactive Sputtering 18

2.2.2 Reactive Evaporation 19

2.2.3 Thermal Oxidation 20

2.2.4 Sol-Gel Methods 21

2.2.5 Other Methods 21

2.3 Optical Properties of VO_2 Thin Film 22

2.4 Doping Effects in VO_2 Thin Film 28

2.5 Applications of VO_2 Thin Film 32

3 THERMO-OPTICAL STUDY OF VO_2 THIN FILM 33

3.1 Synthesis of VO_2 Thin Film 33

3.2 Semiconductor-to-Metal Phase Transition 37

3.3 Thermo-Optical Switching of VO_2 Thin Film 40

3.3.1 Theory of Multilayer Matrix Calculation 40

3.3.2 Thermo-Optical Switching Spectra 45

TABLE OF CONTENTS
(Continued)

Chapter **Page**

3.3.3 Effect of VO_2 Thickness 49

3.4 Microstructure Characterization 51

3.5 Effect of the Hysteresis on Light Modulation 58

4 DESIGN AND ANALYSIS OF VO_2 LIGHT MODULATOR 65

4.1 Thermal Modeling 65

4.1.1 Thermal Isolation Pixel Structure 65

4.1.2 Thermal Conductance Analysis 68

4.1.3 Thermal Finite Element Simulation 70

4.2 Optical Modeling 74

5 MICROFABRICATION OF VO_2 LIGHT MODULATOR 79

5.1 Integration of VO_2 into Micromachining Process.......... 79

5.2 Microfabrication Process and Results.......... 81

5.3 Experimental Characterization and Discussions 89

5.3.1 Surface Planarity 89

5.3.2 Stress in VO_2 Thin Film.......... 89

5.4 Thermo-Optical Modulation Testing 98

5.5 Effects of Oxygen Plasma 101

6 SUMMARY AND CONCLUSIONS 103

REFERENCES 105

LIST OF TABLES

Table **Page**

2.1 Various Vanadium Oxides and Their Resistivity Jump at Phase Transition 17

3.1 Interference Color Variation during Vanadium Oxidation 34

3.2 List of Instruments Used in above Setup.. 38

4.1 Geometrical Dimension and Material Properties of the Pixel 71

4.2 Thermal Properties of Light Modulator Pixel 73

5.1 Stress Measurement Result for Vanadium and VO_2 Thin Film 96

LIST OF FIGURES

Figure **Page**

1.1 DMD mirror pixels with torsional hinges. The mirror is fabricated above CMOS silicon substrate that hosts the addressing and controlling circuits. The mirror is electrostatically actuated and operates between "on" and "off" states, which is the reason that it's called digital mirror [3]................................ 3

1.2 The WaveStar™ MEMS mirror by Lucent Technologies. The mirror can tilt along two axes and be continuously actuated to greater than ± 6°, which operates as an analog mirror [4] 4

1.3 The schematic (top) and operation principle (bottom) of the deformable grating light valve (GLV). The aluminum beams are actuated by the electrostatic force and operate between "on" and "off" states [3]................ 5

1.4 Variation of the electrical resistivity of vanadium dioxide thin film with the temperature at the semiconductor-to-metal transition. The VO_2 film was grown by reactive e-beam evaporation of vanadium in oxygen ambient on (0001) sapphire single-crystal substrate [7].. 8

1.5 Optical transmittance (solid line) and reflectance (dashed line) of VO_2 thin film on silica substrate (a) at room temperature (b) at 100 °C. The thickness of the VO_2 film is 85 nm [7].. 9

1.6 Schematic of the VO_2 thermo-optical light modulator pixel investigated in this research. The thermal isolation platform is surface micromachined and anchored on the substrate. The reflectance and the transmittance of the VO_2 film are controlled by the pixel temperature.. 11

2.1 Tetragonal unit-cell of the metal phase (top) and the monoclinic unit-cell structure of the semiconductor phase (bottom) of vanadium dioxide. The crystalline distortion from the rutile structure is illustrated [19]................. 15

2.2 Band diagram of the semiconductor and metal phases of vanadium dioxide suggested by J. Goodenough [20]. It should be noted that the predicted 0.7 eV band gap in this model disagrees with the experimental result of 2.5 eV 16

2.3 Typical optical transmission spectra for VO_2 thin film. The sample is 80-nm-thick VO_2 film on (0001) sapphire substrate by reactive evaporation [7] 23

2.4 Comparison of the transmittance spectra for standard (bronze) and anomalous (blue) VO_2 film in the visible region. The sample was 150-nm VO_2 films on quartz [28].. 24

LIST OF FIGURES
(Continued)

Figure		Page
2.5	Real part of the dielectric constant of VO_2 (top) at semiconductor phase, and (bottom) in metal phase [6]..	26
2.6	Imaginary part of the dielectric constant of VO_2 film at semiconductor phase (top) and metal phase (bottom) [6]..	27
2.7	Variation of the phase transition temperature (T_c) of VO_2 film with the doping levels of tungsten and fluorine. The effect of T_c reduction is less pronounced for co-doped film than single-doped film [49]....................................	29
2.8	Effect of the tungsten and fluorine doping on the optical switching property of VO_2 films. The transition temperature (T_c) is significantly reduced, but the switching magnitude is also adversely affected [50]............................	30
2.9	Shifting of the absorption edge (λ_k) of VO_2 film caused by the fluorine doping. The tungsten doping seems doesn't have as significant effect [49]......	31
3.1	Thickness variation of vanadium films with oxidation time (oxidized in room atmosphere, T = 370 ^oC)..	36
3.2	Experimental setup for testing the temperature-reflectance curve of VO_2 film..	38
3.3	Temperature-reflectance curve of VO_2 film on vanadium substrate (a) and the phase transition temperature T_c (b). The starting vanadium thickness is 115 nm. The VO_2 film is obtained by oxidizing for 12 minutes at 390 ^oC in air on hot plate (wavelength = 635.5 nm)..	39
3.4	Plane wave incident on a single thin film...	41
3.5	Simulated and measured infrared transmittance spectra (a) and reflectance spectra (b) for 614 nm VO_2 on sapphire [7]..	46
3.6	Simulated and measured transmittance spectra of 120 nm VO_2 on glass [35]...	47
3.7	Comparison of the measured and simulated UV-Visible spectra of thermally oxidized VO_2 on borofloat glass (a) ~ 35 nm (b) ~ 200 nm	48
3.8	Evolution of the reflectance contrast of VO_2 film with thickness (wavelength = 635.5 nm)..	50

LIST OF FIGURES
(Continued)

Figure **Page**

3.9 Surface grain microstructure and the temperature-reflectance curve of the VO_2 film by oxidizing 115 nm vanadium for 2 minutes at 390 °C (λ = 635.5 nm)... 52

3.10 Surface grain microstructure and the temperature-reflectance curve of the VO_2 film by oxidizing 115 nm vanadium for 12 minutes at 390 °C (λ = 635.5 nm).. 53

3.11 Surface grain microstructure and the temperature-reflectance curve of the VO_2 film by oxidizing 115 nm vanadium for 25 minutes at 390 °C (λ = 635.5 nm) 54

3.12 Evolution of the surface microstructure from columnar grains (a) to oriented crystalline texture (b) for 115 nm vanadium oxidized for 35 minutes 56

3.13 Asymmetrical hysteresis loop for VO_2 film with oriented textures compared with the columnar grain structure (a) and explanation with overlap of two hysteresis loops from differently oriented textures suggested by W. Haidnger (b) [62].. 57

3.14 Measured minor-loops of VO_2 film (a) when it was swept with temperature excursion less than the hysteresis width (b). The film was obtained by oxidizing 115 nm vanadium at 390 °C for 12 minutes. (λ = 635.5 nm).......... 60

3.15 Decreasing of the slope of the reflectance-temperature curve at the heat-up branch with the decrease of the temperature-sweeping excursion. The VO_2 film is obtained by oxidizing 115 nm vanadium at 390 °C for 12 minutes. (λ = 635.5 nm).. 61

3.16 Recorded temperature variation (a) the corresponding reflectance variation of the VO_2 thin film for small-signal operation testing (b). The VO_2 film is obtained by oxidizing 115 nm vanadium at 390 °C for 12 minutes. (λ = 635.5 nm).. 62

3.17 Experimental result that shows the reflectance-switching curve following same loop when the VO_2 film is cooled down to full semiconductor state. The VO_2 film is obtained by oxidizing 115 nm vanadium at 390 °C for 11 minutes. (λ = 635.5 nm).. 63

3.18 Measured reflectance of VO_2 film (a) when the film is held constantly at the phase transition temperature of 65 °C (b). The VO_2 film is obtained by oxidizing 115 nm vanadium at 390 °C for 11 minutes (λ = 635.5 nm).......... 64

LIST OF FIGURES
(Continued)

Figure **Page**

4.1 Schematic drawing of the light modulator pixel structure (a) and its equivalent lumped circuit model (b).. 66

4.2 Steady-state thermal simulation result for the light modulator pixel (a) temperature increase under different heat input (b) temperature distribution 72

4.3 Transient thermal ANSYS simulation result for the light modulator pixel........ 73

4.4 Cross-section view of the multi-layer light modulator pixel structure............, 74

4.5 Simulated transmittance spectra (a) and reflectance spectra (b) of a device structure consists of VO_2 (35nm) / SiO_2 (200nm) / Air-Gap (2.25um) / Glass-substrate.. 75

4.6 Simulated transmittance spectra (a) and reflectance spectra (b) of a device structure consists of VO_2 (50nm) / SiO_2 (200nm) / Air-Gap (2.25um) / Glass-Substrate 76

4.7 Simulated transmittance spectra (a) and reflectance spectra (b) of a device structure consists of SiO_2 (20nm) / VO_2 (35nm) / SiO_2 (200nm) / Air-Gap (2.25um) / Glass-Substrate 77

5.1 Illustration of a metal lift-off process to pattern metal films 80

5.2 Process flow of the light modulator.. 82

5.3 SEM micrograph of selected area of the microfabricated VO_2 pixel array before sacrificial releasing 87

5.4 SEM micrograph of selected area of the microfabricated VO_2 pixel array after sacrificial releasing.. 87

5.5 SEM image of single VO_2 pixel after sacrificial releasing 88

5.6 SEM image shows the VO_2 thin film on top of the SiO_2 pixel platform 88

LIST OF FIGURES
(Continued)

Figure **Page**

5.7 Wyko™ Optical profilometer measurement result on the pixel with good planarity 90

5.8 Wyko™ optical surface profile measurement result on the curled-up pixel..... 91

5.9 SEM image shows the curvature of the VO_2 pixel due to the residual stress 92

5.10 SEM image shows that the broken beams by the excess VO_2 stress in the worst case 92

5.11 Laser scanned wafer bow before and after vanadium evaporation for measurement of the stress 94

5.12 Laser scanned wafer bow after VO_2 oxidation for measurement of the stress... 95

5.13 Change of the VO_2 thin film stress with the temperature 97

5.14 Measured and simulated transmittance spectra of VO_2 testing structure 99

5.15 Thermo-optical modulation testing result (a) temperature setup (b) measured LED intensity variation 100

5.16 Temperature-reflectance curves of VO_2 film before and after O_2 plasma treatment........ 102

CHAPTER 1

INTRODUCTION

1.1 Micromachined Light Modulator

The Micro-Electro-Mechanical Systems (MEMS) technology refers to the field of fabrication of miniaturized sensors and actuators generally using processing and tools that originally developed for integrated circuits (IC) industry [1]. The micromachined sensors and actuators are superior to their macro counterparts in terms of smaller size, reduced power consumption, faster response time, and sometimes novel functions that are impossible in macro world. The MOEMS (Micro-Opto-Electro-Mechanical Systems) represents an important and unique class of MEMS devices, which integrate optical, electrical and mechanical functions on one chip. A tremendous variety of micromachined optical devices have been developed to date. The spectrum covers the emitter sources, waveguides, microlenses, light mixers, optical switches and modulators, and optical detectors. The application areas of MOEMS include optical communication, digital image acquisition and processing, display and projection, biomedical imaging, as well as industrial control, just to name a few.

A spatial light modulator (SLM) is a real-time reconfigurable device that can modify certain parameter of the transmitted light signal as a function of position across the wavefront [2]. The parameters that can be modulated include intensity (amplitude), frequency, phase, or polarization of the light signal. The spatial light modulator is a critical device in optical information acquisition and processing systems. A large format two-dimensional SLM enables parallel processing of a large data array (10^6 for

1000 × 1000 array, for example). Applications of SLM include scene simulation, dynamic spatial frequency filtering, optical switching, and image projection, etc. [2].

Micromachined devices are advantageous for interacting with light. First, the structural dimensions of the micromachined devices are on the same order as the light wavelength. The control of the light can be achieved with relatively small motion. Second, it offers advantages in size, weight, power and flexibility, which are general characteristics of MEMS devices. Today, numerous MOEMS light modulators have been developed based on mechanisms of reflection, transmission, interference, or diffraction modulation. A brief review of the representative devices is provided below.

The reflective optical modulator or switch is typically based on micromirror or micromirror array. The micromirror generally has a highly reflective surface. The reflection path of the light is altered by tilting the mirror. The most successful demonstration of the micromirror switch has been the digital micromirror device (DMD) by Texas Instrument [3]. As shown in Figure 1.1, the DMD pixel consists of an aluminum mirror suspended above silicon substrate by a torsional hinge. The mirror is deflected electrostatically by the applied potential between the mirror and the underlying electrodes. The controlling CMOS circuits are fabricated in the silicon substrate. The DMD devices have been successfully applied for the high-definition TV, high performance printers and projectors. Recent interest in developing micromirror matrix was for the optical cross-connect (OXC) and optical add/drop multiplexer (OADM) in fiber-optic communication systems. Dozens of micromirror prototypes have been reported with electrostatic, electromagnetic, or thermo-mechanical actuation mechanisms. One example, as illustrated in Figure 1.2, is the electrostatic tilting mirror developed by

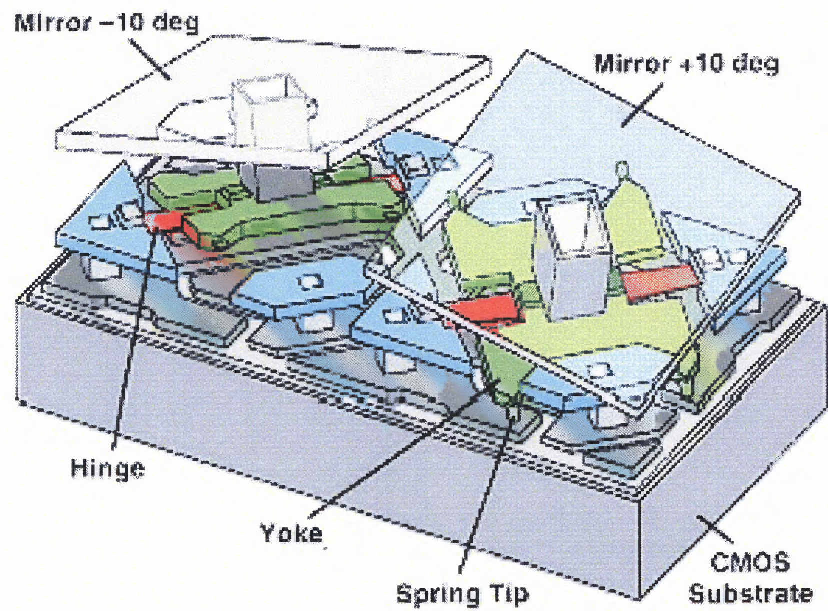

Figure 1.1 DMD mirror pixels with torsional hinges. The mirror is fabricated above CMOS silicon substrate that hosts the addressing and controlling circuits. The mirror is electrostatically actuated and operates between "on" and "off" states, which is the reason that it's called digital mirror [3].

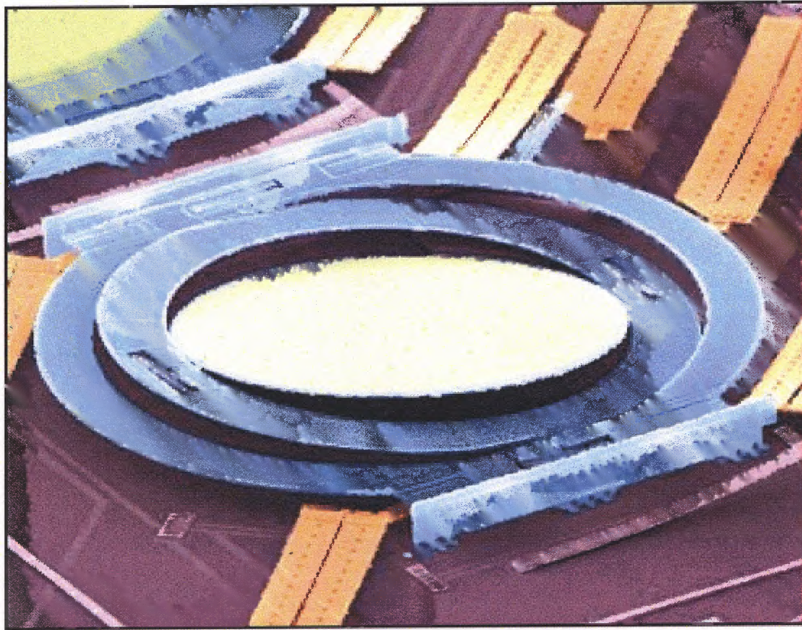

Figure 1.2 The WaveStar^{TM} MEMS mirror by Lucent Technologies. The mirror can tilt along two axes and be continuously actuated to greater than ± 6 degree, which operates as an analog mirror [4].

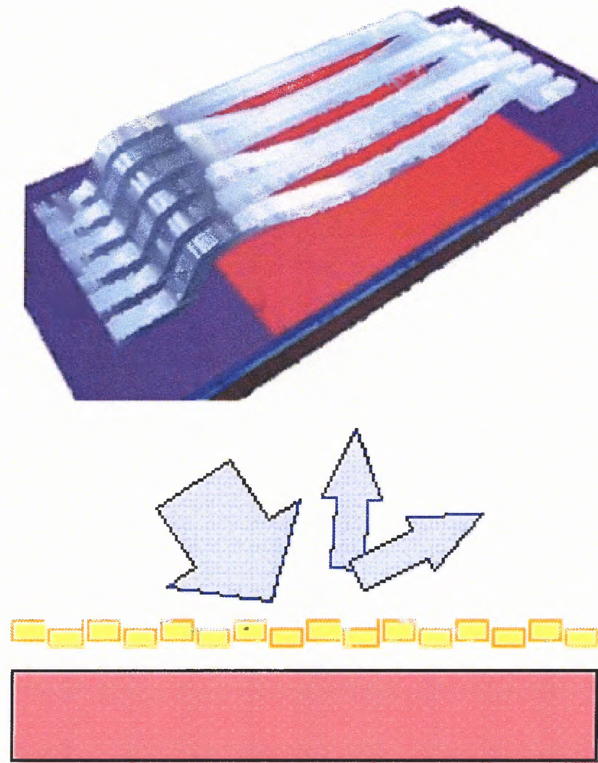

Figure 1.3 Schematic (top) and operation principle (bottom) of the deformable grating light valve (GLV). The aluminum beams are actuated by the electrostatic force and operate between “on” and “off” states [3].

Lucent Technologies [4]. It is a three-dimensional or so-called analog mirror, which means it can rotate along two axes and operate at multiple angles continuously (reported ± 6 degree travel range).

The representative device of the diffractive light modulator is the deformable grating light valve (GLV) by Silicon Light Machines, as shown in Figure 1.3 [3]. It has an array of aluminum beams that can be actuated electrostatically. When the beams are not actuated, the incident light is reflected back to the source and the GLV is at the "off" state. When it is actuated, the array diffracts light to certain angle and the GLV is at the "on" state. Every six beams form one pixel. The maximum diffraction intensity is obtained when the beams are actuated by $\lambda/4$, where λ is the light wavelength.

The reported transmission mode MEMS light modulators operate with certain mechanisms that interrupt the transmission of the light. They are generally electrostatically actuated micro-shutters that interrupt the path of the light passing through the substrate [1]. With the shutter actuated in or out of the light path, the signal is turned between "off" and "on" states.

However, all of above mentioned micromachined light modulators are mechanical devices. There are several challenges for the mechanical light modulators, including the speed, long-term reliability, and manufacturability. The reliability is always an issue for the MEMS devices. It is particularly important for light modulators that need to switch on and off constantly. The stiction and fatigue of the moving parts are of great concern for a huge array of mirrors. For the electrostatic actuation, high driving voltage is required to compensate the low force potential. To extend the travel range or precisely control the

tilting angle, electrical feedback is typically needed for the moving mirror array. The added circuits will increase the fabrication cost and complexity [1, 3].

In this dissertation, a thermo-optical light modulator is investigated. It is based on the semiconductor-to-metal phase transition properties of vanadium dioxide (VO_2) thin film. The optical properties of the VO_2 film change drastically before and after the phase transition. The modulator can be switched between high transmission to high reflection by controlling the pixel temperature. There are no moving parts required. The potential advantages of the thermo-optical light modulator include the high reliability and the simplicity for fabrication.

1.2 Principles of VO_2 Thermo-Optical Light Modulator

It's well known that vanadium dioxide undergoes a reversible semiconductor-to-metal phase transition at about 68 ^{o}C, which is accompanied by abrupt changes in its electrical and optical properties [5-6]. The sharp electrical resistivity change has been observed of as great as five orders for VO_2 single crystals and three to four orders for thin films (Figure 1.4) [7]. Optically, there're large variation in both the real and imaginary parts of the refractive index of VO_2, which will cause drastic change of its optical transmittance and reflectance upon the phase transition, as shown in Figure 1.5 [8].

As seen in figure 1.5, the large optical contrast is generally only observed in the infrared range. However, with proper interference structures, high optical contrast can also be achieved for the visible light [9]. It is possible to fabricate both reflective and transmissive light modulators. For the reflective modulator, the VO_2 thin film is deposited on a highly reflective metal layer. The thickness of the VO_2 is selected to

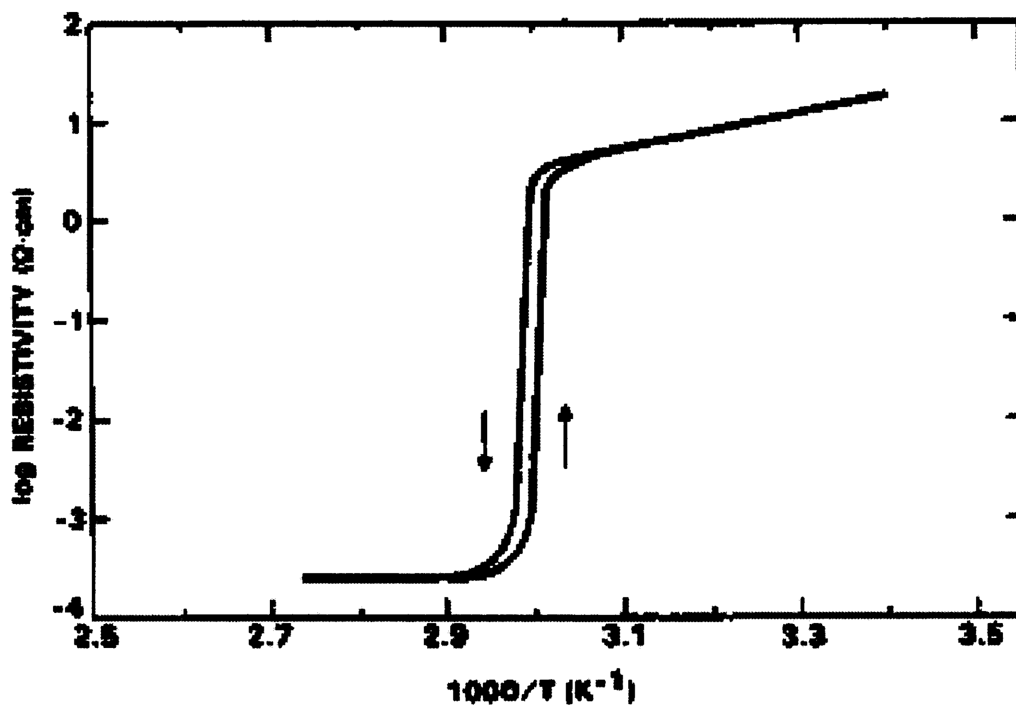

Figure 1.4 Variation of the electrical resistivity of vanadium dioxide thin film with the temperature at the semiconductor-to-metal transition. The VO_2 film was grown by reactive e-beam evaporation of vanadium in oxygen ambient on (0001) sapphire single-crystal substrate [7].

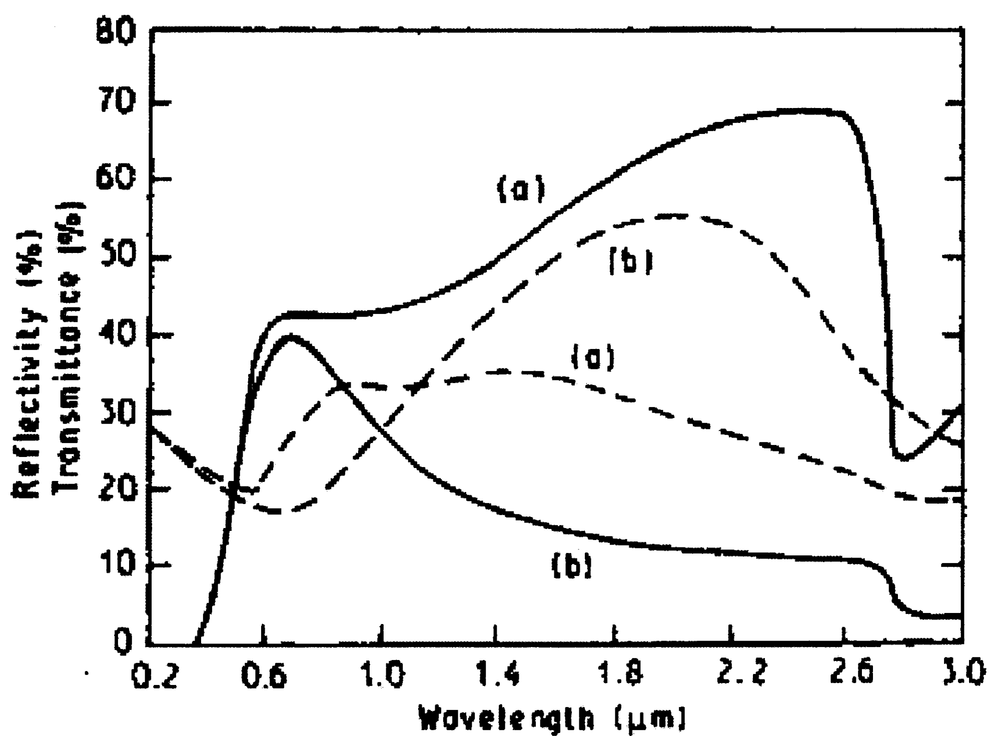

Figure 1.5 Optical transmittance (solid line) and reflectance (dashed line) of VO_2 thin film on silica substrate (a) at room temperature and (b) at 100 °C. The thickness of the VO_2 film is 85 nm [8].

satisfy the anti-reflection condition in one phase and be highly reflective in another phase. To operate in transmissive mode, the substrate must have a high optical transmission in the working wavelength.

Several light modulators have been proposed based on the thermo-optical switching property of VO_2 films [10-14]. The general principle of a VO_2 light modulator is as following: firstly, the VO_2 film is thermally biased at a temperature within its hysteresis loop. Heat is momentarily injected or removed from VO_2 film to locally increase or decrease the temperature of the VO_2 film. This local temperature variation will produce a spot that exhibits optical contrast to other areas. If the heat injection is spatially addressed, the VO_2 film will act as a 2-D spatial light modulator [10]. However, the cross talk between the adjacent spots and the large thermal mass of the bulk film make such device impractical [12].

The MEMS technology is the most practical method to fabricate a large format, high-resolution, high speed VO_2 SLM. First, because the optical property of VO_2 is extremely temperature-sensitive, good thermal isolation is required to prevent cross talk between adjacent pixels as well as temperature deviations across the array. Second, the thermal mass of the pixel needs to be minimized to compensate the high thermal isolation to reduce the thermal time constant, which determines the switching speed of the modulator. The good thermal insulation also helps to reduce the power consumption. The MEMS technology is well suitable to fabricate such large array of thermal isolated pixels, as have been proven in the infrared thermal detector technology [15-17].

A schematic of the thermo-optical light modulator pixel is shown in Figure 1.6. Each pixel is a micromachined thin film platform that suspended with long and thin

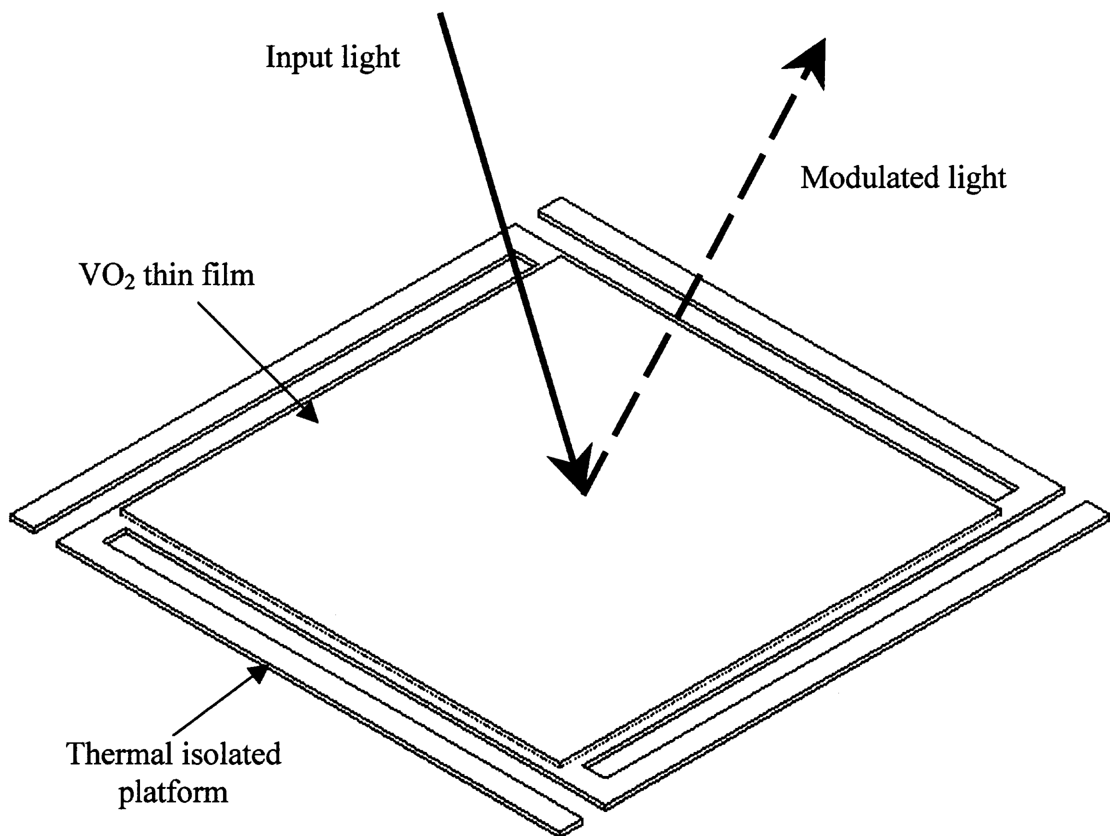

Figure 1.6 Schematic of the VO_2 thermo-optical light modulator pixel investigated in this research. The thermal isolation platform is surface micromachined and anchored on the substrate. The reflectance and the transmittance of the VO_2 film are controlled by the pixel temperature.

beams. Material with low thermal conductance is chosen for the platform and suspension beams. Vanadium dioxide is deposited on the top of the platform. The light signal is switched between high reflectance state and high transmission state by control the temperature of the pixel. The temperature can be controlled with integrated resistive heater on each pixel or spatially addressed radiation heat sources.

The objective of this research is to develop a VO_2 thermo-optical light modulator by surface micromachining technology. There are two major steps to reach the objective. First, we need to synthesis VO_2 thin film with high optical switching capability. The VO_2 film needs to be characterized to optimize the deposition process in terms of high optical modulation. Second, a micromachining process is to be developed to fabricate the pixel array with good uniformity. The VO_2 deposition step needs to be integrated into the microfabrication process, which is a key step for the realization of the light modulator. Correspondingly, the dissertation consists of two main parts. The first part is the synthesis and thermo-optical study of the VO_2 thin film. The second part is the microfabrication and experimental characterizations of the VO_2 light modulator.

1.3 Dissertation Organization

Chapter 2 provides a literature review on VO_2 thin films. It covers the basic mechanism of the semiconductor-to-metal phase transition, the comparison of various deposition methods, the optical properties, and applications of VO_2 thin film.

Chapter 3 presents the experimental results of the VO_2 thin film fabrication and the studies of the thermo-optical properties of the VO_2 thin films. The VO_2 film was produced by e-beam evaporation of vanadium metal film followed by thermal oxidation.

The optical switching properties are measured and explained with a multi-layer interference model. The optical properties are simulated and compared with experimental results. The microstructures of the films are characterized and their effects on the optical switching are discussed. The switching hysteresis is discussed in terms of its effects on the thermo-optical switching of the VO_2 light modulator.

Chapter 4 describes the design and simulation of the light modulator pixel. The thermal isolation property of the pixel is described analytically and simulated with finite element method. The tradeoff between the speed and power consumption is discussed. The optical behavior is simulated with thin film optic software.

Chapter 5 presents the experimental results of the microfabrication, characterization and testing of the light modulator. The light modulator is fabricated by surface micromachining. A polyimide sacrificial layer is used. PECVD SiO_2 was used to form the thermal isolation platform. VO_2 film was patterned by lift-off. The light modulator was realized in a 64×64 format.

Finally, Chapter 6 concludes the dissertation and presents the future work.

CHAPTER 2

LITERATURE REVIEW ON VO_2 THIN FILM

2.1 Semiconductor-to-Metal Phase Transition

The semiconductor-to-metal phase transition in VO_2 was firstly observed by Morin in 1959 [18]. The first-order transition occurs at about 68 °C and is accompanied with a crystallographic distortion. As shown in Figure 2.1, the high-temperature phase of VO_2 has a tetragonal rutile structure with V^{4+} ions occupy the *bcc* positions and the center position of the O^{2-} ions octahedral. At temperatures lower than the phase transition temperature (T_c = 68 °C), the VO_2 crystalline lattice is distorted into a monoclinic structure. The V^{4+} ions at the body corner displace along the rutile c-axis and cause the unit-cell size to double [19]. Several theoretical models have been proposed to explain the phase transition phenomenon based on this lattice distortion [5]. However, no single model can explain all the properties related to the phase transition. The mechanism behind the phase transition is still not fully understood.

One generally accepted model was developed by J. B. Goodenough based on molecule field and crystal field theories [20]. As illustrated in Figure 2.2, in the metallic phase ($T > T_c$), the $3d^1$ energies of the vanadium atom split into twofold-degenerate E_g states and triply degenerate T_{2g} levels. The E_g orbitals are strongly hybridized with the $2p$ orbitals of the oxygen atom and form σ and σ^* bands. On the other hand, the three T_{2g} orbitals split into two π and π^* bands and one $d_{//}$ band along the c-axis. The bands of $d_{//}$ and π^* overlap at the Fermi level, which leads to the metal state at high temperature. In the room temperature state, the V-V bond becomes stronger due to the lattice distortion.

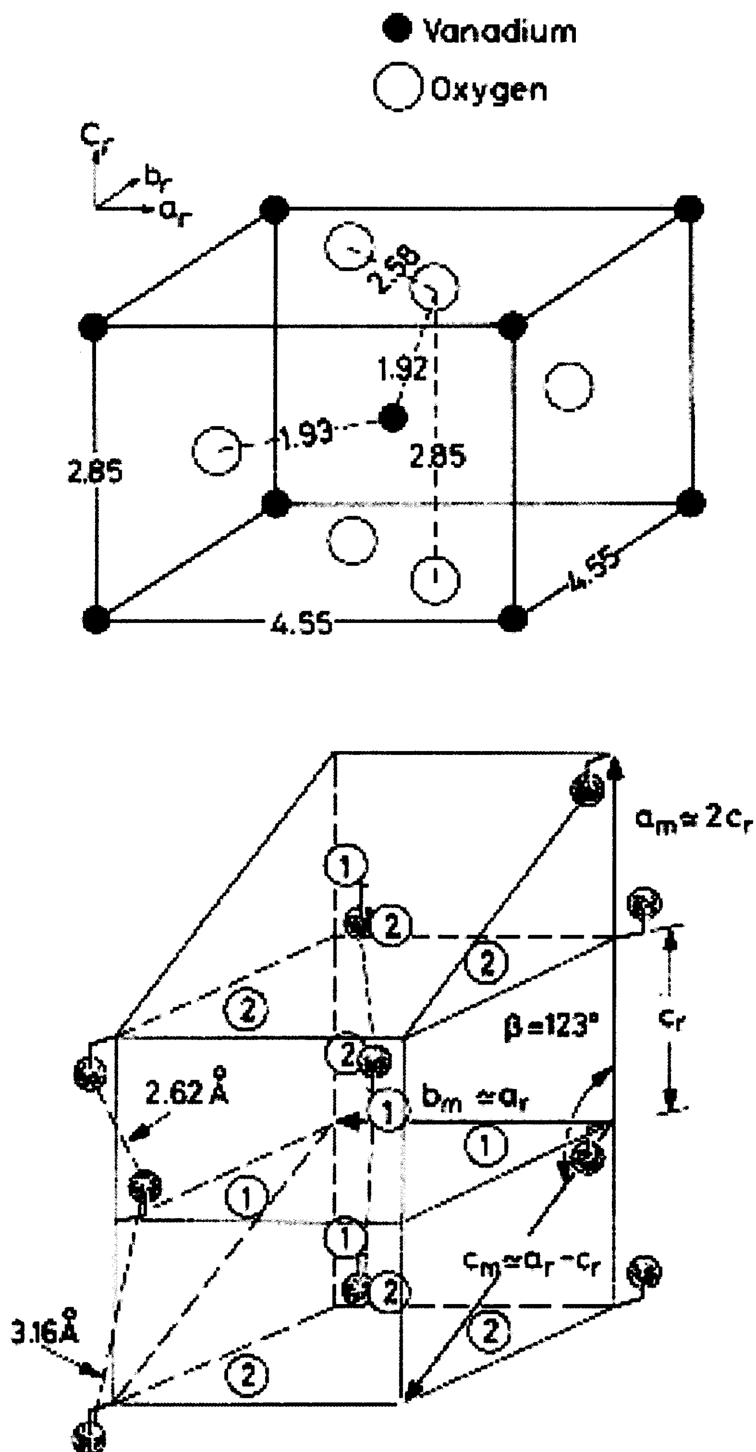

Figure 2.1 Tetragonal unit-cell of the metal phase (top) and the monoclinic unit-cell structure of the semiconductor phase (bottom) of vanadium dioxide. The crystalline distortion from the rutile structure is illustrated [19].

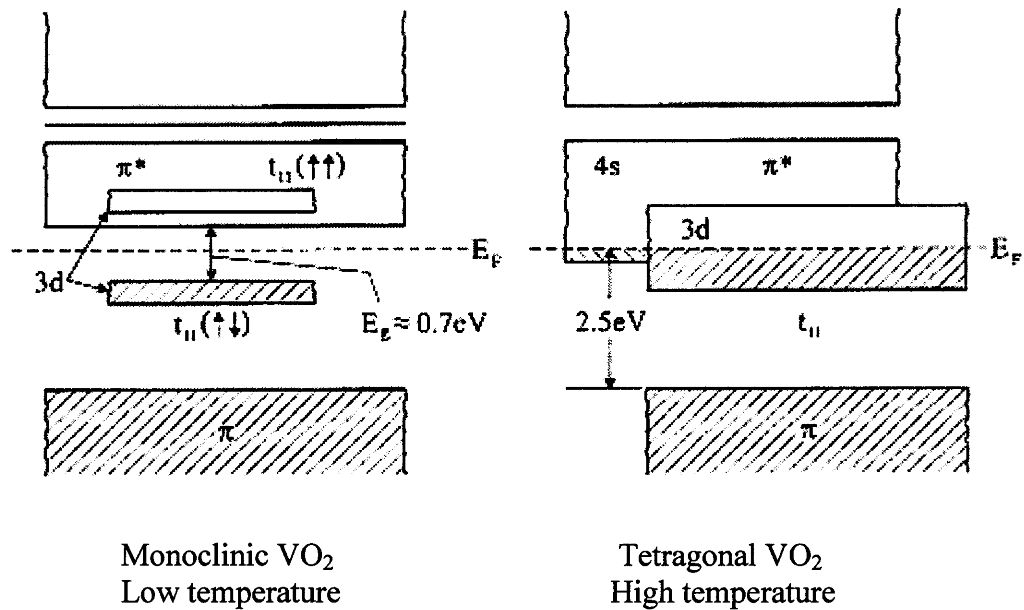

Figure 2.2 Band diagram of the semiconductor and metal phases of vanadium dioxide suggested by J. Goodenough [20]. It should be noted that the predicted 0.7 eV band gap in this model disagrees with the experimental result of 2.0 - 2.5 eV [8].

The π* is raised above the Fermi level, which is energetically favorable. The $d_{//}$ band split into one empty band and one filled band because of the unit cell volume doubling. However, the predicted 0.7 eV band gap disagrees with some experimental results [8].

There are other materials, i.e. certain compounds of some transition and rare earth metals, also display the phase transitions properties. Vanadium itself is a multi-valence metal and forms dozens of different oxides. Most vanadium oxides undergo phase transition at certain temperatures. Table 2.1 summarizes the phase transition temperatures and the associated electrical resistivity jump of those vanadium oxides [5, 21]. Among them, VO_2 has been mostly studied because that its phase transition temperature is well close to the room temperature and offers tremendous potential applications in electronic and optics. This chapter presents a literature review on VO_2 film. It covers the deposition methods and the relationships between the film properties and processing parameters.

Table 2.1 Various Vanadium Oxides and the Resistivity Jump at Their Phase Transition

Valence	Compound	T_c (°C)	Resistivity jump
+2	VO	Metal	
+3	V_2O_3	- 105	10^{10}
	V_3O_5	155	10^2
	V_4O_7	- 13	10^3
	V_5O_9	- 138	10^6
Magnel series	V_6O_{11}	- 103	10^4
V_nO_{2n-1}	V_7O_{13}	Metal	
(n = 3 – 9)	V_8O_{15}	- 205	10^1
	V_9O_{17}	- 193	10^1
+4	VO_2	68	10^5
	V_3O_7	Insulator	
	V_6O_{13}	- 123	10^5
+5	V_2O_5	Semiconductor	

2.2 Review of VO_2 Deposition Methods

Numerous methods have been developed to fabricate VO_2 thin films, including reactive sputtering [22-26], reactive evaporation [27-31], chemical vapor deposition [32-33], thermal oxidation [9, 34-36], as well as sol-gel methods [37-40]. The stoichiometry and microstructure of the VO_2 film are strongly dependent on the deposition method and process parameters, which in turn determine the electrical and optical properties of the VO_2 film. It was shown that single-crystal VO_2 displays the largest electrical swing of five orders and smallest hysteresis of only 1 ^oC [7]. The drawback of VO_2 single-crystal is that it will crack after several switching due to the lattice distortion with the phase transition, which prevents it from practical applications. No VO_2 thin film has ever achieved equivalent properties to those of single-crystal. For the light modulator application, the optical switching properties in terms of the switching magnitude of reflectance and transmittance, the hysteresis width and the phase transition temperature are most important parameters. In this section, various deposition methods are reviewed with emphasis on the effects of deposition parameters on the VO_2 properties.

2.2.1 Reactive Sputtering

The reactive sputtering of the VO_2 film is typically carried out by sputtering pure vanadium target in an argon-oxygen mixture atmosphere. Various sputtering techniques include dc-sputtering, RF-sputtering, and ion-assisted sputtering have been studied to deposit VO_2 film. The properties of the VO_2 film can be controlled by adjusting the sputtering parameters of oxygen gas ratio, temperature and biasing of the substrate, and the ion bombardment. It was shown that the stoichiometry of the sputtered VO_2 film is extremely sensitive to the oxygen fraction in the sputtering ambient. The increase of the

oxygen gas fraction leads to oxygen-rich films, which mixed with higher valence oxide such as V_6O_{13} or V_2O_5 [23-24, 26]. Only a narrow range of oxygen percentage can produce switchable VO_2 film. In C. H. Griffiths' study [24], different phases of vanadium oxides have been identified by electron diffraction for films created at different sputtering oxygen partial pressure. The microstructure of the film is strongly influenced by the substrate temperature (T_s). E. E. Chain [25] studied the effects of substrate temperature in ion-beam sputtering. It was found that the strongest effect of T_s is related to the film structure. The increased T_s produced films with large grain size and improved electrical switching. The temperature dependence growth of the sputtered film was modeled with the Thornton's zone model. Other researchers also reported that the VO_2 film sputtered at lower T_s were in amorphous state [24, 26]. The effects of biasing and annealing were studied by A. Razavi [22]. The *in situ* anneal was found to improve the stoichiometry, modify the optical contrast and increase the grain size. The bias of substrate will cause ion bombardment on the film and degrade the optical contrast.

2.2.2 Reactive Evaporation

Some "anomalous" VO_2 films have been deposited by reactive evaporation method [27-28]. The typically produced VO_2 film is in brown color and displays high optical switching only in the infrared range. But those anomalous films are in blue and display enhanced optical contrast even in visible range. The contrast is so pronounced that the color of the film can be visually observed to change from bright blue to dark when it is heated through the phase transition. G. A. Nyberg firstly reported this phenomenon and attributed it to improved stoichiometry [27]. F. C. Case reproduced such film by annealing pre-evaporated film in oxygen flow [28]. She assumed that the anomaly was

due to the large grain and grain boundary in the film and the blue-to-dark color change came from the scattering from the large grain. In her other reports, she studied the activated-reactive-evaporation (ARE) of VO_2 film [31]. Compared to conventional reactive evaporation, the electrons in the ARE method were accelerated to promote the ionization of background gas atoms. It resulted in an improved VO_2 film for the infrared switching. Also, with the ion-assisted evaporation, the switchable VO_2 film can be fabricated at low temperature of 300 °C [30].

2.2.3 Thermal Oxidation

Vanadium metal can be easily oxidized in oxygen ambient at elevated temperature. The thermal oxidation has been studied for both vanadium bulk metal [9, 36] and vanadium metal films [34-35]. One advantage of this method is its simplicity. The vanadium film can be deposited on the substrate by sputtering or evaporation. Typically, oxidation just in the air can produce reasonable good film. It was found that the stoichiometry of the oxidized film depends on both the temperature and time of oxidation. S. Jiang [35] studied the oxidation of vanadium film at 400 °C in air. For a 120 nm vanadium film, the best VO_2 film was obtained after 3 hours oxidation. The film thickness increased about 2.3 times after fully oxidation. A. Z. Moshfegh oxidized bulk vanadium (about 0.7 mm thickness) in atmosphere-pressure pure oxygen at 400 – 600 °C [36]. Though his primary interest was to produce V_2O_5, it was found that VO_2 was formed at 400 °C.

2.3.4 Sol-Gel Methods

The sol-gel process is based on the hydrolysis and condensation of molecular precursors. The sol-gel method is convenient to produce thin films. The sol-gel processes developed for VO_2 have been based on precursors of tetravalent alkoxide such as vanadium tetrabutoxide [39] or pentavalent vanadium such as vanadium oxo-isopropoxide and vanadium pentoxide [40-41]. J. Livage derived VO_2 film from vanadium alkoxides [$VO(OR)_3$, R = alkyl group] precursor [39]. The vanadium alkoxides were synthesized by reaction of ammonium vanadate with alcohol. The alkoxide solution was spin-coated onto silica substrate and rapidly dried at 80 ^{o}C. The film needs to be thermally treated in a reducing ambient to remove the organics and form crystalline VO_2. The resulted film shows about three-order switch of electrical resistivity. D. Yin reported an inorganic sol-gel method [40]. It uses V_2O_5 powder as precursor. The V_2O_5 is melted at high temperature and quenched in DI water to form V_2O_5 sol. The spin-coated film is vacuum heated to form VO_2 film. The synthesized VO_2 film exhibits the best resistivity switching of 4 to 5 orders.

2.3.5 Other Methods

The other deposition methods for VO_2 films have been chemical vapor deposition (CVD) [32-33], pulsed laser deposition [42], as well as thermal reduction from V_2O_5 [43]. However, the first four methods have been mostly studied. The processes and film properties are better understood.

2.3 Optical Properties of VO_2 Thin Film

The most prominent optical property of VO_2 film is its phase transition related optical switching ability. There are both theoretical and practical interests in studying the optical switching properties of VO_2 film. From a theoretical point of view, a study on the optical switch especially at the temperature close to the phase transition will shed light on the nature of the phase transition. In the practical perspective, one wants to enhance the optical contrast of the switching to improve the light modulation ability.

However, there have been a lot of disagreements in the reported optical properties of VO_2 films. First, the magnitude of optical switching is wavelength dependent. It is generally very small in the visible and near-infrared range but accentuated in the infrared region. Second, the optical properties are sensitive to the stoichiometry and surface microstructures of the VO_2 films. Films prepared by different deposition methods or under different processing parameters will behave differently. Also, it's well known that the optical behavior of thin film is a function of the film thickness. Most time it is hard to directly compare the results from different authors because they experimented at different film thickness.

A typical transmittance spectrum of VO_2 film is shown in Figure 2.3. It was taken on an 80-nm-thick film on (0001) single-crystal sapphire prepared by reactive e-beam evaporation [7]. The cut-off beyond 5 um is from the substrate. One feature of the spectrum is the sharp cutoff below 0.4 um. It comes from the inherent absorption of VO_2. It also should be noted that there is very little contrast in the visible spectrum. This type of VO_2 film was typically cited as "conventional", "bronze" film, in comparison with the "anomalous", "blue" VO_2 films [27-28]. The big difference is the enhanced visible

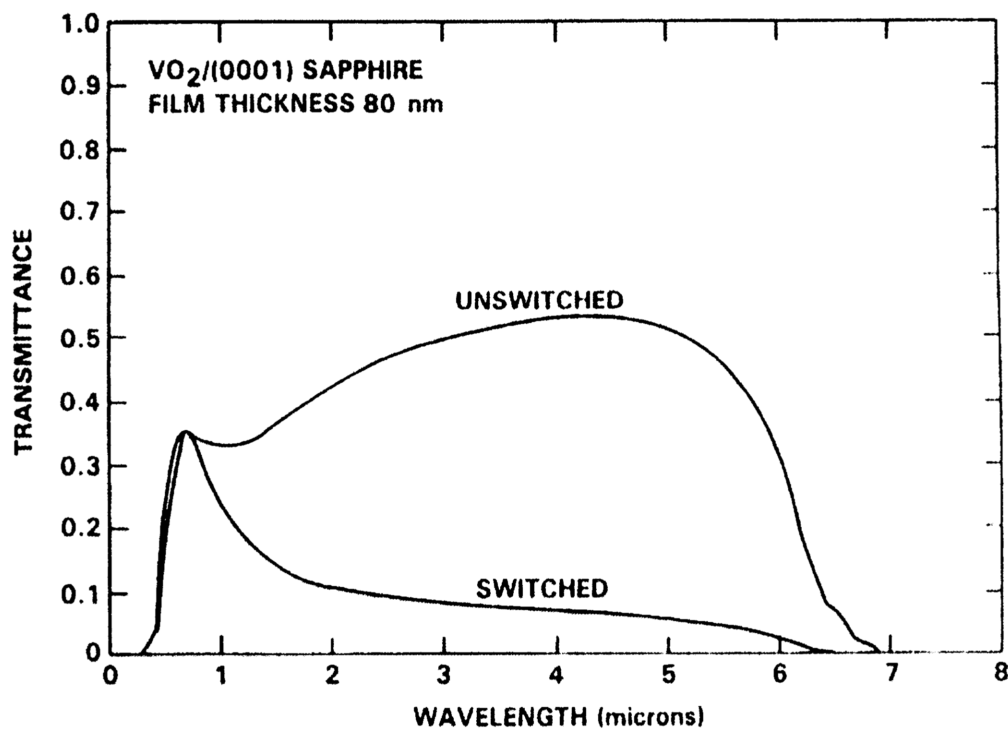

Figure 2.3 A typical optical transmission spectra for VO_2 thin film. The sample is 80-nm-thick VO_2 film on (0001) sapphire substrate, formed by reactive evaporation [7].

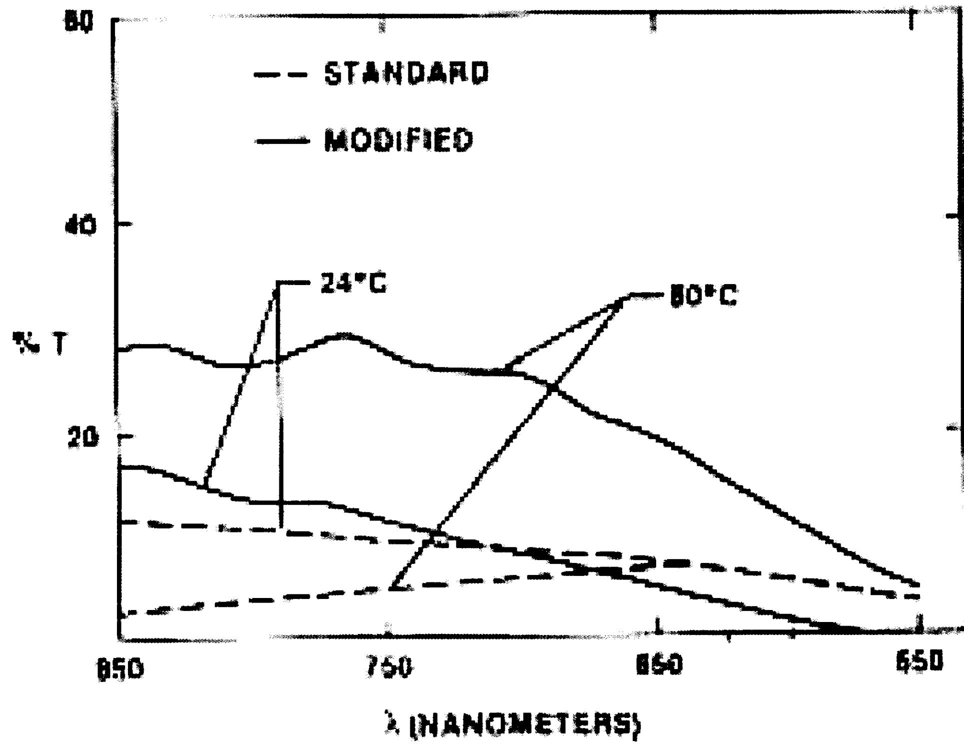

Figure 2.4 Comparison of the transmittance spectra for standard bronze and modified anomalous blue VO_2 film in the visible region. The sample was 150-nm VO_2 films on quartz [28].

optical contrast for the "blue" film (Figure 2.4). It was firstly reported by G. A. Nyberg and he attributed the difference to the stoichiometry [27]. F. C. Case reproduced this type of film and she observed 42% decrease of the imaginary refractive index for the "blue" film at phase transition, comparing to a 19% increase for the "brass" film [28].

It was believed that the optical switching comes from the variation of the complex refractive index during the phase transition. The refractive index is an important parameter in designing thin film optical structure. H. W. Verleur derived the optical constants from the reflective and transmissive spectra [6]. Figure 2.5 and 2.6 illustrate his results. Other authors have derived refractive index over limited spectral range or at single wavelength from reflection and transmission spectra or by ellipsometry methods [44-45]. The VO_2 film shows high absorption at wavelength less than 500 nm. The absorption edge at the metal phase was attributed to the 2p-3d absorption, while it was interpreted as the band gap absorption for the semiconductor phase [27].

Concerning the switching speed of VO_2 film, several studies suggested that the switching time for VO_2 itself is at the order of pico-second [44-45]. The switching speed for a subsystem including VO_2 film will be determined by the thermal constant of the pixel design and the rate of the energy injection and removal [46].

Other features related to the optical switching of VO_2 include the hysteresis width and phase transition temperature (T_c). The hysteresis width is believed to be connected with the grain structure of a host of individual grains that each transforms at its own temperature. A large distribution of grain size and orientation will result in an enlarged hysteresis. The T_c is significantly influenced by the doping effect and is discussed separately in next section.

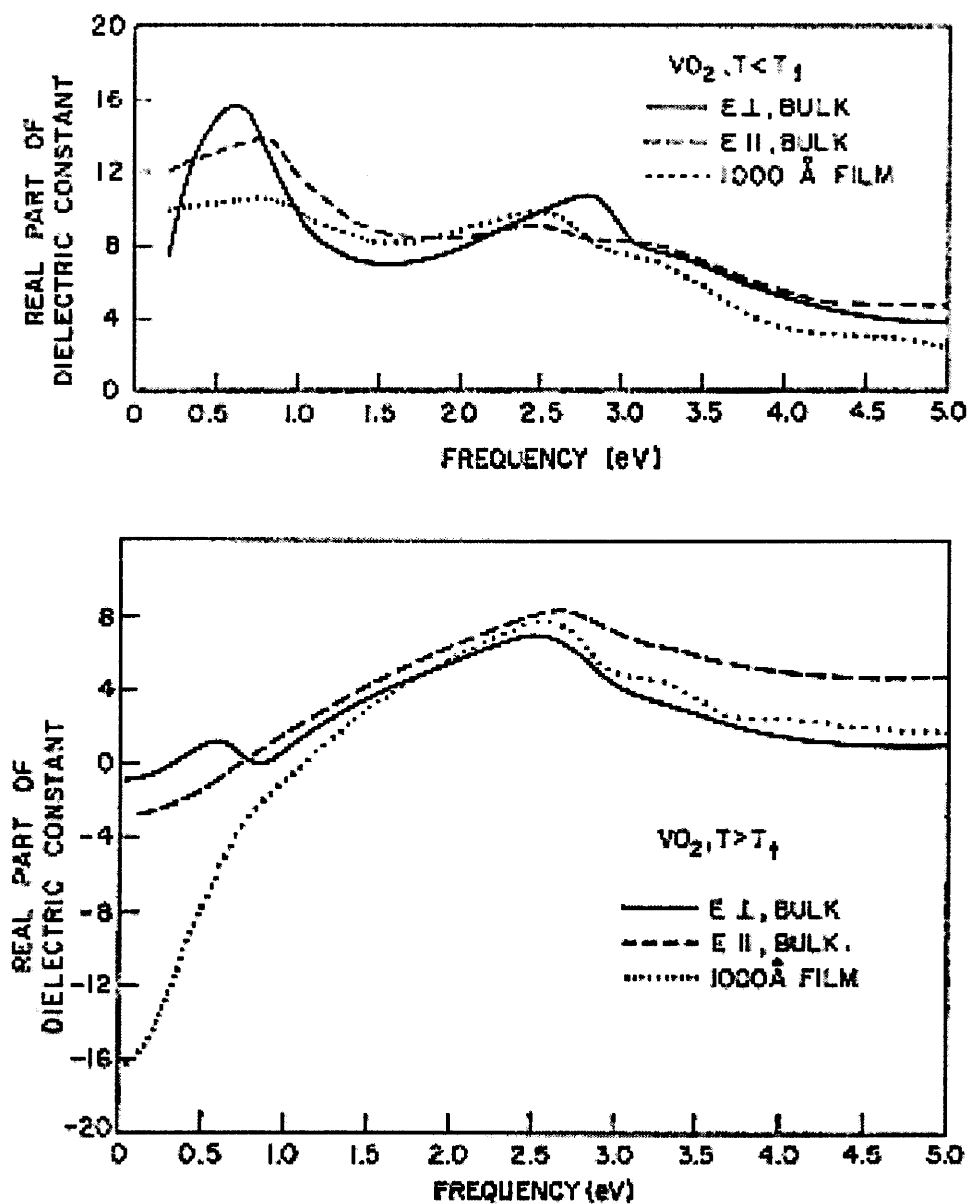

Figure 2.5 Real part of the dielectric constant of VO_2 at semiconductor phase (top) and in metal phase(bottom) [6].

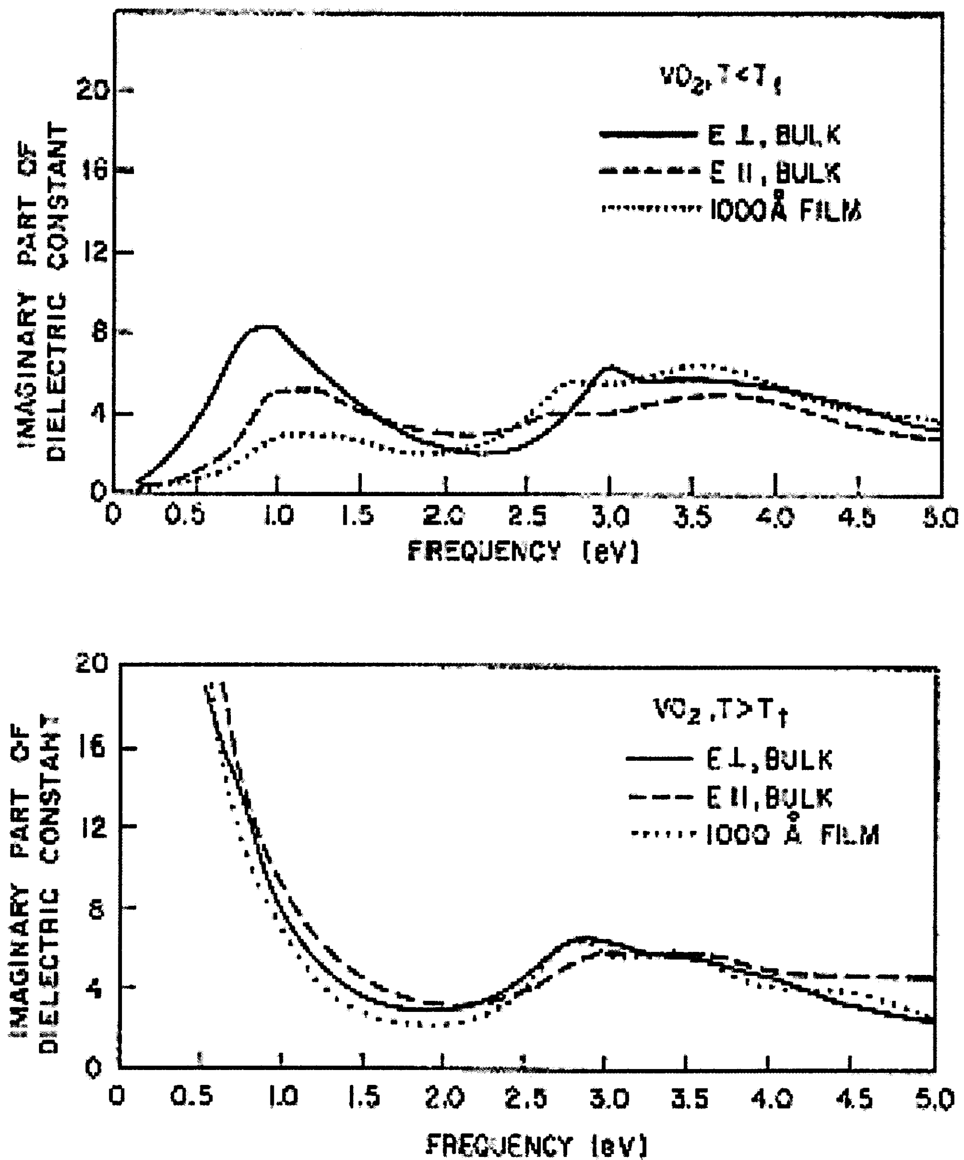

Figure 2.6 Imaginary part of the dielectric constant of VO_2 film at semiconductor phase (top) and metal phase (bottom) [6].

2.4 Doping Effects in VO_2 Thin Film

Doping is an effective method to reduce the phase transition temperature of VO_2 film. The mostly used dopant is tungsten with a reported effect of about –23 K/at.%W up to concentration of several percent. Other dopants include fluorine at –20 K/at.%F, rhenium at –18 K/at.%Re, and molybdenum at –10 K/at.%Mo [47]. The incorporation of the dopant can be done by co-sputtering [48] or ion implantation followed by annealing [49]. W. Burkhardt studied the effects of W and F co-doping in the VO_2 film [47-48]. The W was from a tungsten target and F was from the fluoromethane in the sputtering gas. Figure 2.7 shows the decreasing of the T_c with the doping concentration of F and W. The two dopants affect the T_c almost independently. The mechanism of reducing the T_c by doping was suggested as that the incorporation of dopant atoms leads to the loss of V^{4+}-V^{4+} pairs, which destabilize the semiconductor phase. Consequently, the semiconductor-to-metal transition will occur at a lower temperature [48]. P. Jin reported the incorporation of tungsten doping by high-energy (1 MeV) ion implantation [49]. A reduction rate of about –24 $^{\circ}$C/at.%W has been achieved.

The adverse effect of doping on the optical property of VO_2 film is the degradation of the optical switching contrast. As illustrated in Figure 2.8, the optical contrast of both W and F doped films has degraded compared to undoped film. However, it was seen that the W doping doesn't degrade the switching as much as the F doping. The other influence of the doping is to shift the VO_2 absorption edge to smaller wavelength. As shown in Figure 2.9, a fluorine dopant level of 2 at.% shifts the absorption edge of 0.15 eV and results in a colorless film [48].

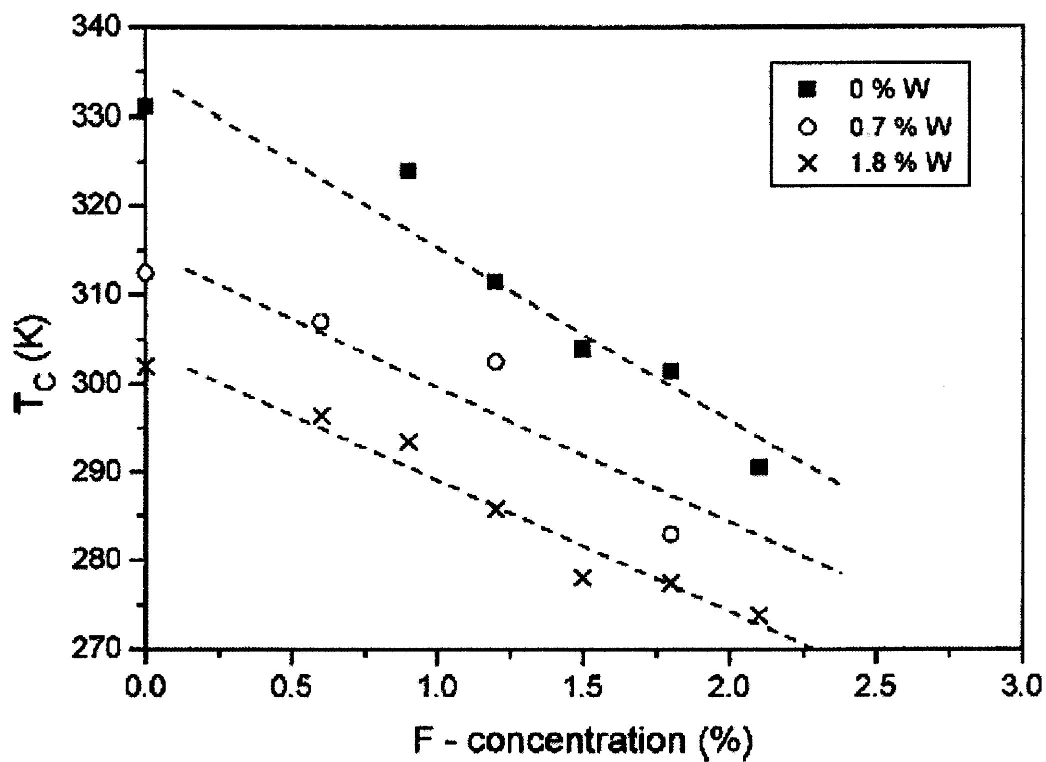

Figure 2.7 Variation of the phase transition temperature (T_c) of VO_2 film with the doping levels of tungsten and fluorine. The effect of T_c reduction is less pronounced for co-doped film than single-doped film [49].

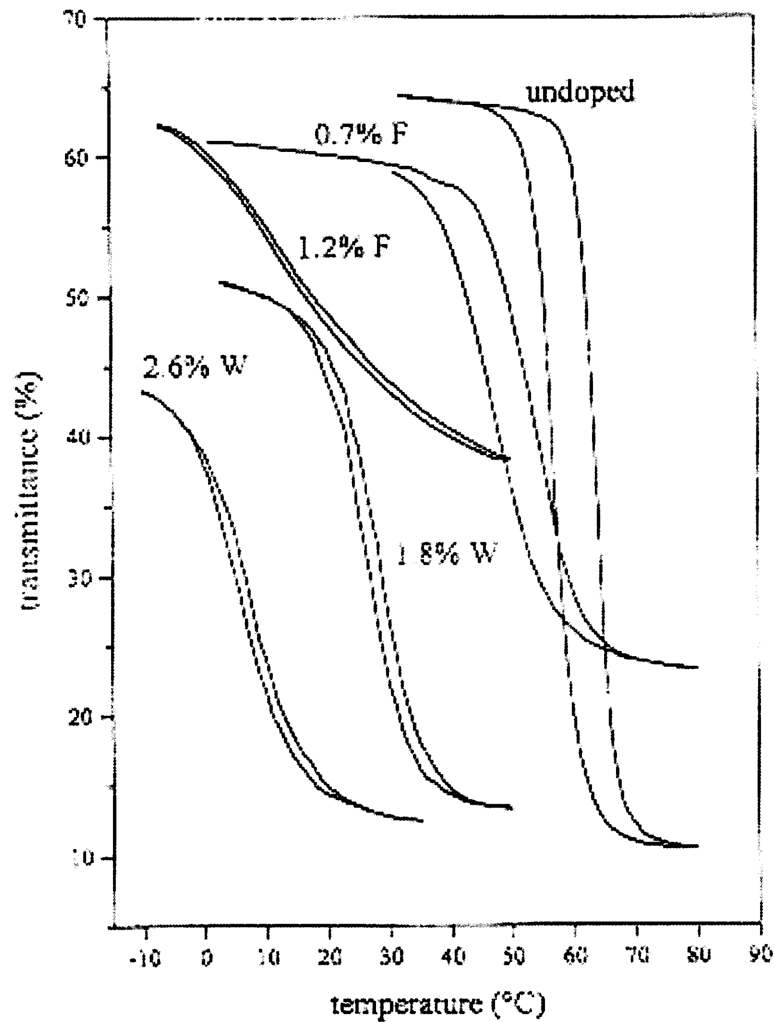

Figure 2.8 Effect of the tungsten and fluorine doping on the optical switching property of VO_2 films. The transition temperature (T_c) is significantly reduced, but the switching magnitude is also adversely affected. Undoped and tungsten-doped films are 120 nm. Fluorine-doped films are 80 nm. All films are reactive RF sputtered on quartz. Data ere taken at 2-um wavelength [50].

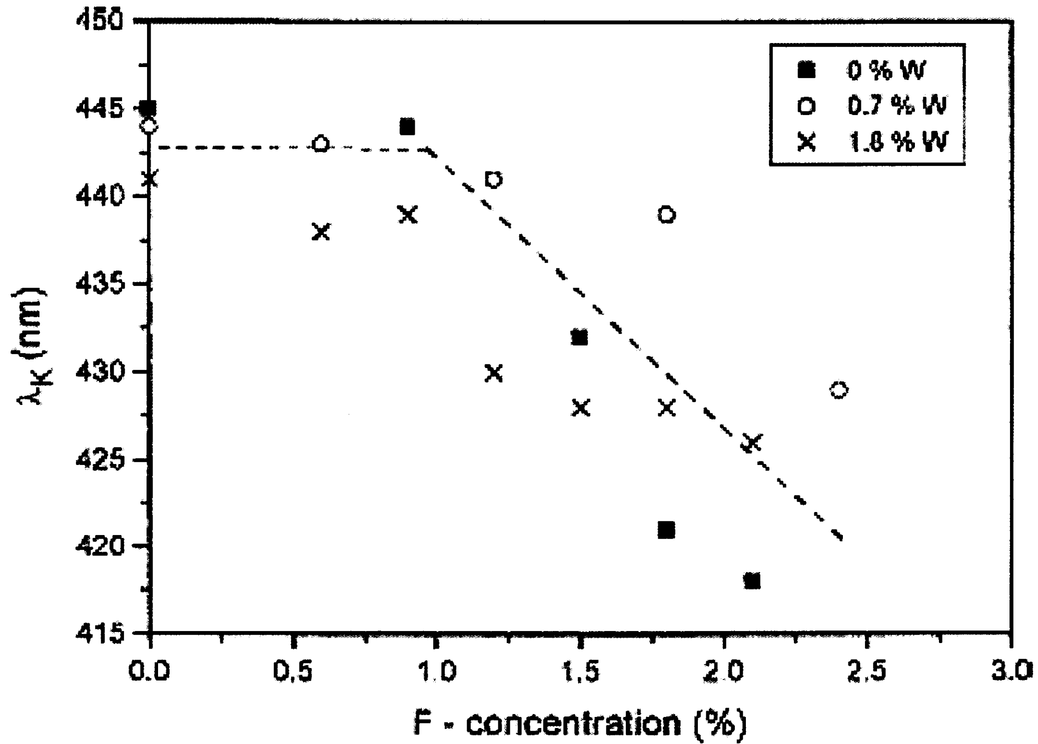

Figure 2.9 Shifting of the absorption edge (λ_k) of VO_2 film caused by the fluorine doping. The tungsten doping seems doesn't have as significant effect [49]. A band gap of about 2.5 eV can be calculated from the absorption edge, which disagrees with the 0.7 eV band gap predicted by Goodenough (see Figure 2.2).

2.5 Applications of VO_2 Thin Film

Based on its unique electrical and optical properties, VO_2 thin films have found a variety of practical applications in electronic and optic fields. The most significant one was in the infrared bolometers [50]. The principle for the VO_2 bolometer is that a temperature variation caused by the infrared radiation will produce a change in the electrical resistance of VO_2 film. So the key merits for a bolometric material is its thermal coefficient of resistance (TCR). The TCR of VO_2 film exceeds 4% per degree for single VO_2 resistor and 2% for bolometer array [51]. A typical pixel structure for a VO_2 bolometer is based on a bridge-like thermal isolated 0.5-um-thick silicon nitride (Si_3N_4) platform. A 50 nm thin layer of polycrystalline VO_2 is encapsulated in the center of the platform. The readout circuit is fabricated on the underlying substrate. Several companies have licensed to fabricate multi-pixel focal plane arrays (FPA) based on this technology from Honeywell [52]. Other applications of VO_2 film that have been investigated include optical storage devices [9, 53-54], optical switches [55-56] and variable reflectance mirror [57], etc.

CHAPTER 3

THERMO-OPTICAL STUDY OF VO_2 THIN FILM

3.1 Synthesis of VO_2 Thin Film

In this research, VO_2 thin films are synthesized by evaporation of vanadium metal film followed by oxidation in air at temperature of 350 to 390 °C. The vanadium metal film is e-beam evaporated from pure vanadium target (99.9%). The substrates used include borofloat silica and silicon with thermal oxide on the surface. The reason for choosing the thermal oxidation method was that it's simple and doesn't involve many processing variables. Another consideration is that it can be easily integrated into the micromachining process using metal lift-off technique.

The oxidation was done on hot plate. The temperature of the hot plate was monitored by a thermocouple and controlled within ± 2 °C by a PID controller. For vanadium films thicker than 50 nm, the oxidation progress can be observed by the continuous color changing of the vanadium film. The color for the vanadium film before any oxidation is silver. It begins to change to slight yellow after being put on the hot plate for several seconds. After half minutes, the color becomes brown. With further oxidation, the color changes to violet, dark blue, blue, green, and yellow. After 20 minutes oxidation, the film turns to violet color again. This observation agrees with the experiment by I. Balberg [9]. A series of VO_2 films with different colors were made by oxidizing for different time. Table 3.1 summarizes the observed colors for VO_2 films from different oxidation time. These colors come from the interference system that consists of VO_2 film on top of a vanadium layer. After about 45 minutes oxidation for a 115 nm vanadium

Table 3.1 Interference Color of Vanadium Films Oxidized for Different Time

115 nm Vanadium		150 nm Vanadium	
Time (min)	Color	Time (min)	Color
2	Blue-Violet	10	Blue
4	Blue	11	Green
5	Blue-Violet	12	Blue
6	Green	14	Yellow
7	Green	16	Yellow-Red
8	Blue	18	Yellow-Red
9	Yellow	20	Yellow-Red
10	Yellow	22	Violet
11	Green	24	Violet
12	Yellow-Red	26	Yellow-Red
14	Yellow-Red	28	Violet
16	Green	30	Violet

film, the film started to become transparent to some degree. The final color was brown and wouldn't change after further oxidation. For the 20-nm-thick vanadium on the borosilicate substrate, the film became transparent after only several minutes oxidation and the systematic color variation as for the thicker film wasn't observed. The thickness variation during the oxidation has been measured for 20 and 30 nm vanadium film with a Tencor P-10 surface profilometer. The result was shown in Figure 3.1.

Most samples in Table 3.1 exhibited a visually observable color change when they were heated through the phase transition temperature. It was one of the characteristics of the anomalous "blue" VO_2 films reported by Nyberg [27] and Case [28]. This sharp color change reveals a relatively large optical switching in the visible wavelength. At room temperature, all the samples display uniform interference colors. Larger pieces of vanadium film of 5×5 cm^2 have been used to test the oxidation uniformity of the hot plate. After 12 minutes oxidation, the 5×5 cm^2 VO_2 film appear visually uniform. The reflectance taken at different points through the wafer revealed very good uniformity. The optical properties of the VO_2 films created from different oxidation conditions were examined with emphasis on the light modulation properties.

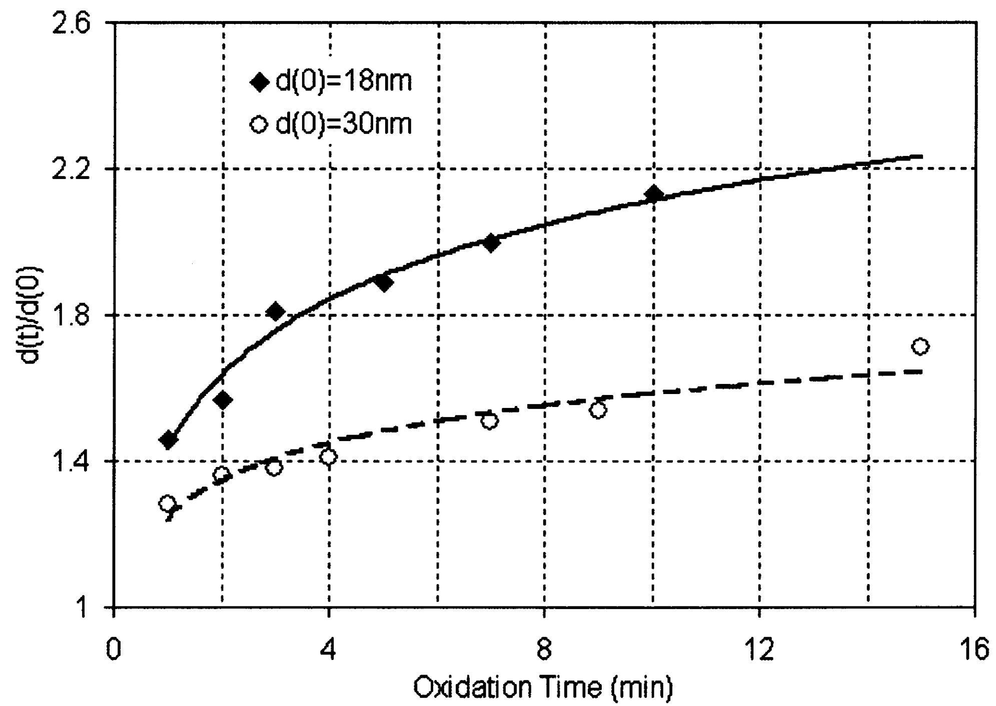

Figure 3.1 Thickness variation of vanadium films with oxidation time (oxidized in room atmosphere, T = 370 °C).

3.2 Semiconductor-to-Metal Phase Transition

The semiconductor-to-metal phase transition of the synthesized VO_2 films was detected by measuring its temperature-reflectance behavior. The experimental setup was shown in Figure 3.2. The light source was a 635.5 nm wavelength laser. The reflected or transmitted light was collected with a photodiode. The current of the photodiode was converted into voltage with a lock-in amplifier, which helps to suppress the noise. The laser was electrically chopped at frequency of 1 KHz. The photodiode was reverse-biased and parallel connected with a 1- MΩ resistor. The input impendence of the lock-in amplifier is 100 MΩ. The VO_2 film was heated with a resistive heater, whose temperature was controlled and logged with a computer. The temperature of the VO_2 samples were cycled between room temperature and above 85 °C. The varied output voltage from the lock-in amplifier was collected with a multimeter and recorded synchronously with the VO_2 temperature variation. The temperature-reflectance curve was constructed from those two sets of data. An aluminum mirror was used as a 100% reflectance reference. Table 3.2 listed the instruments used in this experimental setup.

Figure 3.3 (a) shows the measured hysteretic temperature-reflectance loop of one of the VO_2 samples in Table 3.1. It consists of a heat-up branch and a cool-down branch. If we define the phase transition temperature (T_c) as the point where the temperature-reflectance curve shows the largest slope, we get a T_c of about 65 °C [Figure 3.3 (b)]. Because there is no other vanadium oxide shows a phase transition in this temperature range, it confirms that the dominant composition for synthesized film is VO_2.

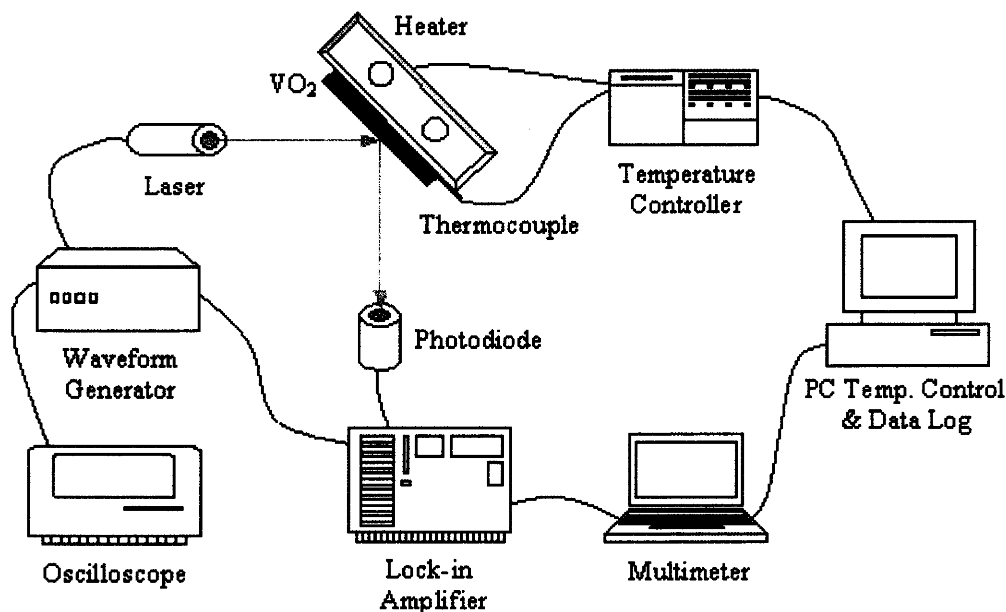

Figure 3.2 Experimental setup for testing the temperature-reflectance curve of VO_2 film.

Table 3.2 List of Instruments Used in above Setup

Instrument	Maker and Model
Waveform Generator	B+K Precision 3022 2MHz
Lock-in Amplifier	Princeton Applied Research 186A
Digital Multimeter	Agilent 34401A
Oscilloscope	Tektronix 2245 100MHz
Temperature Controller	Cole-Parmer Digi-Sense
Laser (λ = 635.5 nm)	Imatronic LDM115G/633/1
Photodiode	Perkin Elmer VT3085

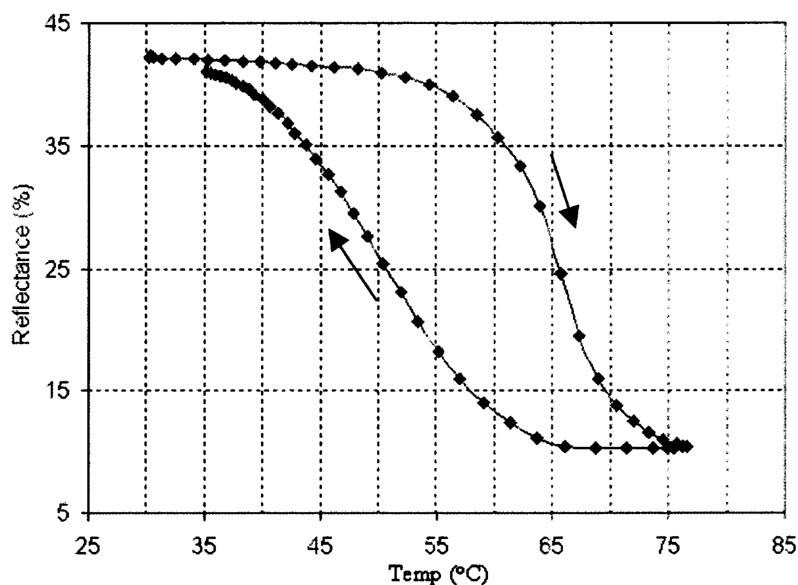

(a)

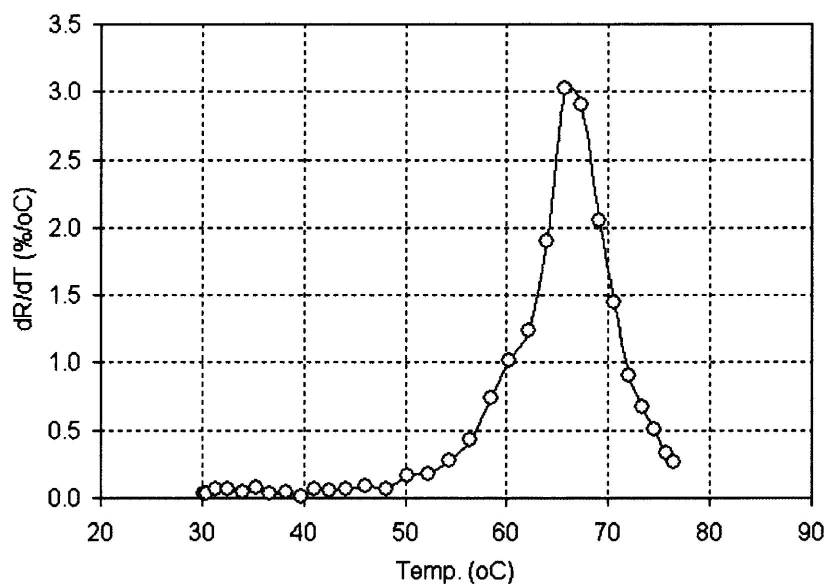

(b)

Figure 3.3 Temperature-reflectance curve of VO_2 film on vanadium substrate (a) and the phase transition temperature T_c (b). The starting vanadium thickness is 115 nm. The VO_2 film is obtained by oxidizing for 12 minutes at 390 °C in air on hot plate (wavelength = 635.5 nm).

3.3 Thermo-Optical Switching of VO_2 Thin Film

3.3.1 Theory of Multilayer Matrix Calculation [58]

If it was assumed that the optical contrast for VO_2 thin film at its phase transition comes solely from the variation of its refractive index, one can actually predict the magnitude of the thermo-optical switching with proper optical models. There have been many numerical methods and computer programs to predict the multi-layer thin film performance. In this section, the most popular method of matrix calculation was introduced.

An ideal multi-layer stack consists of a total m layers on a substrate that has a complex refractive index ($n_s - ik_s$). Each layer of the stack is represented with a physical thickness (t_m) and refractive index ($n_m - ik_m$). To derive the matrix formulation for the multi-layer stack, a simple structure with a thin parallel film on a substrate was firstly considered, as illustrated in Figure 3.4. Normal incidence radiation and optically homogeneous film were assumed. From electromagnetic field theory, the electric field vector (E_{m-1}) and magnetic field vector (H_{m-1}) at the incident boundary are related to the electric field vector (E_m) and magnetic field vector (H_m) at adjacent boundary by the product of the characteristic matrix per layer.

The tangential components of the electric field E and magnetic field H at the interface of m layer are:

$$\begin{aligned} E_m &= E_m^+ + E_m^- \\ H_m &= \eta_1 H_m^+ + \eta_1 H_m^- \end{aligned} \tag{3.1}$$

where symbol + denotes positive-going wave and symbol – means negative-going wave.

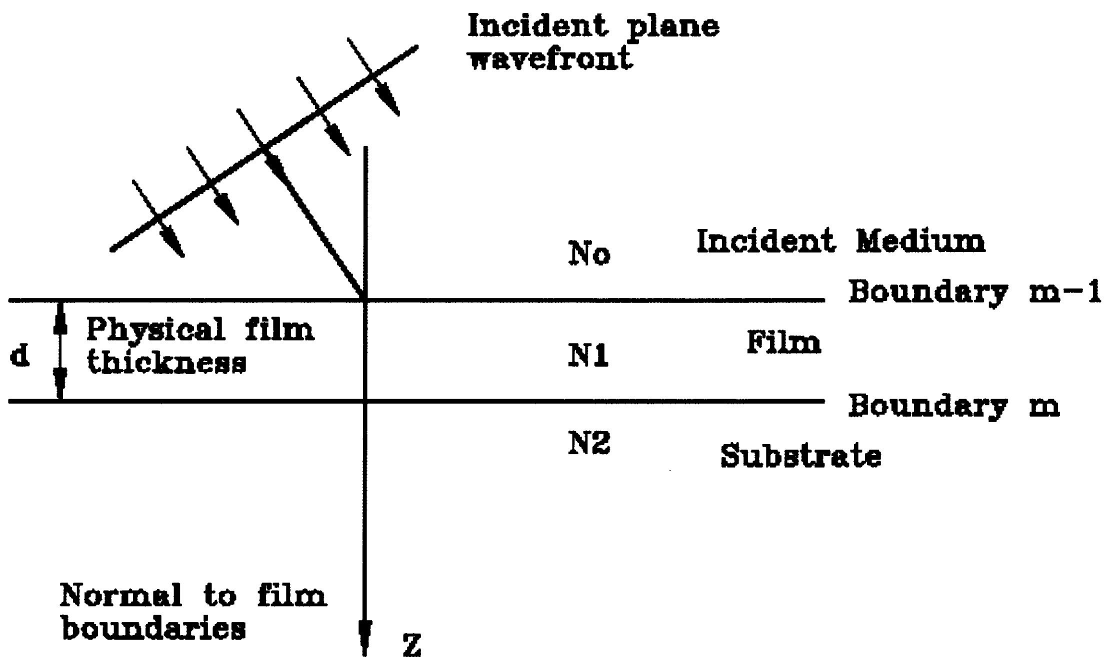

Figure 3.4 Plane wave incident on a single thin film.

The electric field and magnetic field are related by the tilted optical admittance as:

$$\eta_1 = \frac{H_1}{E_1} \tag{3.2}$$

Neglecting the common phase factors and with E_m and H_m represent the resultants, then:

$$\begin{aligned} E_m^+ &= \frac{1}{2}\left(H_m / \eta_1 + E_m \right) \\ E_m^- &= \frac{1}{2}\left(-H_m / \eta_1 + E_m \right) \\ H_m^+ &= \frac{1}{2}\left(H_m + \eta_1 E_m \right) \\ H_m^- &= \frac{1}{2}\left(H_m - \eta_1 E_m \right) \end{aligned} \tag{3.3}$$

The fields at the *m-1* interface at the same time instant and at a position with identical x and y coordinates are determined by multiplying with the phase factors of the waves to allow for a shift in the z direction from *0* to *-d* given by $e^{i\delta}$ and $e^{-i\delta}$ where:

$$\delta = 2\pi N_1 d \cdot \cos\theta_1 / \lambda \tag{3.4}$$

in which N_1 is the complex refractive index, λ is the wavelength, θ_1 may be complex.

The values of *E* and *H* at *m-1* interface are therefore given by:

$$\begin{aligned} E_{m-1}^+ &= \frac{1}{2}\left(H_m / \eta_1 + E_m \right) \cdot e^{i\delta} \\ E_{m-1}^- &= \frac{1}{2}\left(-H_m / \eta_1 + E_m \right) \cdot e^{-i\delta} \\ H_{m-1}^+ &= \frac{1}{2}\left(H_m + \eta_1 E_m \right) \cdot e^{i\delta} \\ H_{m-1}^- &= \frac{1}{2}\left(H_m - \eta_1 E_m \right) \cdot e^{-i\delta} \end{aligned} \tag{3.5}$$

With the trigonometric identities for $e^{ix} = \cos x + i\sin x$ and $e^{-ix} = \cos x - i\sin x$, so that:

$$E_{m-1} = E_{m-1}^{+} + E_{m-1}^{-} = E_m \cos\delta + H_m \frac{i\sin\delta}{\eta_1}$$
$$H_{m-1} = H_{m-1}^{+} + H_{m-1}^{-} = E_m \frac{i\sin\delta}{\eta_1} + H_m \cos\delta \tag{3.6}$$

Equation 3.6 can then be written in matrix notation as:

$$\begin{bmatrix} E_{m-1} \\ H_{m-1} \end{bmatrix} = \begin{bmatrix} \cos\delta & i\sin\delta/\eta_1 \\ i\eta_1 \sin\delta & \cos\delta \end{bmatrix} \begin{bmatrix} E_m \\ H_m \end{bmatrix} \tag{3.7}$$

The 2 × 2 matrix on the right side of above equation is known as the *characteristic matrix of the thin film.*

By normalizing Equation 3.7 over E_m, a matrix was obtained as:

$$\begin{bmatrix} B \\ C \end{bmatrix} = \begin{bmatrix} E_{m-1}/E_m \\ H_{m-1}/E_m \end{bmatrix} = \begin{bmatrix} \cos\delta & i\sin\delta/\eta_1 \\ i\eta_1 \sin\delta & \cos\delta \end{bmatrix} \begin{bmatrix} 1 \\ \eta_2 \end{bmatrix} \tag{3.8}$$

where B and C are normalized electrical and magnetic fields respectively. Above matrix is known as the *characteristic matrix of the assembly.*

If another layer of thin film was added on the top of *m-1* layer, the characteristic matrix of the new assembly can be obtained by analogy to Equation 3.8 as:

$$\begin{bmatrix} B \\ C \end{bmatrix} = \begin{bmatrix} \cos\delta_1 & i\sin\delta_1/\eta_1 \\ i\eta_1 \sin\delta_1 & \cos\delta_1 \end{bmatrix} \begin{bmatrix} \cos\delta_2 & i\sin\delta_2/\eta_2 \\ i\eta_2 \sin\delta_2 & \cos\delta_2 \end{bmatrix} \begin{bmatrix} 1 \\ \eta_3 \end{bmatrix} \tag{3.9}$$

And the results can be readily extended to the general case of a stack of q layers, where the characteristic matrix is simply the product of individual matrices taken in their sequential order and given by:

$$\begin{bmatrix} B \\ C \end{bmatrix} = \left\{ \prod_{m=1}^{q} \begin{bmatrix} \cos\delta_m & i\sin\delta_m/\eta_m \\ i\eta_1 \sin\delta_m & \cos\delta_m \end{bmatrix} \right\} \begin{bmatrix} 1 \\ \eta_s \end{bmatrix} \tag{3.10}$$

where m denotes for m^{th} layer and s for substrate or exit medium. Equation 3.10 is of prime significance in optical thin film work and forms basis for almost all calculations. The meanings of other symbols in above equation are as follows:

$$\delta_m = 2\pi N_m d_m \cos\theta_m / \lambda \tag{3.11}$$

and

$$\begin{aligned} \eta_m &= y N_m \cos\theta_m \quad \text{for s-polarization (TE)} \\ \eta_m &= y N_m / \cos\theta_m \quad \text{for p-polarization (TM)} \end{aligned} \tag{3.12}$$

and

$$\begin{aligned} \eta_s &= y N_s \cos\theta_s \quad \text{for s-polarization (TE)} \\ \eta_s &= y N_s / \cos\theta_s \quad \text{for p-polarization (TM)} \end{aligned} \tag{3.13}$$

where the admittance of free space is given by:

$$y = \sqrt{\varepsilon_0 / \mu_0} = 0.002654 \quad \Omega^{-1} \tag{3.14}$$

If the incidence angle θ_0 is given then the exit angle can be found by Snell's law, by:

$$N_0 \sin\theta_0 = N_m \sin\theta_m = N_s \sin\theta_s \tag{3.15}$$

Finally, the reflectance, transmittance, and absorptance are calculated as:

$$R_q = \left(\frac{\eta_0 B - C}{\eta_0 B + C} \right) \left(\frac{\eta_0 B - C}{\eta_0 B + C} \right)^* \tag{3.16}$$

and

$$T_q = \frac{4\eta_0 \operatorname{Re}(\eta_s)}{(\eta_0 B + C)(\eta_0 B + C)^*} \tag{3.17}$$

and

$$A_q = \frac{4\eta_0 \operatorname{Re}(BC^* - \eta_s)}{(\eta_0 B + C)(\eta_0 B + C)^*} \tag{3.18}$$

Based on this model, the thermo-optical switching spectra of VO_2 thin film can be calculated. The calculation was done with a thin film optic software Essential-Macleod^{TM}. The refractive index data of VO_2 were obtained from Ref. [6]. The simulation considered two variables, i.e. different substrate and the VO_2 thickness. The simulation results have revealed that both factors have significant effects on the thermo-optical switching.

3.3.2 Thermo-Optical Switching Spectra

The refractive index data for VO_2 were taken from Ref. [6]. Transmittance and reflectance spectra of VO_2 before and after the phase transition were simulated and compared with experimental results from both previous publications and measurements in this research. Figure 3.5 shows the simulation results of 614 nm VO_2 on sapphire substrate, compared with the measurement results by J. F. De Natale [7]. The simulation results agree well with the measurements. In Figure 3.6, another simulation of 120 nm VO_2 on glass substrate was shown comparing with the experimental results by [35]. It was noticed that the agreement between the simulation and measurement. Considering the fact that the VO_2 films in Ref. [7] and Ref. [35] were made by different methods, the agreement is reasonable. The conclusion is that the refractive index data in Ref. [6] can be used to predict the thermo-optical switching behavior of structure with VO_2.

The UV-Visible spectra of the VO_2 films fabricated by thermal oxidation in this research was measured and compared with the simulation results. Figure 3.7 shows the results for 35 nm and 200 nm VO_2 films. There are also good agreements between the simulation and experimental results. This gives us more confidence on the optical modeling and simulations.

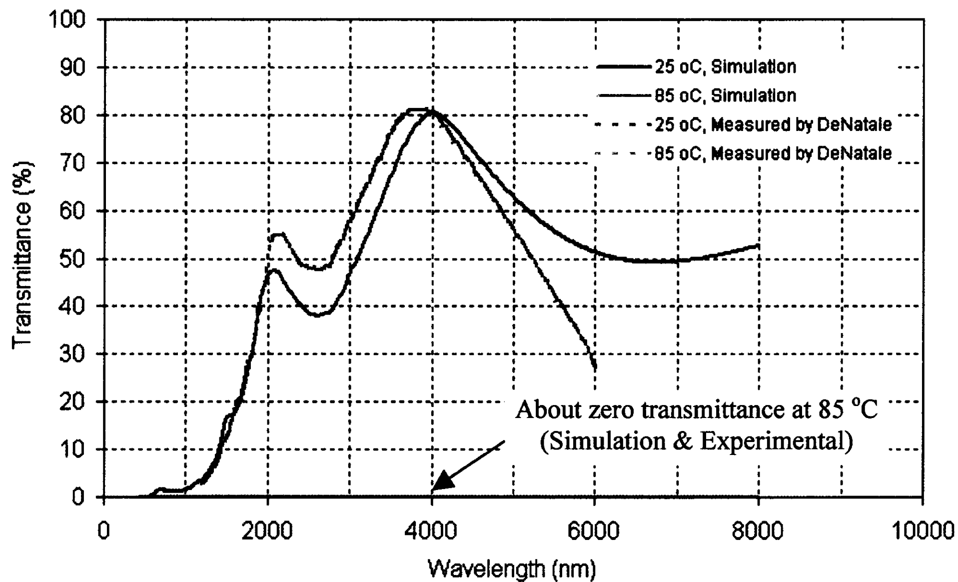

(a)

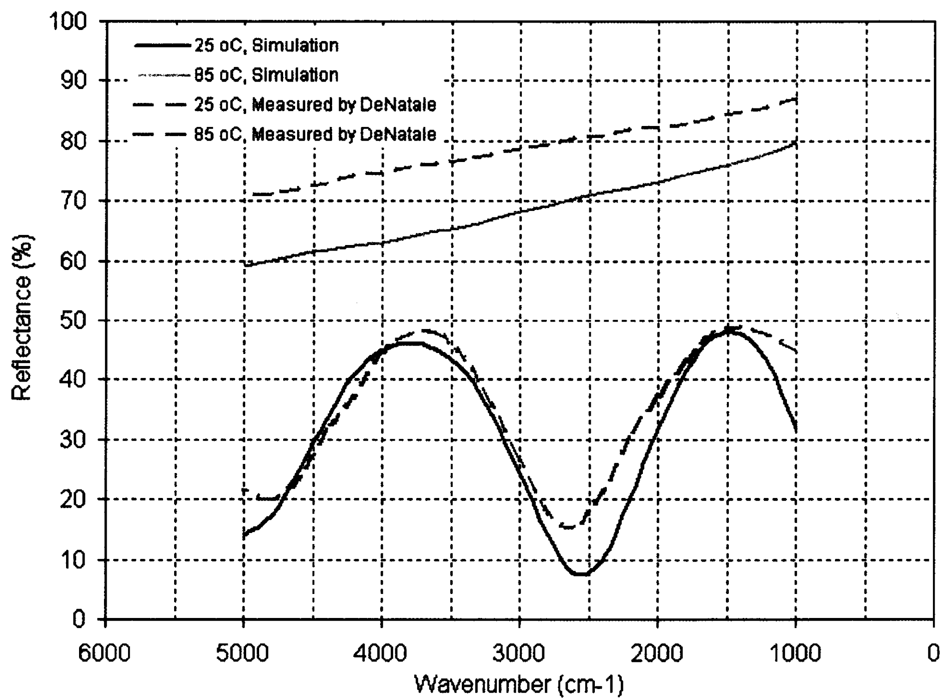

(b)

Figure 3.5 Simulated and measured infrared transmittance spectra (a) and reflectance spectra (b) for 614 nm VO_2 on sapphire [7].

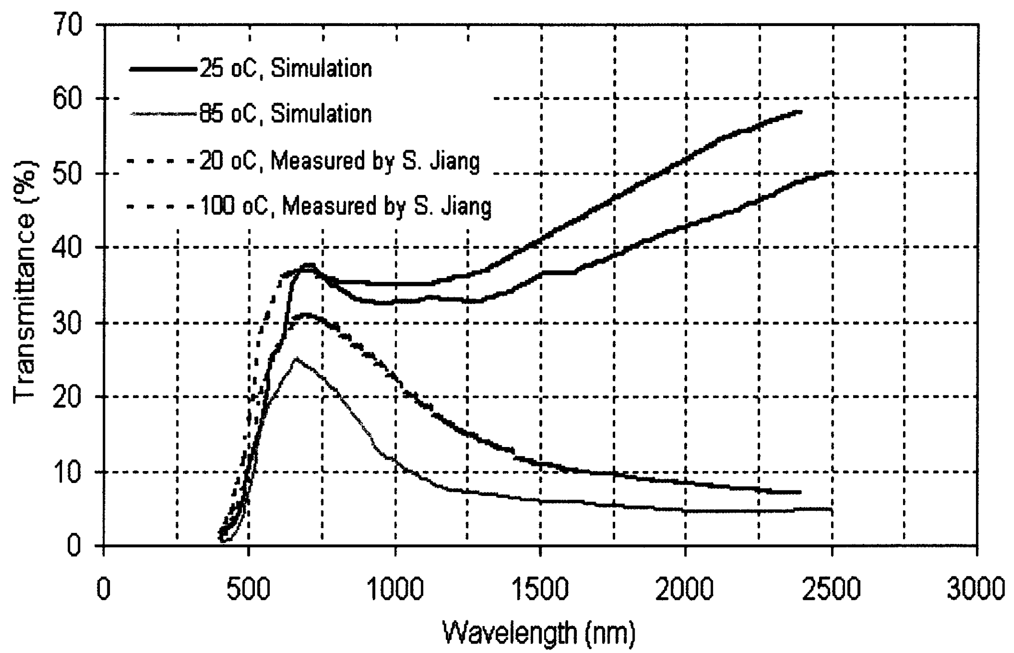

Figure 3.6 Simulated and measured transmittance spectra of 120 nm VO_2 on glass [35].

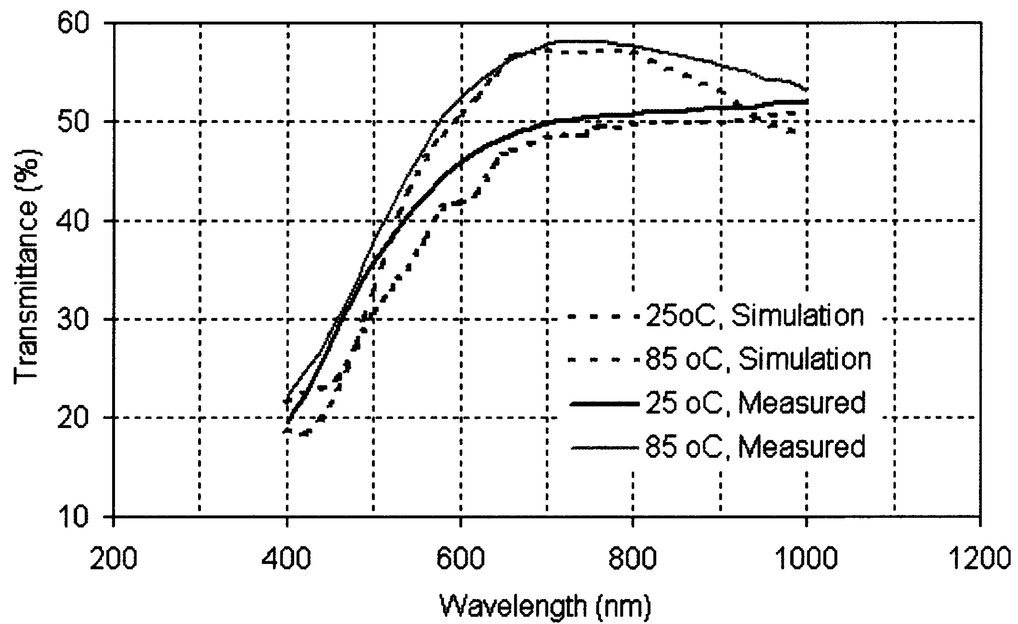

(a)

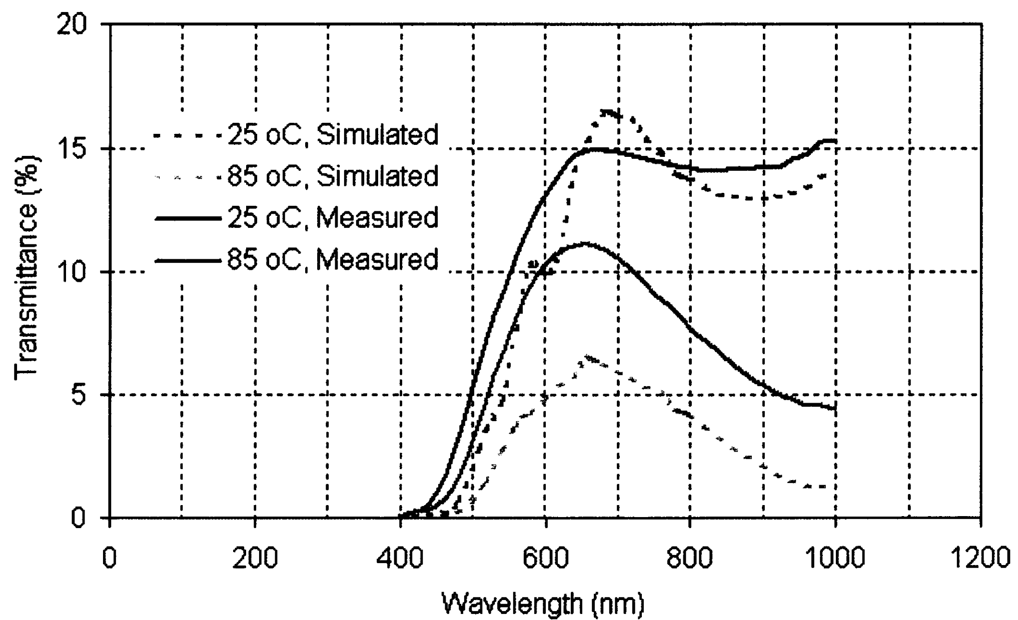

(b)

Figure 3.7 Comparison of the measured and simulated UV-Visible spectra of thermally oxidized VO_2 on borofloat glass (a) ~ 35 nm (b) ~ 200 nm.

3.3.3 Effects of VO_2 Thickness

It was well known that the thickness of the VO_2 film would have significant effects on its optical properties. To investigate the effect of film thickness and find out the thickness that gives maximum optical contrast, a series of VO_2 film with different thickness were made on by oxidizing for different time. The thicknesses of the films were measured by surface profilometer. Then the reflectance contrast before and after the phase transition were measured at 635.5 nm wavelength with the setup described in Section 3.2. Figure 3.9 shows the experimental results of VO_2 film on vanadium substrate, with comparison to the simulation results. From the results, the effect of the VO_2 thickness on its reflectance switching was noticed. There is a general agreement between the simulation and measurement. It seems that the measured reflectance is higher than the simulated reflectance. One reason for this is that we have used the reflectance of an aluminum mirror as 100% reflectance reference. However, we know that the actual reflectance from aluminum is only about 90%. The data in Figure 3.9 were before the correction. Another factor might be that the refractive index values from Ref. [6] didn't totally fit to the films made in this experiment. However, there was qualitative agreement between the simulation and measurements to acceptable degree.

The highest reflectance switching contrast was obtained from the VO_2 film that oxidized for 12 to 25 minutes at 390 °C. It was also noted here that for the VO_2 less than about 50 nm (corresponds to the first few minutes oxidizing) the high temperature phase has higher reflectance. With the increase of oxidation time, it enters the second period and the trend reverted. This also explains the periodic variation of the interference color during the oxidation.

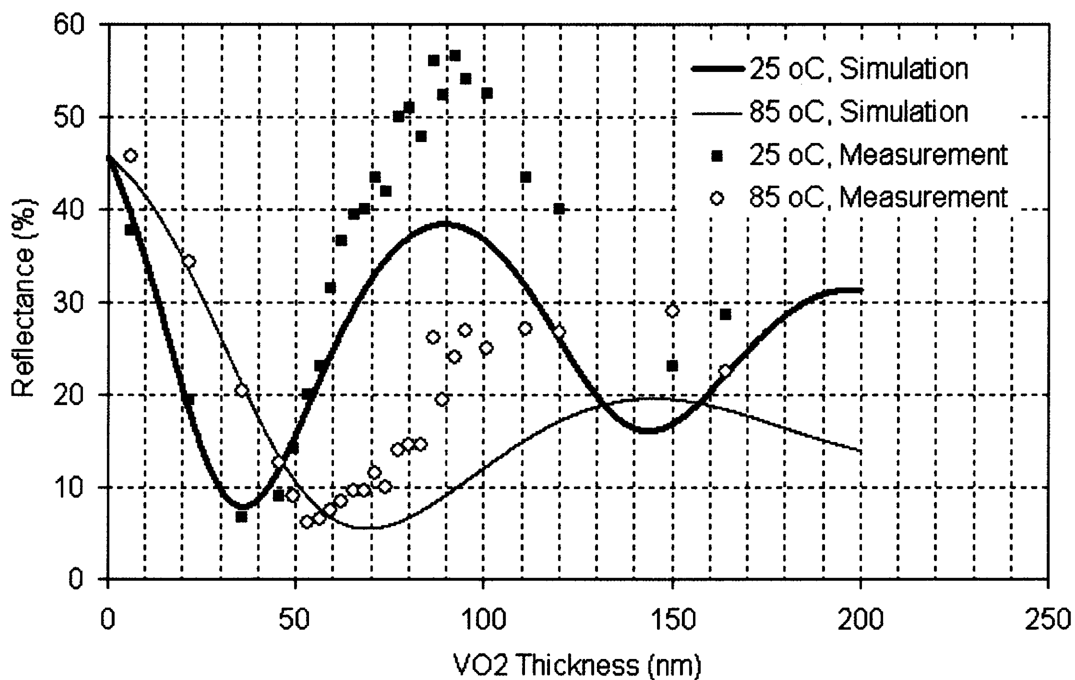

Figure 3.8 Evolution of the reflectance contrast of VO_2 film with thickness (wavelength = 635.5 nm). The VO_2 films are on vanadium substrate. The disagreement between the simulation and measurement may come from the refractive index data, which was taken from literature reference [6].

3.4 Microstructure Characterization

The surface microstructure of the VO_2 film was investigated by scanning electron microscope (SEM). It was observed that the film has a microstructure of disoriented, granular grains of 20 – 50 nm in size. It has been reported that the microstructure has significant effect on the optical switching of VO_2 [25]. It was believed that the sharpness of the switching is related to the degree of disorientation between the adjacent grains. In single crystal, the crystallographic matching at the grain boundaries allow the shear transformation front to propagate easily, which corresponds to a hysteresis width of less than 1 °C. In J. F. DeNatale's work, grain-oriented VO_2 film was produced and the hysteresis was only 2 – 4 °C, compared to the 10 –15 °C hysteresis generally observed for disoriented films [7]. E. E. Chain suggested that the large grain size could enhance the optical contrast of switching [25]. However, in this work, it was found that the optical contrast is primarily determined by the optical thickness of the VO_2 film.

Figure 3.9 to 3.11 illustrate the surface microstructures and the corresponding optical switching curves for VO_2 films oxidized at 390 °C for 2 minutes, 12 minutes and 25 minutes respectively. Obvious change of the grain size with the increase of the oxidation time was not observed. If the hysteresis width was taken as the temperature difference at the middle points of the heat-up and cool-down branches, the hysteresis width increases with the oxidation time. It was obvious that the enlargement of the hysteresis is not related to the grain size. However, it was observed that for the VO_2 film oxidized for 35 minutes, in certain areas of the film, the surface texture becomes oriented locally, as shown in Figure 3.12. As compared in Figure 3.13 (a), the hysteretic loop for the 35 minutes film becomes more asymmetrical than that of the 12 minutes film.

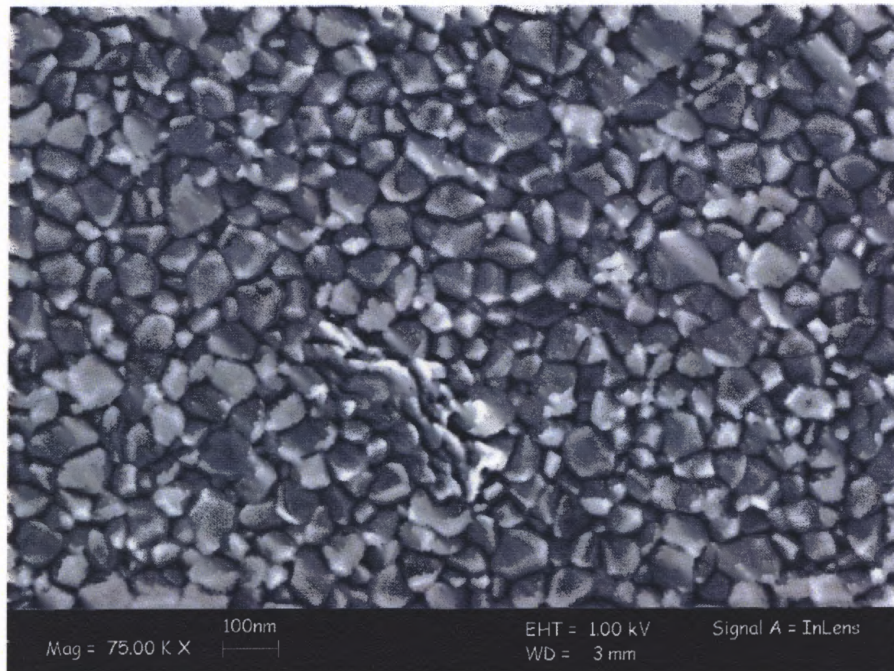

(a)

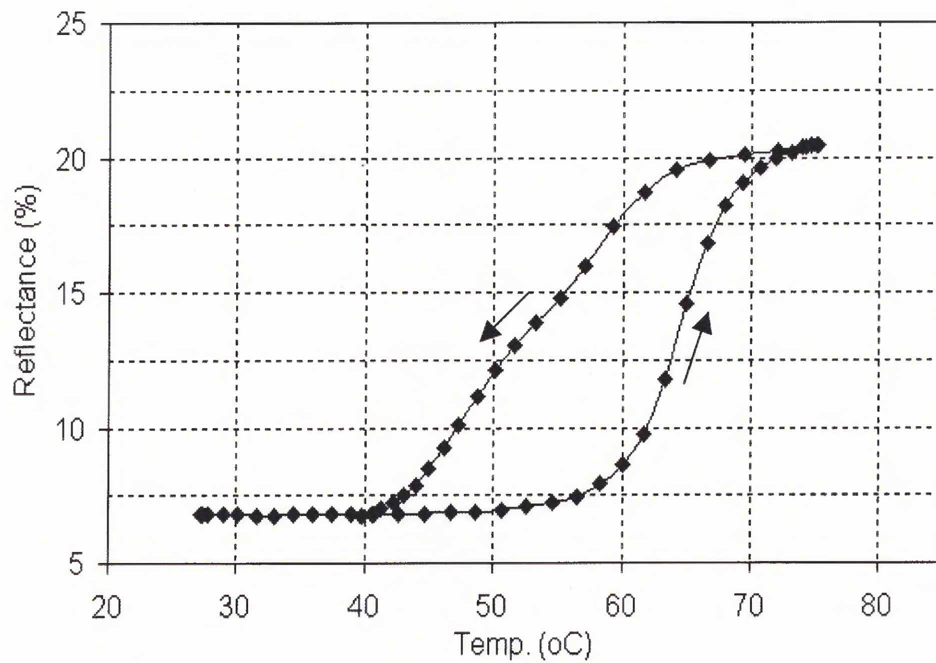

(b)

Figure 3.9 Surface grain microstructure and the temperature-reflectance curve of the VO_2 film by oxidizing 115 nm vanadium for 2 minutes at 390 °C (λ = 635.5 nm).

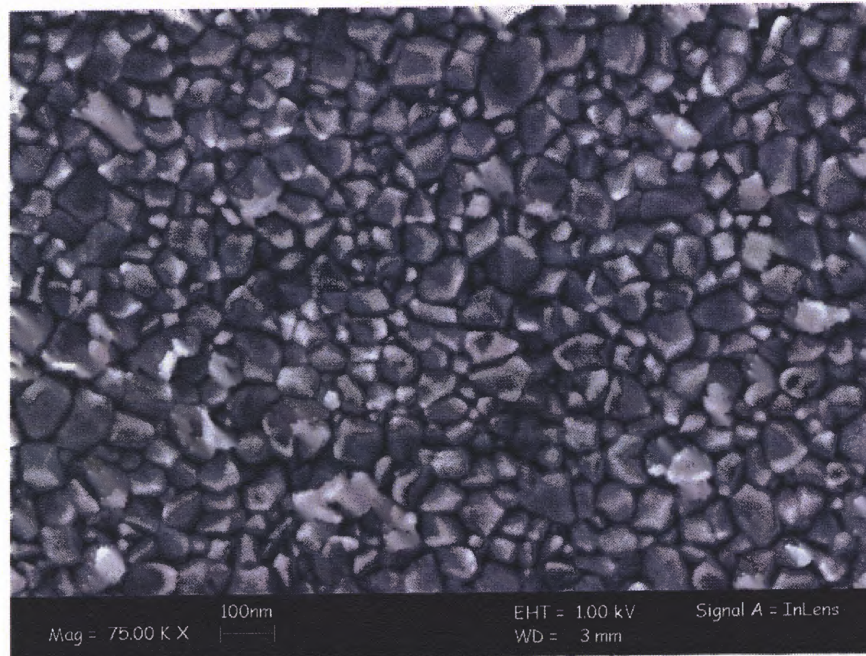

(a)

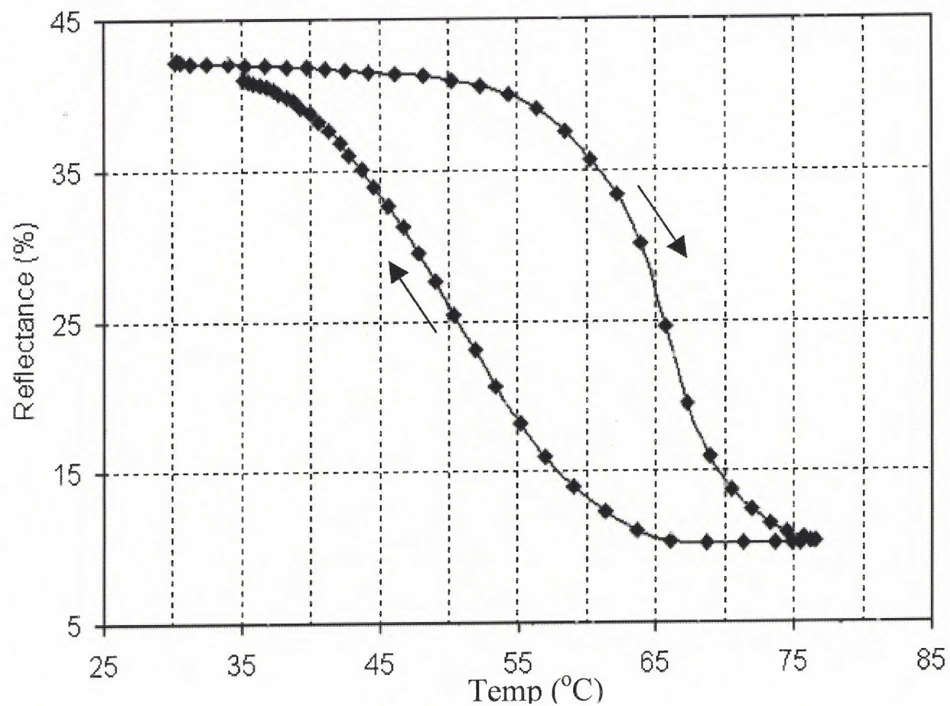

(b)

Figure 3.10 Surface grain microstructure and the temperature-reflectance curve of the VO_2 film by oxidizing 115 nm vanadium for 12 minutes at 390 °C (λ = 635.5 nm).

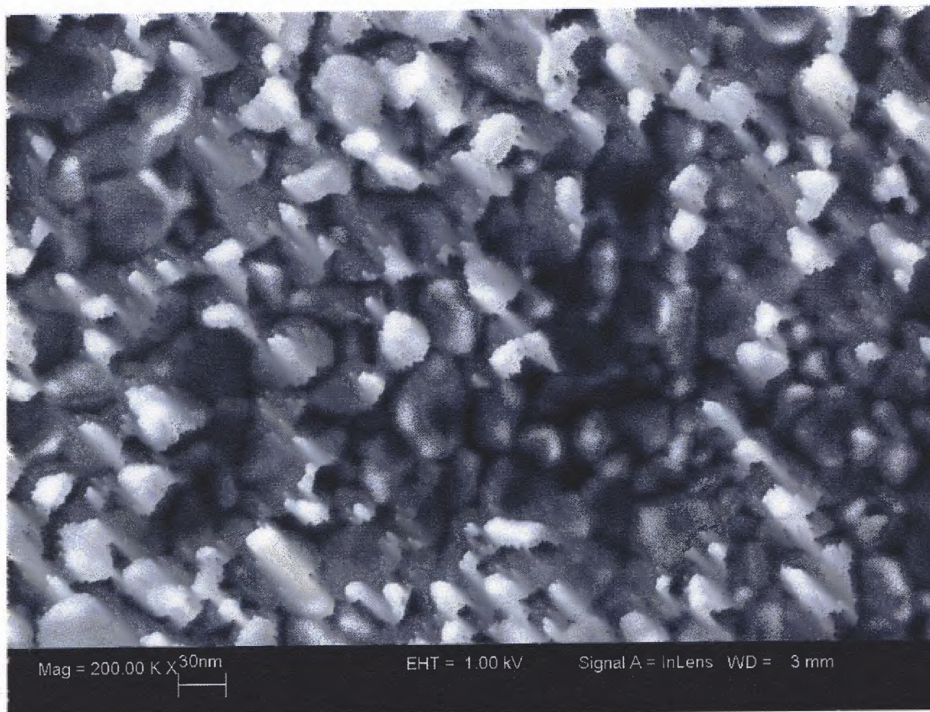

(a)

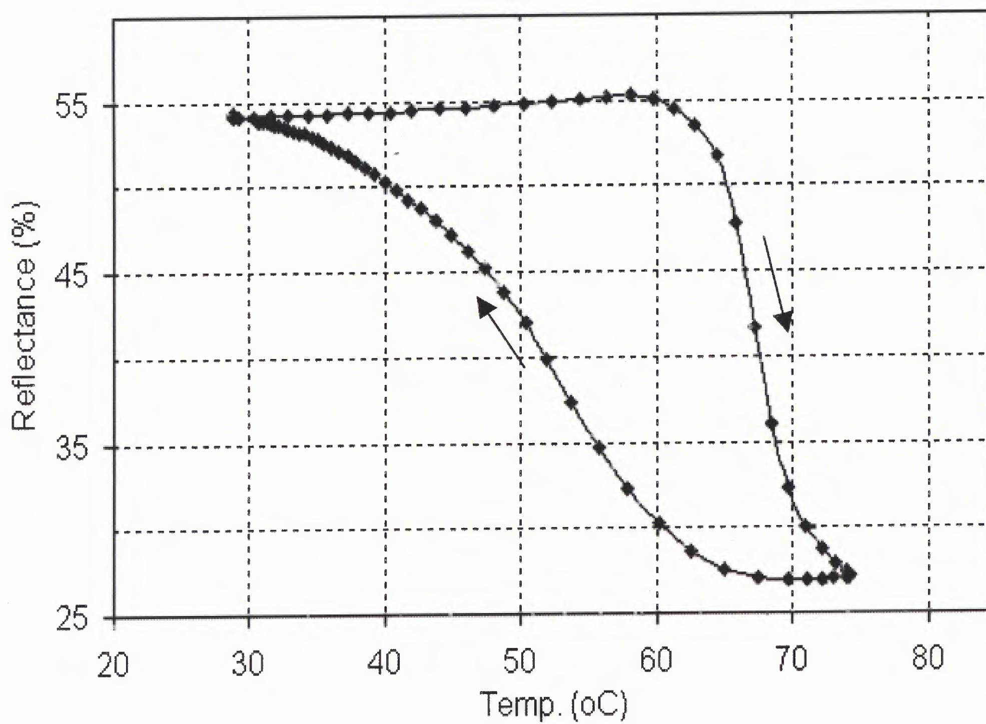

(b)

Figure 3.11 Surface grain microstructure and the temperature-reflectance curve of the VO_2 film by oxidizing 115 nm vanadium for 25 minutes at 390 °C (λ = 635.5 nm).

The evolution of the hysteresis loop from symmetrical for both branches to the asymmetrical hysteresis was also observed by W. Haidinger [59]. In his work, he observed symmetrical hysteresis for samples with (110) texture, and asymmetrical hysteresis for samples with an additional (210) texture. Because the different textures exhibit different hysteresis loops, the overlap of two textures will result in an asymmetrical hysteresis loop [Figure 3.13 (b)]. However, contradictory results have also been reported [60]. It seems that the grain orientation itself can't fully explain the broadening of the hysteresis.

In V. A. Klimov's work [61], he considered not only the difference in the grain size, but also the different degrees of oxygen nonstoichiometry in different grains. It was suggested that the presence of oxygen vacancies would lower the phase equilibrium temperature, which produces an asymmetrical cooling branch. In the thermal oxidation of vanadium into VO_2 film, a gradient of oxygen distribution over the film thickness was expected. This oxygen gradient will become significant with the increase of the oxidation time, because the oxygen need to diffuse through an increased vanadium oxide thickness to induce further oxidation. Consequently, the asymmetrical broadening of the hysteresis loop was tentatively attributed to the increased oxygen gradient in the film.

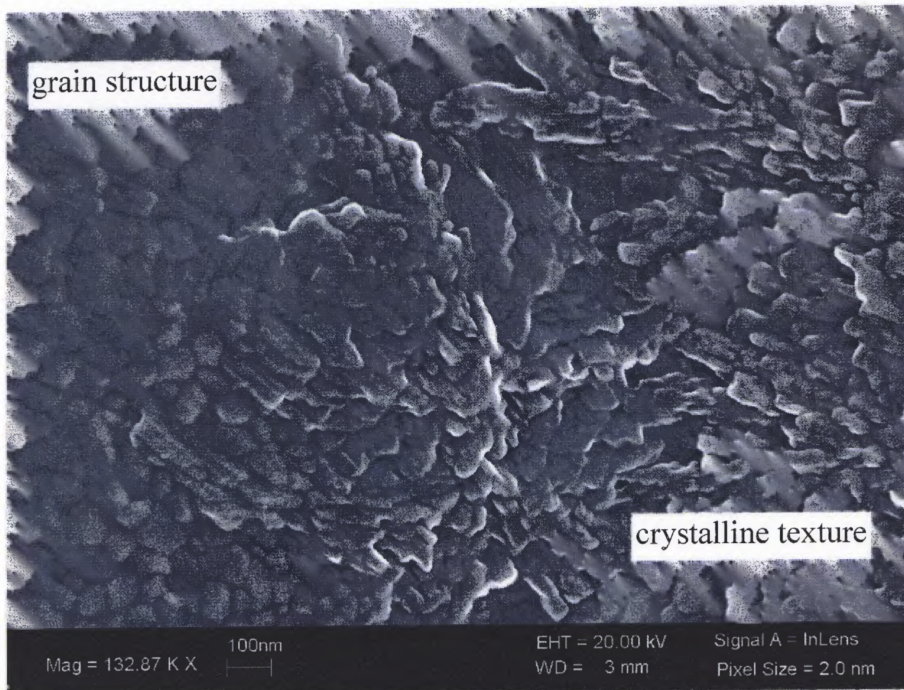

(a)

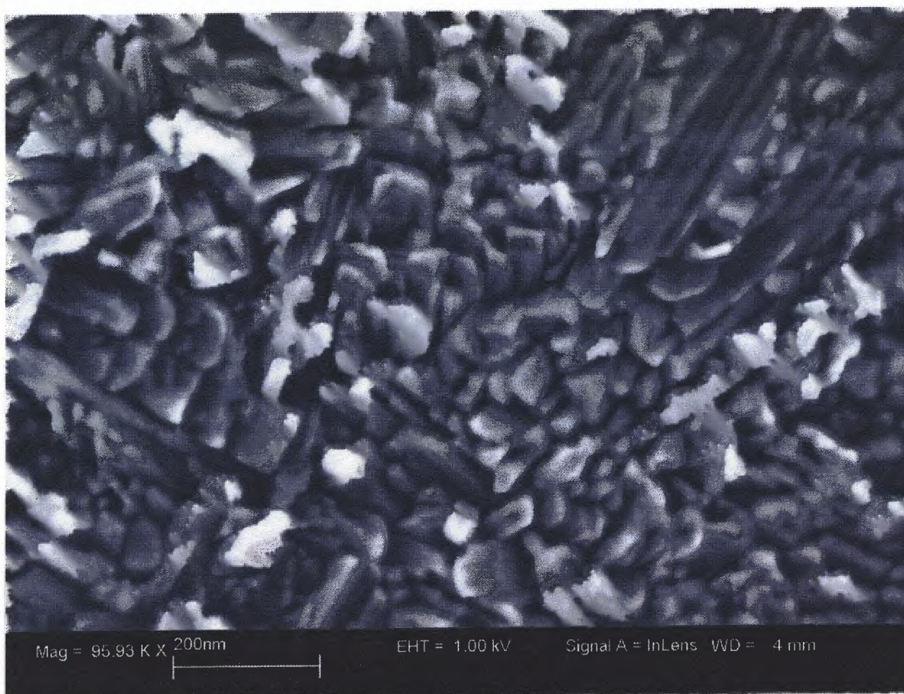

(b)

Figure 3.12 Evolution of the surface microstructure from columnar grains (a) to oriented crystalline texture (b) for 115 nm vanadium oxidized for 35 minutes.

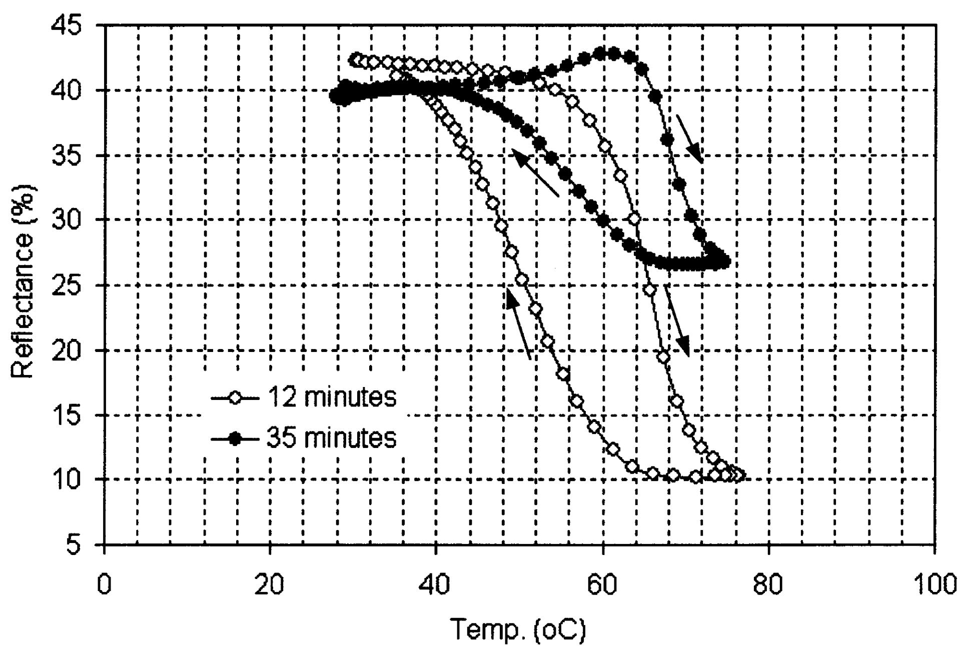

(a)

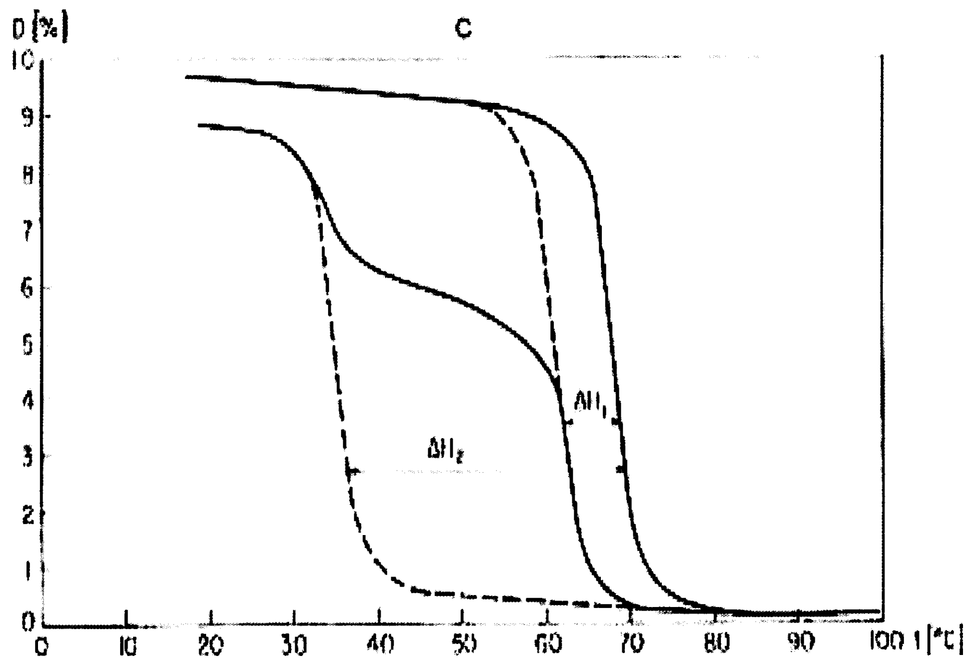

(b)

Figure 3.13 Asymmetrical hysteresis loop for VO_2 film with oriented textures compared with the columnar grain structure (a) and explanation with overlap of two hysteresis loops from differently oriented textures suggested by W. Haidinger [59].

3.5 Effect of the Hysteresis on Light Modulation

The hysteresis of the optical switching will have significant effects on the operation of the light modulator. Unfortunately, there are very few works have been done on this topic. Today, the most successful application of VO_2 is for the infrared bolometers. However, those bolometers operate outside of the transition loop to avoid the complicated operation within the transition. The primary concern is that when the temperature variation in the VO_2 film is less than the hysteresis width, the phase transition will follow a minor loop instead of the major loop. As will be shown, the minor loop has a reduced sensitivity.

Some works have been done to investigate the property of the minor loop of the electrical resistance switching [62-64]. Because both the electrical switching and the optical switching are phase transition related, it was expected that conclusions drawn on the electrical switching would be true for the optical switching also. L. A. Almeida has done the most works on the minor loop study of the VO_2 transition. He proposed to use the Preisach model to describe the hysteresis of VO_2 [62]. The Preisach model was originally proposed to describe the magnetic hysteresis. The simulation results by L. A. Almeida shown that the Preisach model can describe the VO_2 phase transition in terms of the major loop and minor loop over certain temperature range. The same author has reported that under low thermal cycling rate, the smooth and monotonic minor hysteresis loop is unstable and unpredictable [63]. If this conclusion also holds true for the optical switching, it will make the operation of the light modulator at small signal conditions very complicated.

In this research, the minor loop property of the VO_2 optical switching was studied. Figure 3.14 (a) shows a hysteretic reflectance versus temperature curve, which consists of

a major loop from the full phase transition and several minor loops from partial temperature sweepings. The corresponding temperature variation is shown in Figure 3.14 (b). It was noted that when the magnitude of the temperature sweeping becomes less than the hysteresis width, the optical contrast degrades drastically. If we use the slope of the heat-up branch curve (dR/dT) as the indication of the optical modulation efficiency and plot it against the corresponding magnitude of temperature sweeping, we get Figure 3.15. It reveals how the optical contrast degrades with the decreasing of the temperature sweeping magnitude.

The repeatability of the optical switching was also studied when the VO_2 operates under minor loop. The temperature was swept between 50 °C to 60 °C. The actual temperature shows some overshoot because of the mechanism of the PID controller [Figure 3.16 (a)]. The resulted optical switching curve is shown in Figure 3.16 (b). It is noted that although the magnitude of the switching keeps almost constant, the absolute values for the metal phase and semiconductor phase drift. This means that the VO_2 light modulator cannot be switched between any two arbitrary temperature points. This observation agrees with de Almeida's work on the electrical switching [63]. It was explained by the self-organization of the internal film microstructure. It was suggested that the grain boundaries and domains in the VO_2 film are mobile during the phase transition. However, this is possible that the drift comes from the thermal lag between the film temperature and the measured heater temperature. Further investigation will be helpful.

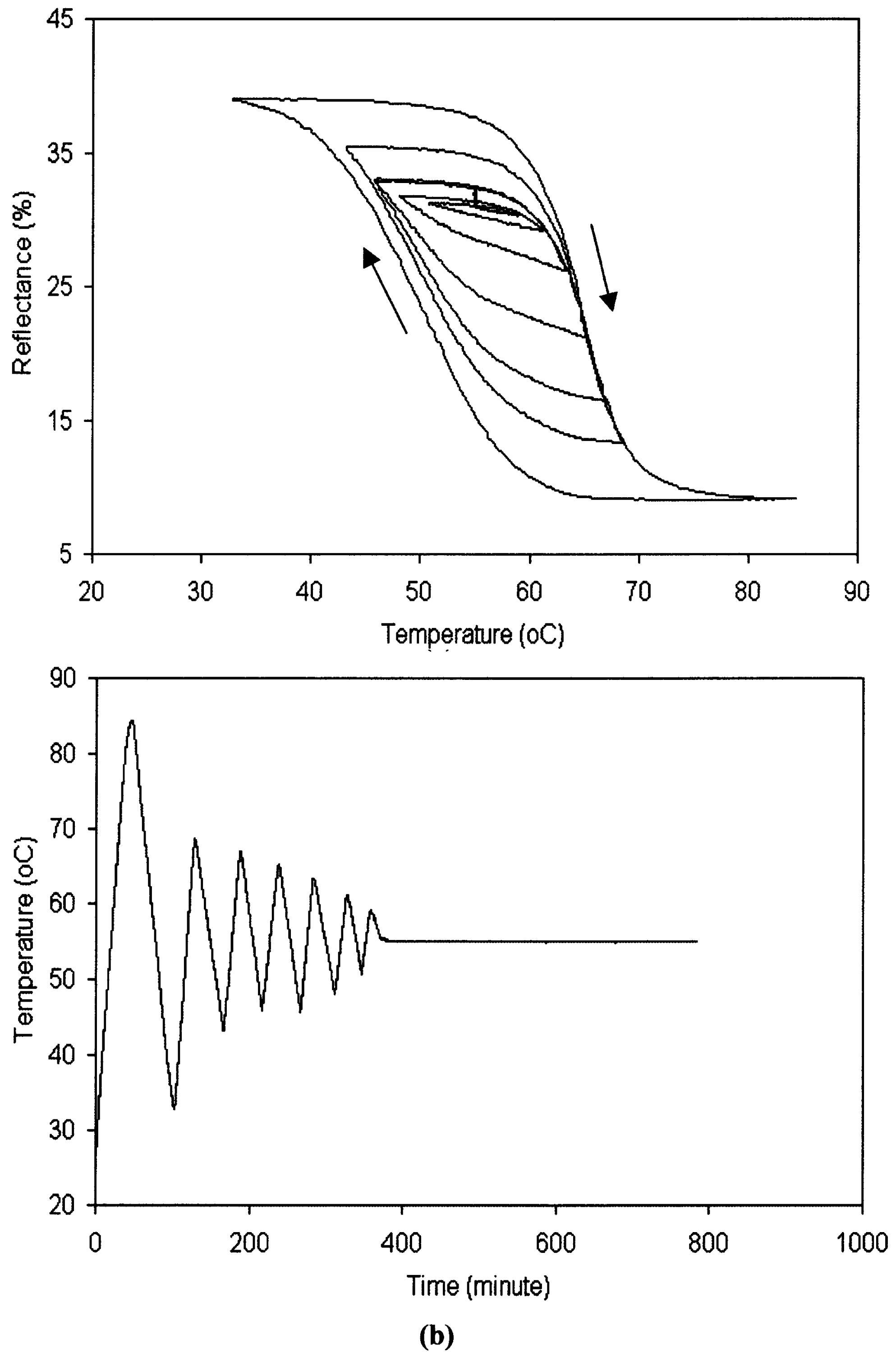

Figure 3.14 Measured minor-loops of VO_2 film (a) when it was swept with temperature excursion less than the hysteresis width (b). The film was obtained by oxidizing 115 nm vanadium at 390 °C for 12 minutes. (λ = 635.5 nm).

To operate the VO_2 light modulator in small signal, it is necessary to ensure that the film is completely brought back to semiconductor state each time. Then, when the VO_2 is heated up, it will follow the major loop, as shown in Figure 3.17. We have monitored the stability of the VO_2 reflectance at fixed temperature point. As shown in Figure 3.18, the reflectance keeps constant over long enough time. It proves that the VO_2 light modulator can operate consistently.

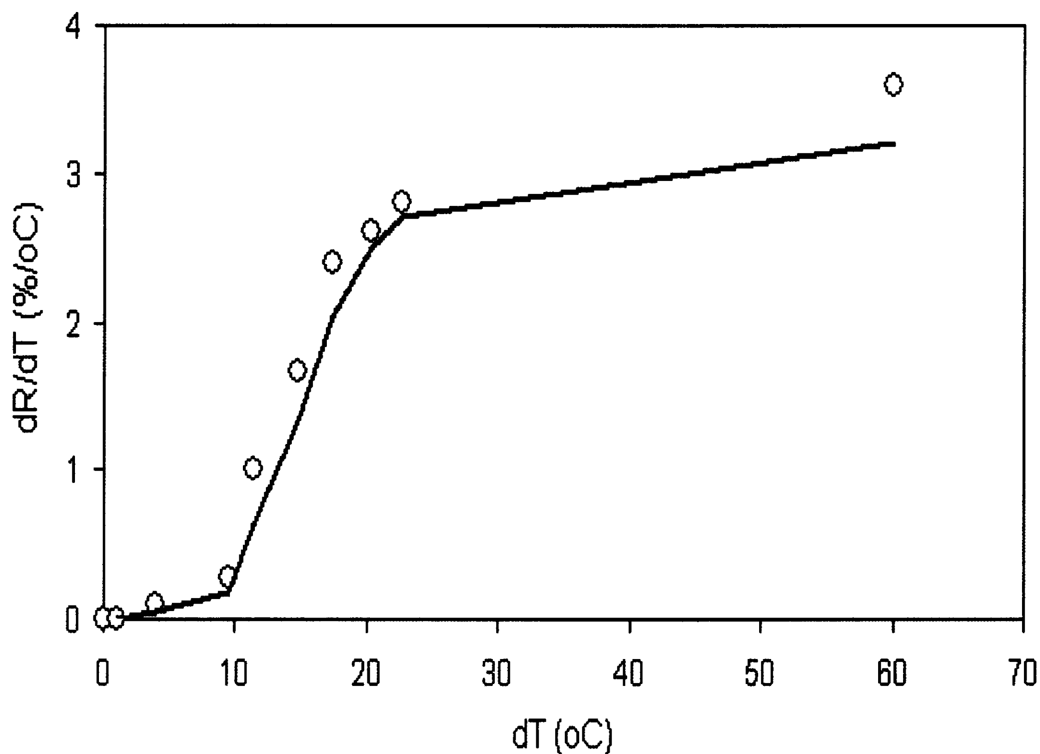

Figure 3.15 Decreasing of the slope of the reflectance-temperature curve at the heat-up branch with the decrease of the temperature-sweeping excursion. The VO_2 film is obtained by oxidizing 115 nm vanadium at 390 °C for 12 minutes. (λ = 635.5 nm).

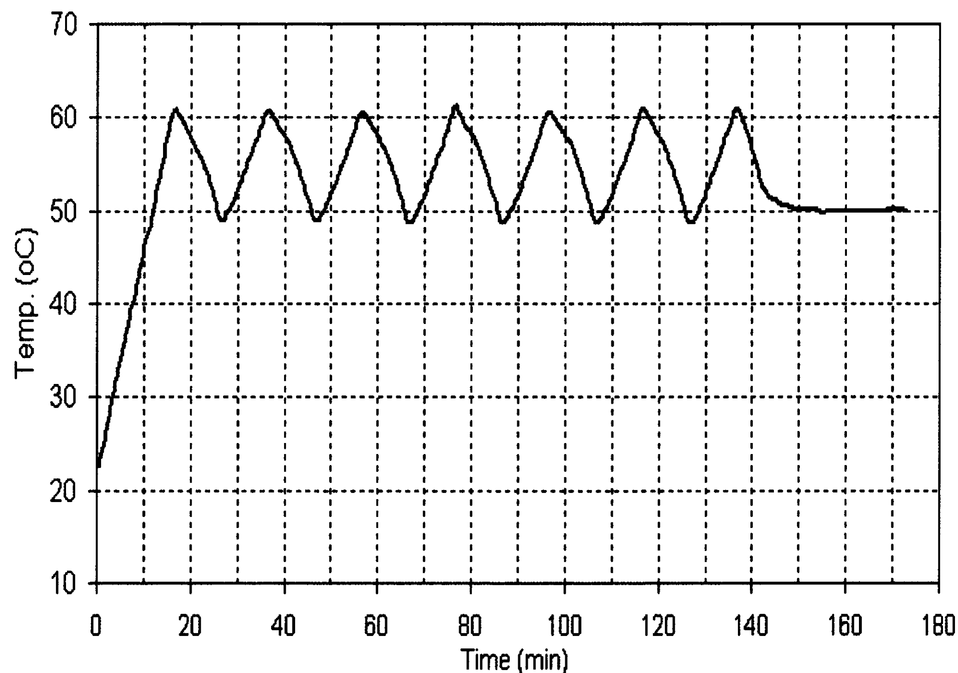

(a)

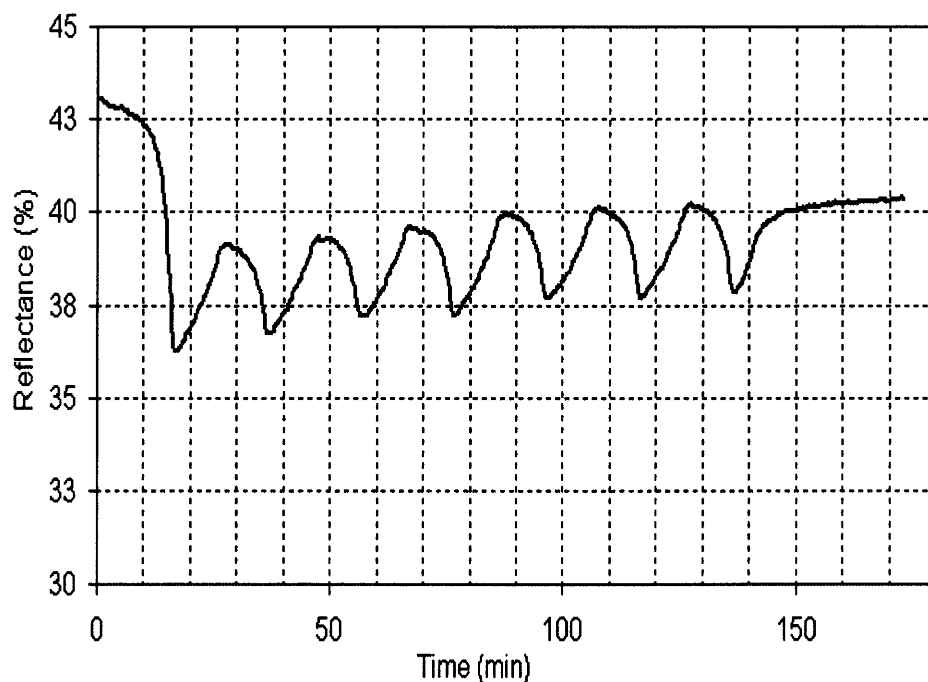

(b)

Figure 3.16 Recorded temperature variation (a) and the corresponding reflectance variation of the VO_2 thin film for small-signal operation testing. The VO_2 film is obtained by oxidizing 115 nm vanadium at 390 °C for 12 minutes. (λ = 635.5 nm).

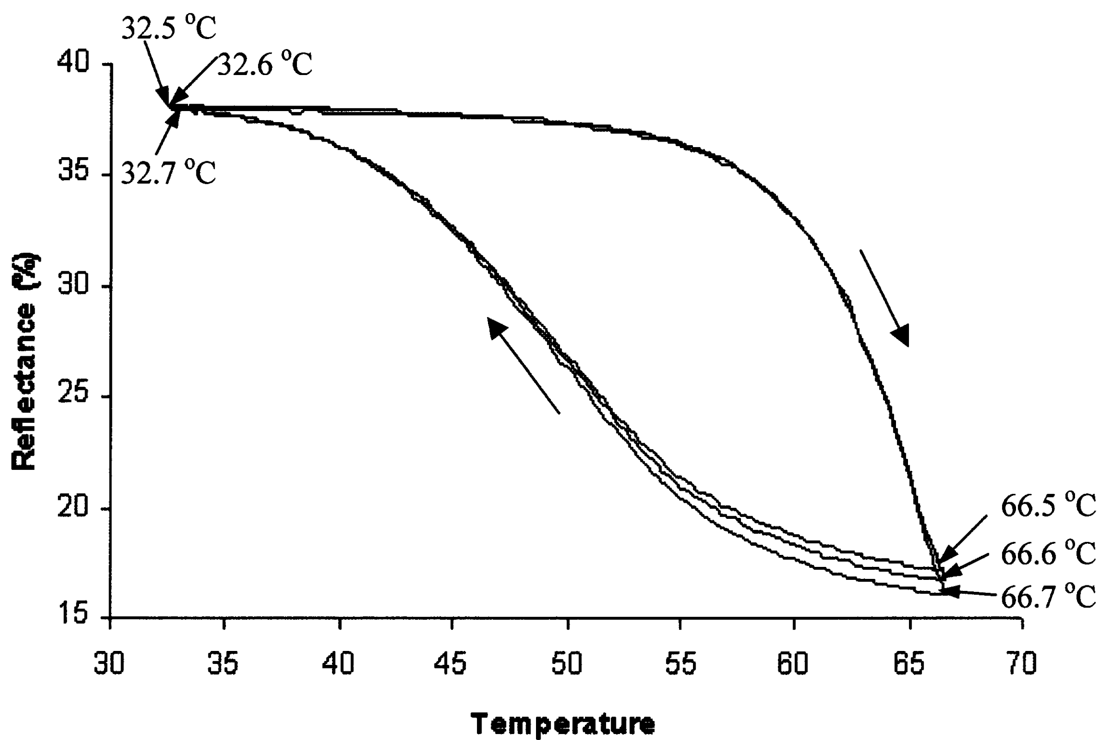

Figure 3.17 Experimental result that shows the reflectance-switching curve following same loop when the VO_2 film is cooled down to full semiconductor state. The VO_2 film is obtained by oxidizing 115 nm vanadium at 390 °C for 11 minutes (λ = 635.5 nm).

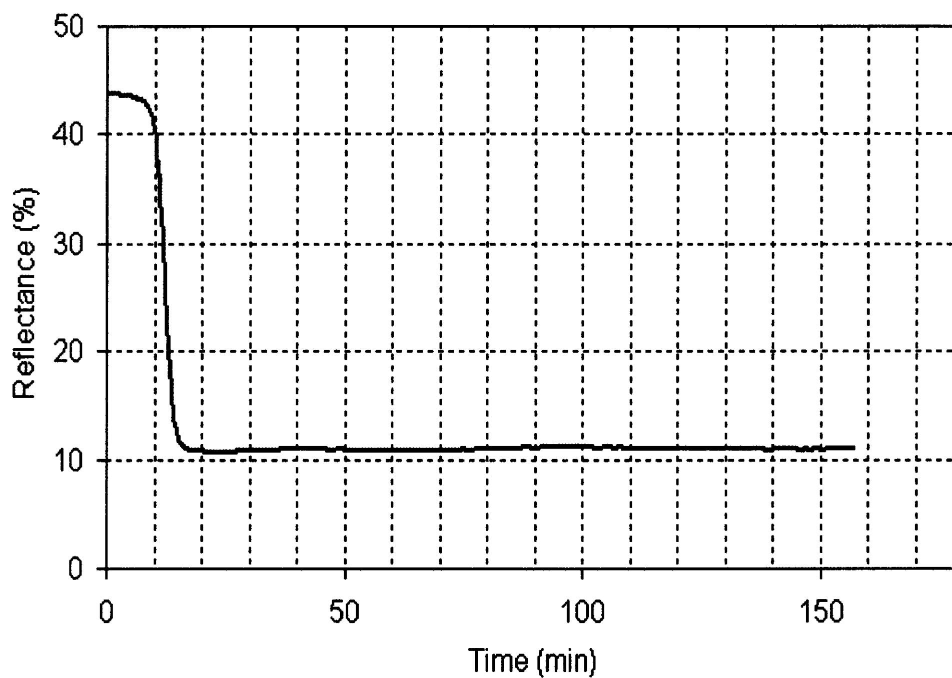

(a)

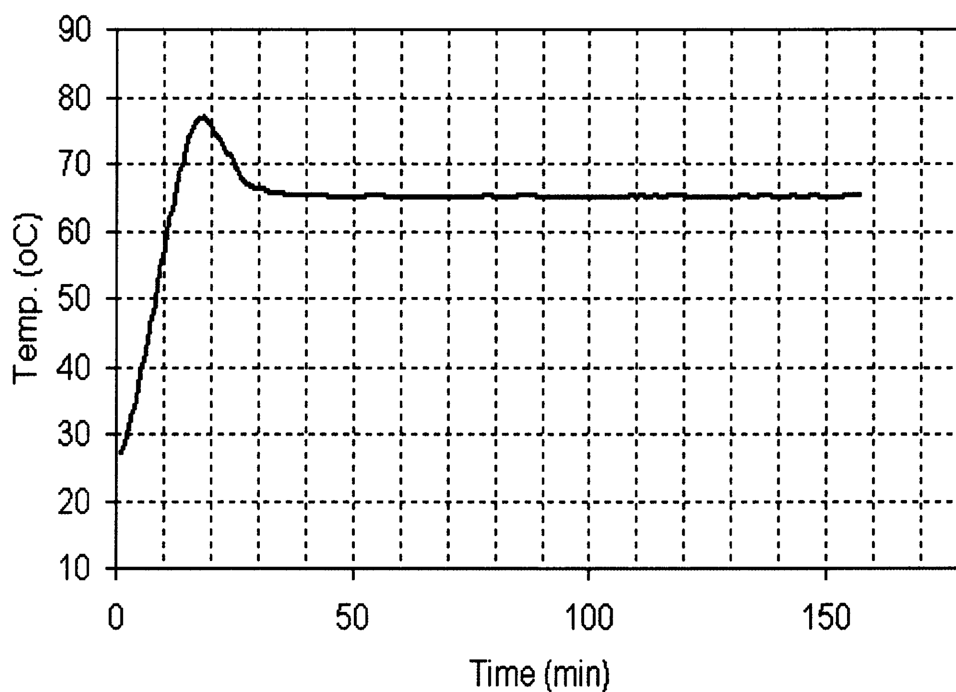

(b)

Figure 3.18 Measured reflectance of VO_2 film (a) when the film is held constantly at the phase transition temperature of 65 °C (b). The VO_2 film is obtained by oxidizing 115 nm vanadium at 390 °C for 11 minutes (λ = 635.5 nm).

CHAPTER 4

DESIGN AND MODELING OF VO_2 LIGHT MODULATOR

4.1 Thermal Modeling

4.1.1 Thermal Isolation Pixel Structure

The thermo-optical light modulator is a two-dimensional array that contains thousands of thermal isolated pixels. The thermal isolation is significant because of the need to reduce the cross talk between pixels. A schematic of the pixel design has been shown in Figure 1.6 and was repeated here in Figure 4.1 (a). It is a bridge-like thin film structure that suspended with long and narrow beams. This structure is typically found in thermal detector or gas sensor design where thermal isolation is important. Material with low thermal conductance is selected to fabricate the pixel and beams. The thermal mass of the pixel needs to be minimized to compensate the high thermal isolation to ensure fast enough thermal time constant. A good thermal isolation also helps to reduce the power consumption.

The thermal isolation pixel can be modeled with a lumped thermal circuit, as shown in Figure 4.1 (b) [65]. The heat capacity or thermal mass of the platform is modeled as an lumped capacitor. Its value is given by:

$$C = V \cdot \rho \cdot c \quad \text{(J/K)} \tag{4.1}$$

where V is the volume of the pixel, ρ is the density and c is the specific heat of the pixel material.

The thermal conductance consists of three independent parts, including the heat conductance through the supporting beams (G_{beam}), the conductance by the ambient (G_{air}),

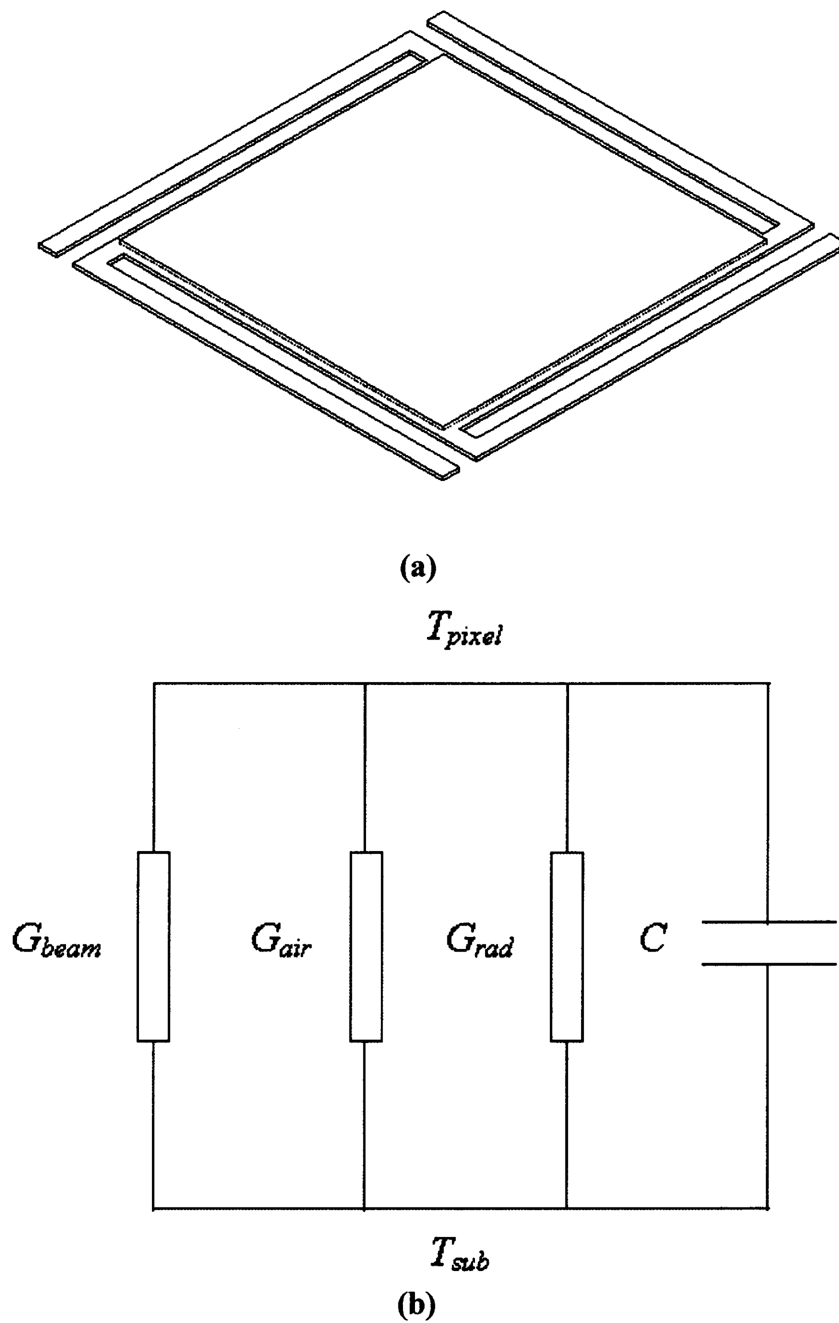

Figure 4.1 Schematic drawing of the light modulator pixel structure (a) and its equivalent lumped circuit model (b).

and the radiation from the pixel surface (G_{rad}). The total thermal conductance is the sum of the three parallel lumped conductance components:

$$G = G_{beam} + G_{air} + G_{rad} \qquad \text{(W/K)} \qquad (4.2)$$

The P represents the thermal source, which can be from resistive heater or radiation source. The power consumption is determined by the thermal resistance and the temperature change needed for certain optical contrast:

$$P = \Delta T_{VO2} \cdot G \qquad \text{(W)} \qquad (4.3)$$

To achieve full scale modulation, the VO_2 film needs to be fully swept through its major hysteresis loop. The ΔT_{VO2} is determined by the intrinsic property of VO_2 and assumed as a constant here. To reduce the power consumption, the thermal conductance of the pixel needs to be minimized.

It was shown that the VO_2 film could switch at speed less than 1 ns. So the modulation speed of the VO_2 light modulator is determined by the thermal time constant (τ) of the platform, which is given by:

$$\tau = \frac{C}{G} \qquad \text{(s)} \qquad (4.4)$$

To achieve high modulation speed, the thermal mass needs to be decrease while the thermal conductance needs to be increase. There is trade-off for the conductance value between the power efficiency and the thermal response time requirements.

4.1.2 Thermal Conductance Analysis

In this section, a theoretical analysis of the thermal conductance of the light modulator pixel was provided. The radiation conductance is the ultimate low limit for the thermal isolation pixel as above and can be calculated as [65]:

$$G_{rad} = 4\sigma\varepsilon_e A_{pixel} \cdot T^3 \qquad \text{(W/K)} \qquad (4.5)$$

where σ is the Stefan-Boltzmann's constant, ε_e is the effective emissivity, A_{pixel} is the surface area of the pixel, T is the absolute temperature of the pixel.

The conductance by the ambient constitutes of both conductance and convection. The light modulator will operate in vacuum package, so the gas convection is neglected. The ambient heat conduction is expressed as:

$$G_{air} = \lambda_{air} \frac{A_{pixel}}{d} \qquad \text{(W/K)} \qquad (4.6)$$

where the λ_{air} is the thermal conductivity of the air and d is the space between the pixel and substrate. The thermal conductivity of the air can be written as:

$$\lambda_{air} = \frac{nvcl}{3} \qquad \text{(W/K·m)} \qquad (4.7)$$

where n is the number of molecules per unit volume, v is the average speed, l is the mean-free path of the molecules. Vacuum packaging can also effectively reduce the conductivity of the air.

The thermal conductance by the beams is determined by the pixel dimension and the thermal conductivity of the beam material. It can be calculated as:

$$G_{beam} = 4\lambda_{SiO2} \frac{A_{beam}}{l_{beam}} \qquad \text{(W/K)} \qquad (4.8)$$

where λ_{SiO2} is the thermal conductivity of the SiO_2 beam material, A_{beam} and l_{beam} are the area and length of the beam respectively. The number of 4 is the number of beams used for the pixel. Silicon dioxide is used because of its low thermal conductivity. To minimize the G_{beam}, long and narrow beam needs to be fabricated. For pixels that use resistive heater, the thermal conductance of the beam will be higher because of the high thermal conductivity of the electrical connection through the beam. Typically the thermal conductance of the beams dominates the overall thermal conductance of the pixel.

Insert the Equations of 4.5, 4.6, and 4.8 into Equation 4.2, the expression for the total thermal conductance of the bridge platform was obtained as:

$$
\begin{aligned}
G &= G_{beam} + G_{air} + G_{rad} \\
&= 4\lambda_{SiO2}\frac{A_{beam}}{l_{beam}} + \lambda_{air}\frac{A_{pixel}}{d} + 4\sigma\varepsilon_e A_{pixel}T^3
\end{aligned} \tag{4.9}
$$

If the light modulator is vacuum packaged, the thermal conductance by the suspension beams will be much larger than the other two components. If the heat exchanges by the means of the air convection and surface radiation were neglected, the power consumption can be expressed as:

$$P = \Delta T_{VO2} \cdot G = \Delta T_{VO2} \cdot 4\lambda_{SiO2}\frac{A_{beam}}{l_{beam}} \tag{4.10}$$

and the thermal time constant:

$$\tau = \frac{C}{G} = \frac{C \cdot l_{beam}}{4\lambda_{SiO2}A_{beam}} \tag{4.11}$$

The above two equations will serve as the guidance in the designing of the thermal isolation pixel structures.

4.1.3 Thermal Finite Element Simulation

In this section, the thermal properties of the pixels were simulated by finite element methods (FEM). The simulation was carried out with ANSYS 6.1 program. Firstly, only the silicon oxide platform without the VO_2 layer was considered because of the lack of data on the VO_2 thermal properties. The addition of a VO_2 layer will only increase the thermal mass because the thermal conductance is determined solely by the SiO_2 beams. A 3-D solid model was created in ANSYS using the geometry dimensions and the material properties listed in Table 4.1. The model was meshed with 8-node thermal brick elements. First, a steady-state simulation is performed. It was assumed that the end of the beam close to the anchor is at constant temperature. A heat flux is applied on the pixel, which corresponds to a thermal power input. The temperature increases under different heat flux were shown in Figure 4.2. From the steady-state simulation, a thermal conductance of 1.21 uW/K was obtained, comparing to the 1.13 uW/K by analytical calculation.

Based on the steady-state simulation, a transient thermal simulation was carried out to characterize the thermal time constant of the pixel. The simulation result is shown in Figure 4.3. It takes about 250 ms for the pixel to reach final thermal balance, which gives a thermal time constant of 50 ms. Considering the thermal mass of the VO_2 film, a larger thermal time constant is expected. However, in the final design we will add heating resistor in each pixel, which will increase the thermal conductance by at least one-order. So the estimated thermal time constant is less than 5 ms for pixels with integrated heater. Table 4.2 summarizes the thermal properties of the pixel from both theoretical calculation and FEM simulations. The results agree with each other very well.

Table 4.1 Geometrical Dimension and Material Properties of the Pixel

Parameter	Unit	Large
Pixel Area	um	75
Beam length	um	80.5
Beam width	um	5
Thickness	um	0.4
Number of beams	-	4
Thermal conductivity	W/m.°C	1.2
Heat capacity	J/kg.°C	800
Density	Kg/m^3	2360

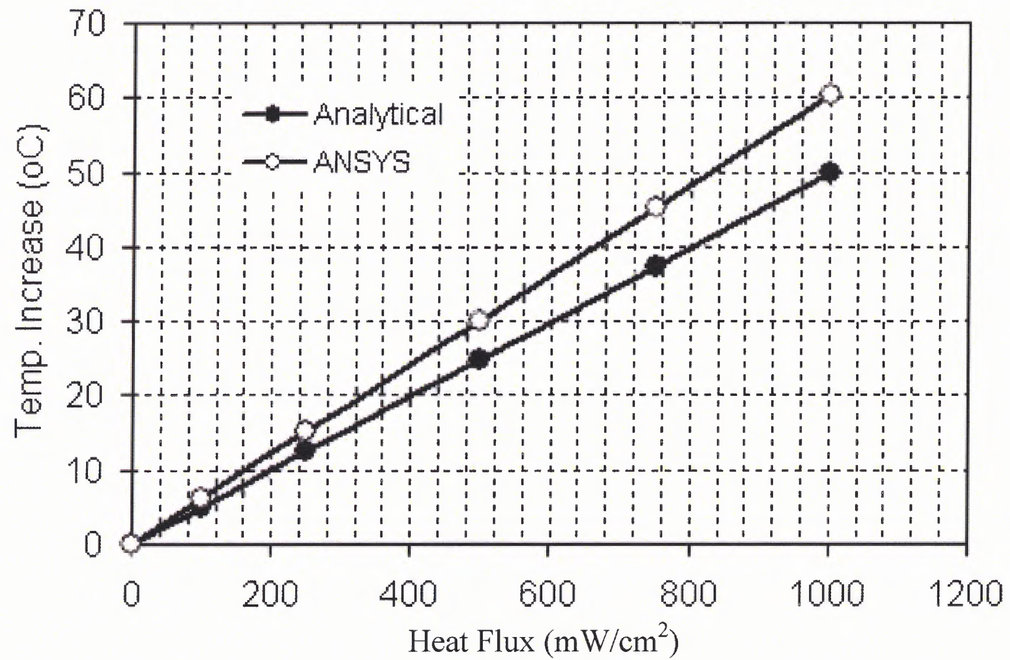

(a)

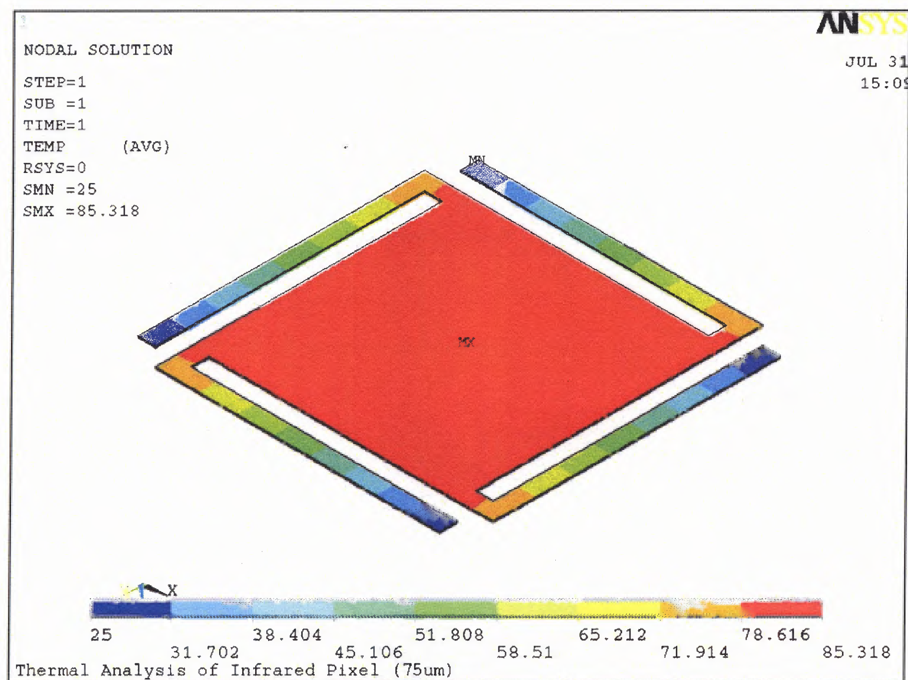

(b)

Figure 4.2 Steady-state thermal simulation result for the light modulator pixel (a) temperature increase under different heat input (b) temperature distribution at 1000 mW/cm^2 heat flux.

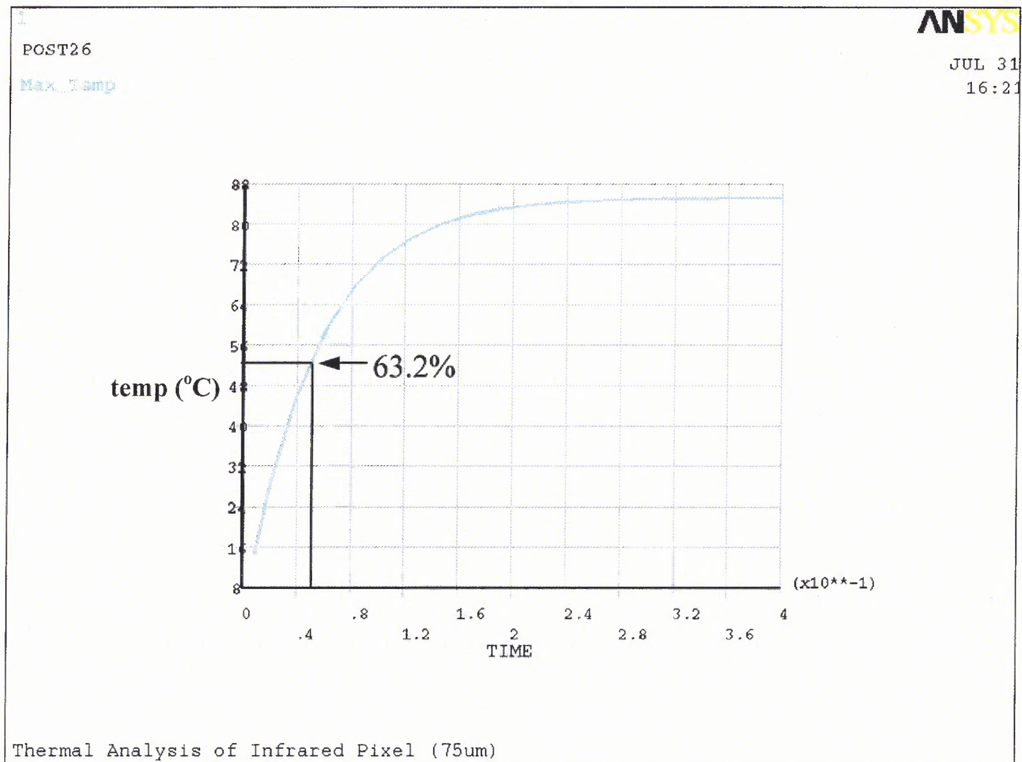

Figure 4.3 Determination of the thermal time constant from a transient thermal simulation by ANSYS.

Table 4.2 Thermal Properties of Light Modulator Pixel

Parameter	Unit	Analytical	Simulation
Thermal mass	J/K	5.53×10^{-9}	-
Thermal conductance	W/K	1.13×10^{-7}	1.21×10^{-7}
Thermal Time constant	ms	49	50

4.2 Optical Modeling

The effect of the temperature-dependent refractive index of VO_2 combined with the optical properties of the underlying layers defines the optical behavior of the light modulator pixel. The optical model of the modulator pixel was calculated using a commercial thin film optic design software Essential-Macleod™ [66], which was based on the multi-layer matrix formulations introduced in Chapter 3. The simulated pixel structure consists of a glass substrate, an air gap, a SiO_2 layer and a VO_2 layer, as displayed in Figure 4.4.

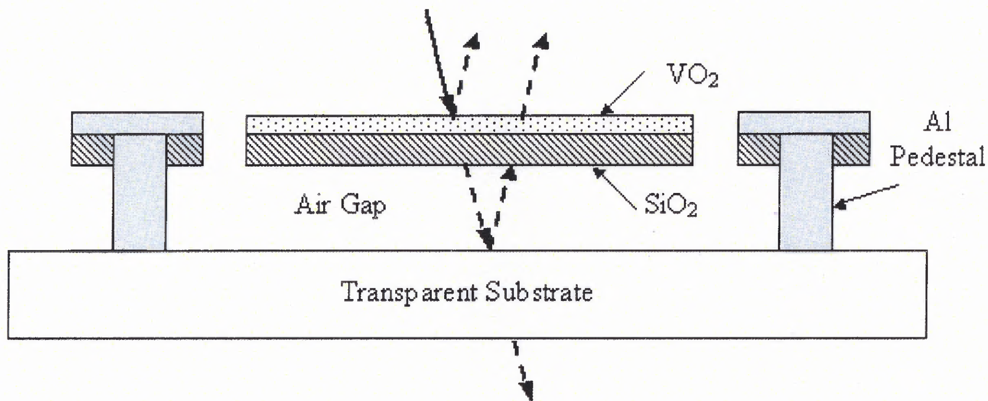

Figure 4.4 Cross-section view of the multi-layer light modulator pixel structure.

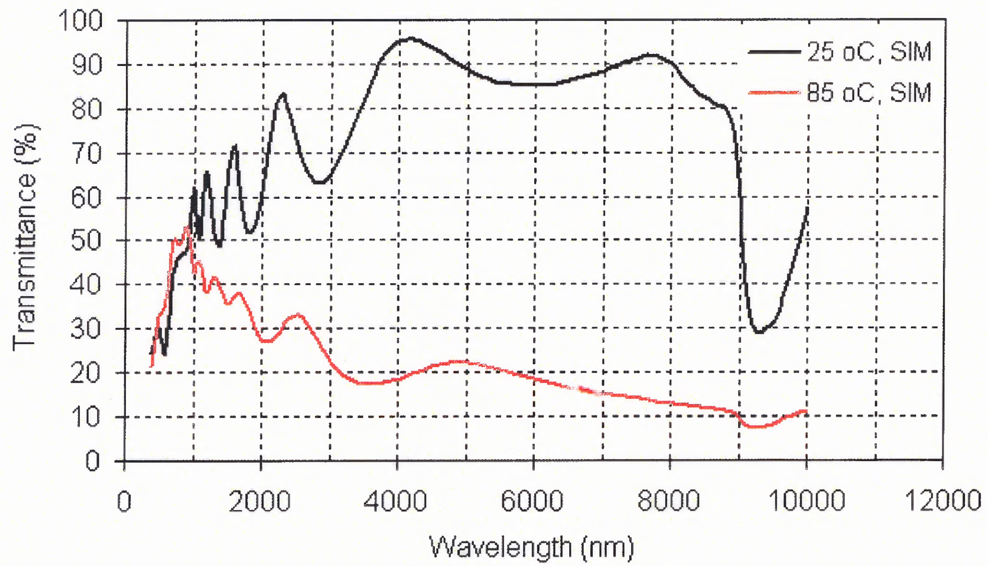

(a)

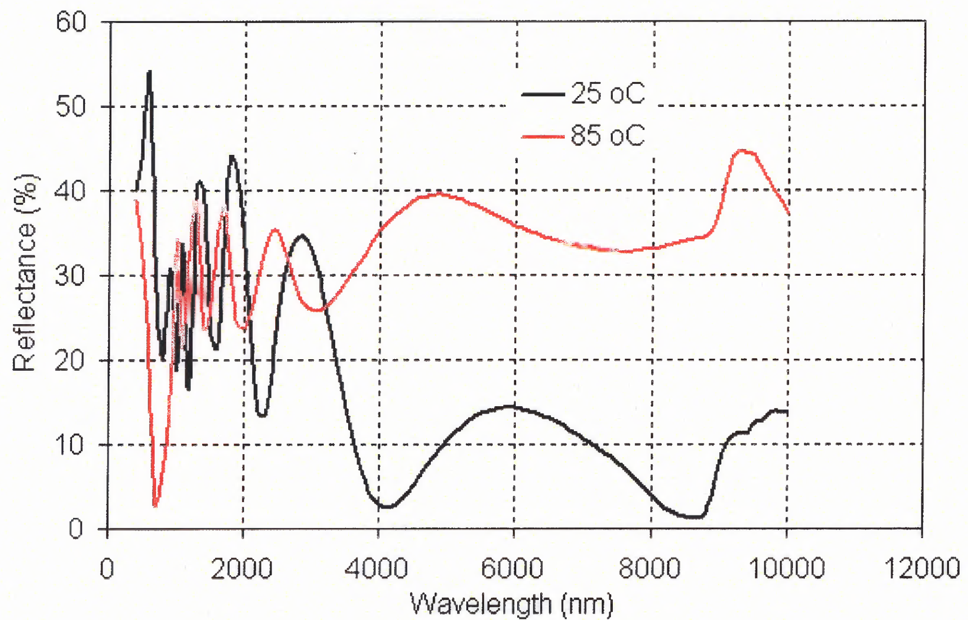

(b)

Figure 4.5 Simulated transmittance spectra (a) and reflectance spectra (b) of a device structure consists of VO_2(35nm)/SiO_2(200nm)/Air Gap(2.25um)/Glass Substrate.

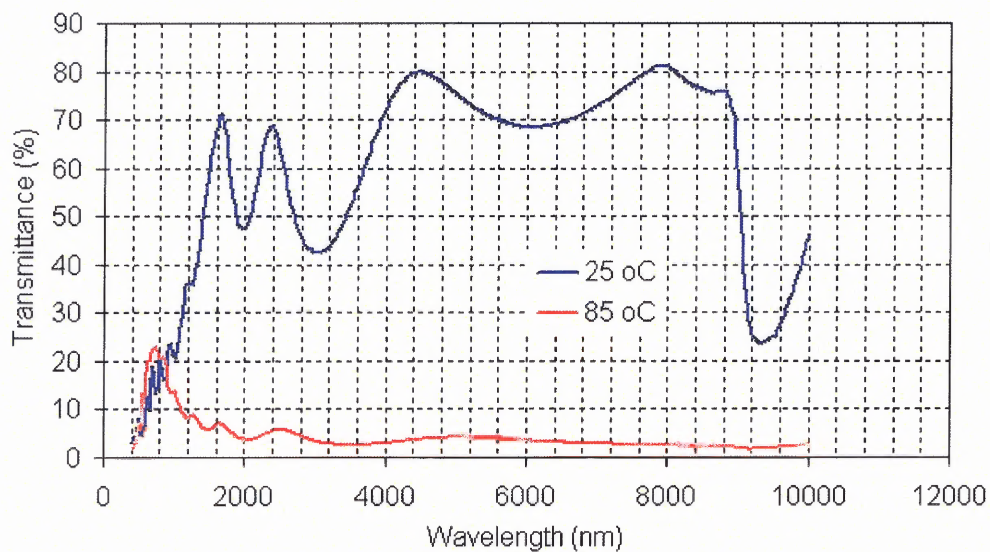

(a)

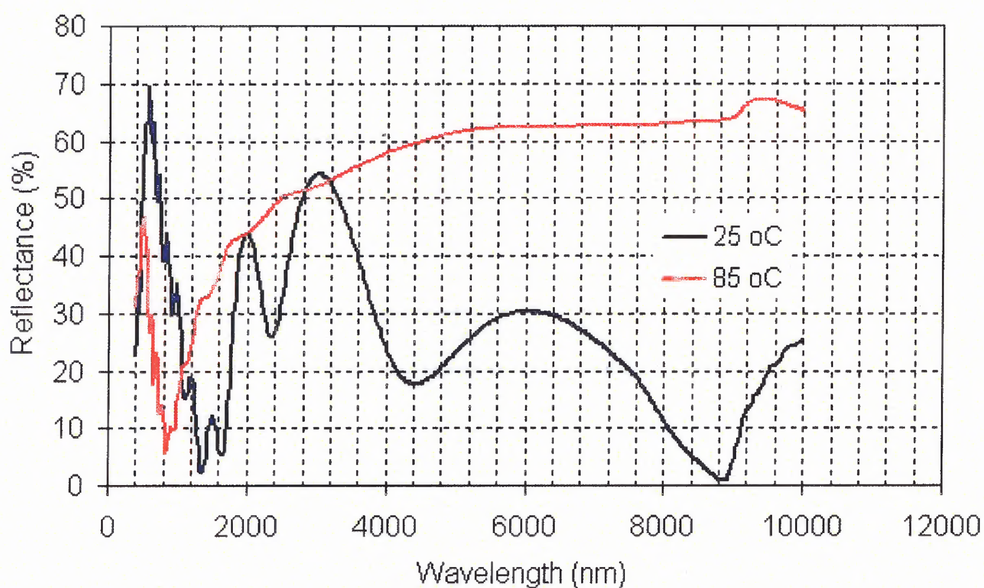

(b)

Figure 4.6 Simulated transmittance spectra (a) and reflectance spectra (b) of a device structure consists of VO_2(50nm)/SiO_2(200nm)/Air-Gap(2.25um)/Glass-Substrate.

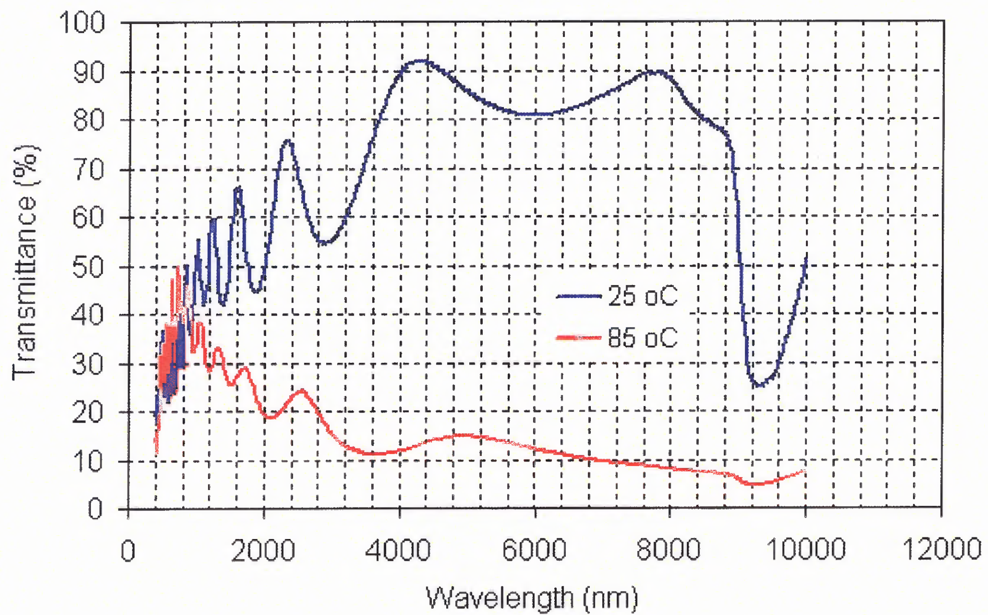

(a)

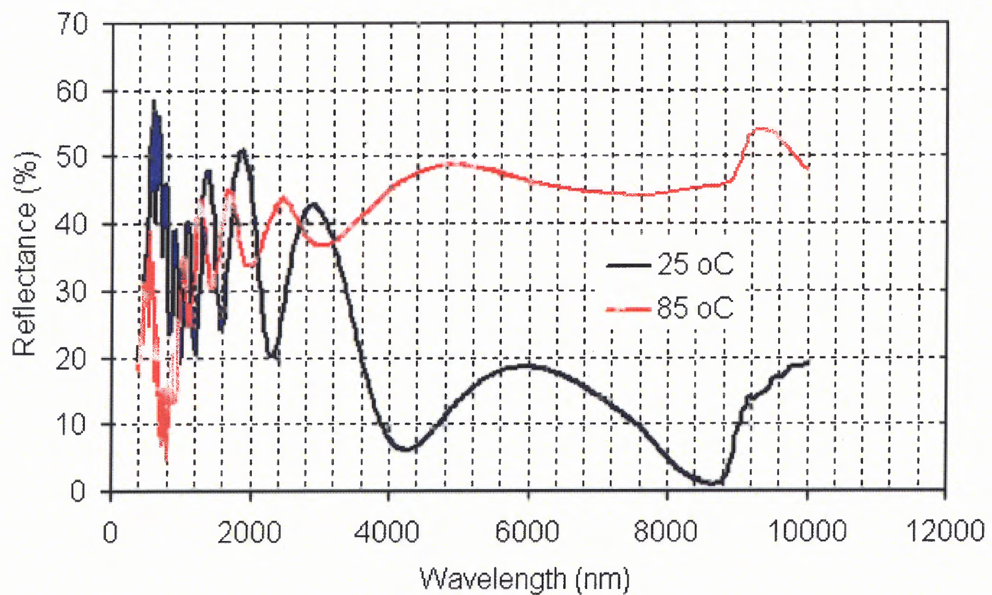

(b)

Figure 4.7 Simulated transmittance spectra (a) and reflectance spectra (b) of a device structure consists of SiO_2(20nm)/VO_2(35nm)/SiO_2(200nm)/Air-Gap(2.25um)/Glass-Substrate.

The transmittance and reflectance spectra of the pixels were simulated by changing the thickness of each layer. Figures of 4.5 to 4.7 show the simulation results. For wavelength less than 2 um, periodic interference characteristics were observed for the multi-layer pixels. It was noticed that the optical contrast accentuates when it enters the infrared region. The optical transmittance contrast is larger than the reflectance contrast in all the simulated structures.

CHAPTER 5

MICROFABRICATION OF VO_2 LIGHT MODULATOR

5.1 Integration of VO_2 into Micromachining Process

In this chapter, the VO_2 light modulator was fabricated with surface micromachining process. One of the processing steps is the growth and patterning of the VO_2 thin film into the MEMS pixels. VO_2 thin films have been used in the uncooled bolometer pixels. However, the processing details are priority and confidential. There is very few information on the etching of VO_2 film in the public literatures [67]. In this research, we use a processing of vanadium metal lift-off followed by thermal oxidation of the patterned vanadium metal film into VO_2. The lift-off patterning is a frequently used process to pattern metal films that are not easily etched. It exploits the fact that the step coverage of most metal deposition methods is very limited. As illustrated in Figure 5.1, a sacrificial mask, typically photoresist is patterned with only the regions where the metal wanted is exposed. After the metal deposition, the sacrificial mask is dissolved away together with the metal on it. The penetration of the lift-off solvent starts at the edge of the photoresist. It is important to have a discontinuity at the step edge of the metal. A vertical or inward sloping profile of the photoresist is desired. A negative tone photoresist tends to undercut after the development to form this type of slope. However, an undercut does not readily form for a positive tone photoresist. To obtain an undercut for the positive photoresist, one can either pre-soak the resist in an aromatic solvent or use the technique of image reversal [68].

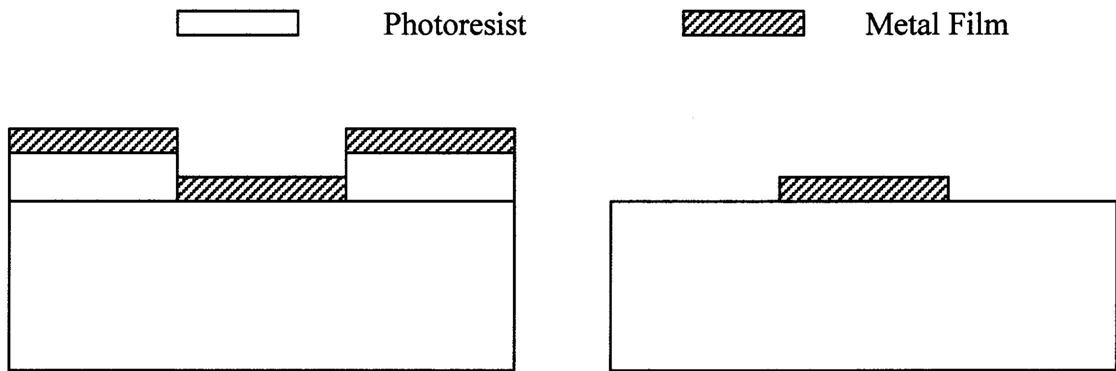

Figure 5.1 Illustration of a metal lift-off process to pattern metal films.

5.2 Microfabrication Process and Results

The fabrication of the light modulator was using surface micromachining. A polymeric sacrificial layer has been used to avoid the stiction problem in the structure releasing. It is a five-mask process. The photo masks were designed in L-Edit. The major fabrication steps are illustrated in Figure 5.2. The process starts with 4-inch diameter silicon or glass wafer. The first step was to grow about 500 nm thermal oxide layer on silicon substrate to improve the adherence of the wafer surface (a).

In the second step, the sacrificial layer of polyimide was applied (b). First, the wafer was soft baked at 175 ^{o}C hotplate for 2 minutes. Then the polyimide was spun-on. The thickness of the polyimide was controlled with the spin speed. Finally the polyimide was cured at higher temperature to about 2 um thickness.

The third step was the 400 nm silicon oxide (SiO_2) deposition on the polyimide by PECVD (c). The deposition was at 240 ^{o}C, using precursor gases of SiH_4 and NO_2. The SiO_2 is for the thermal isolation platform.

The forth step was to deposit the vanadium metal film for the VO_2 pixel. The pattern of the VO_2 pixel was defined by lift-off technology. The lift-off technology is very useful for metals that can't be etched without attacking the substrate. Because there is no standard etching process for the vanadium, the lift-off was selected. The lift-off process takes advantage of the fact that the step coverage of the deposited metal is limited. So when the photoresist is removed, the metal will only adhere to regions where is not covered by the photoresist. As shown in Figure 5.2 (d), Shipley 1045 photoresist was spun-on and patterned by photolithography. Then vanadium film was deposited by e-beam evaporation (e). After the deposition, the wafer was soaked in the photoresist strip

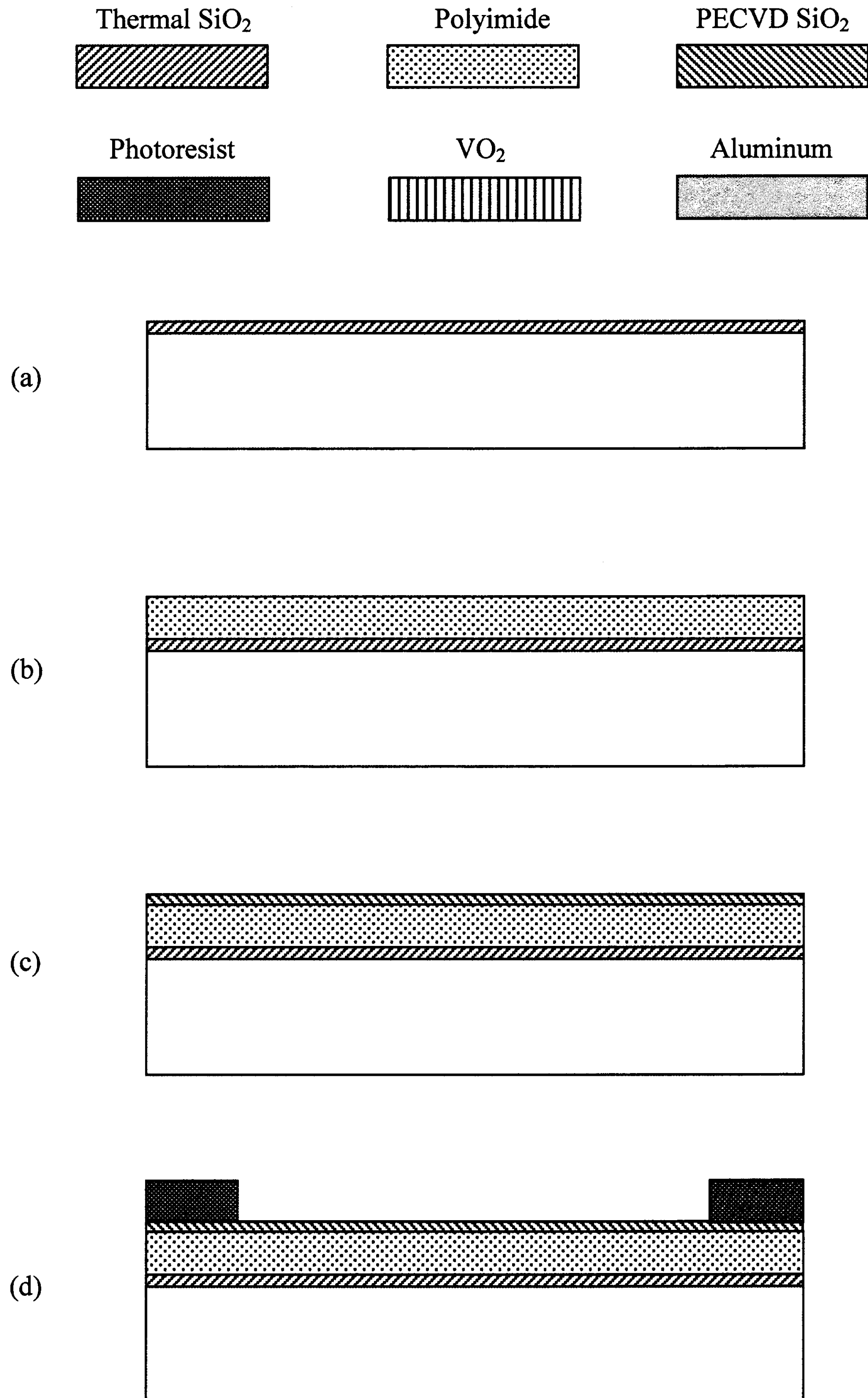

Figure 5.2 Process flow of the light modulator (a) ~ (d).

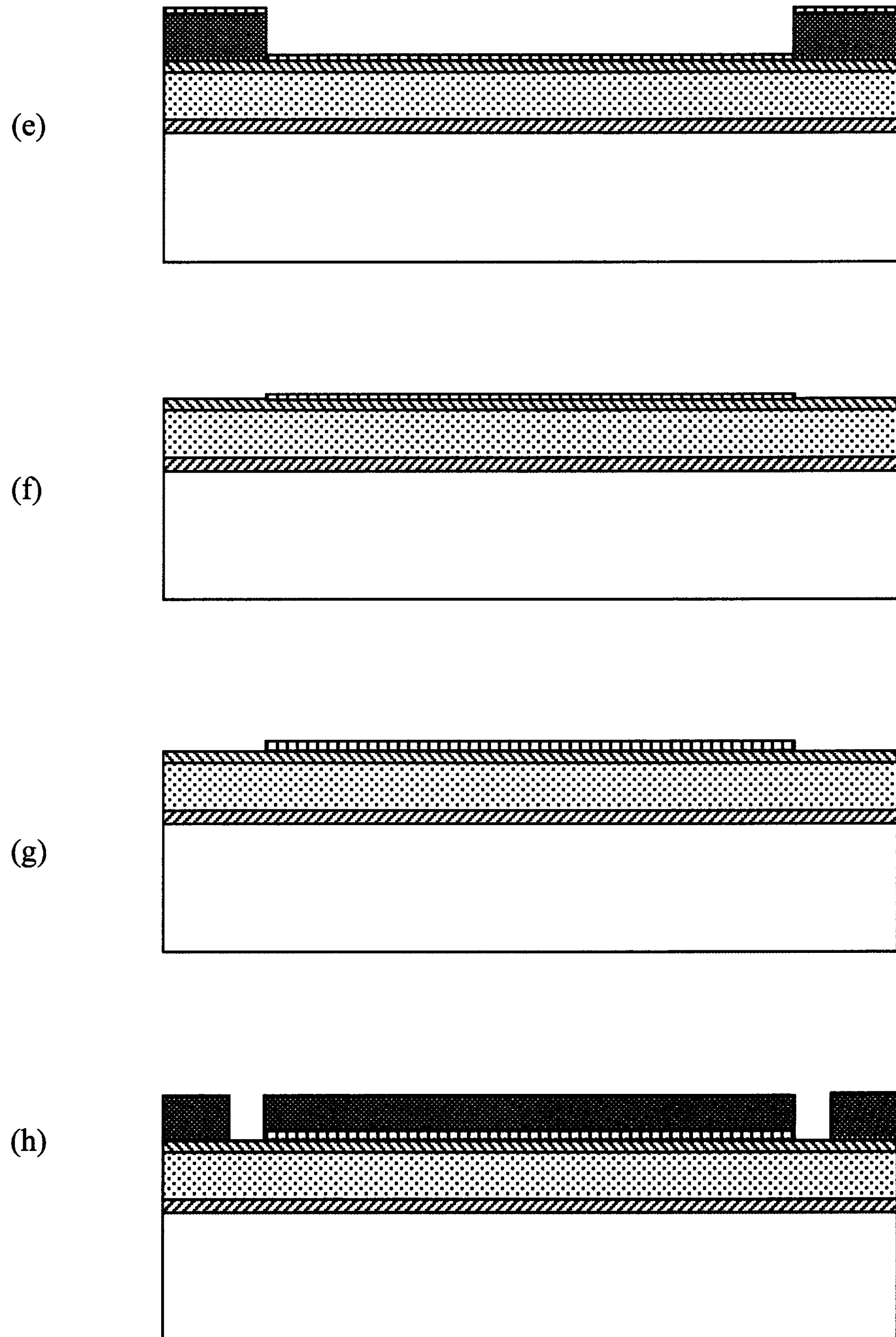

Figure 5.2 Process flow of the light modulator (e) ~ (h).

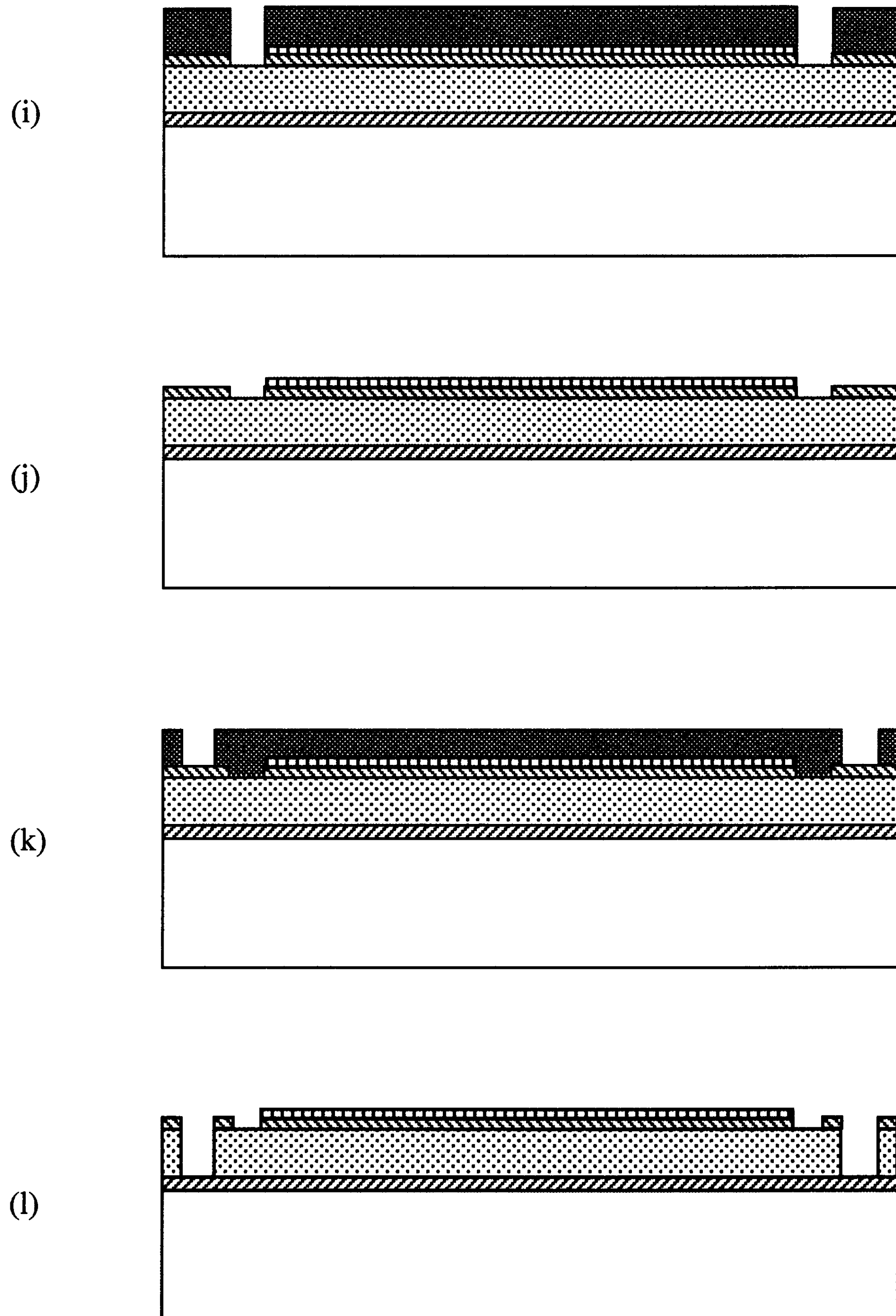

Figure 5.2 Process flow of the light modulator (i) ~ (l).

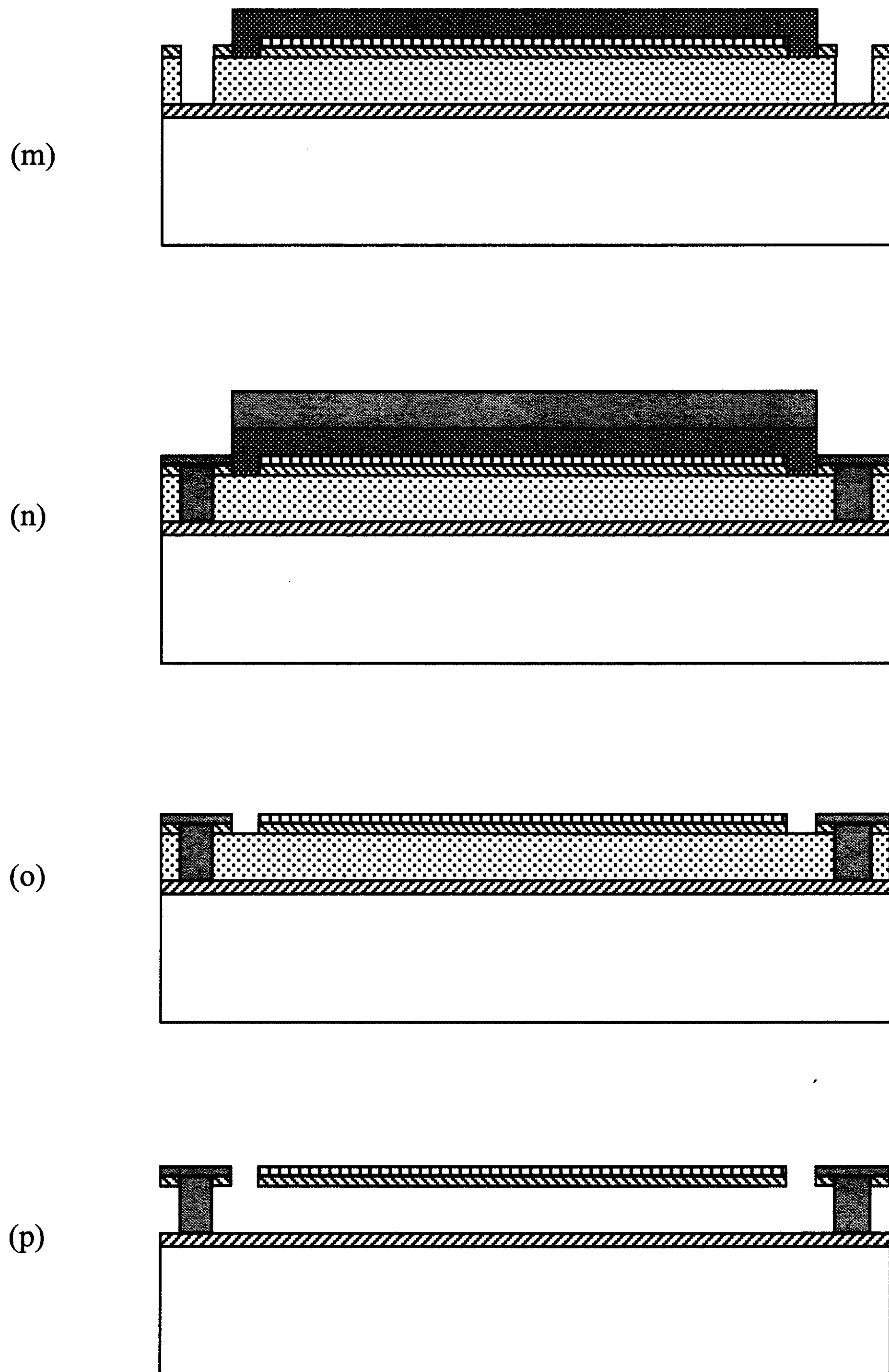

Figure 5.2 Process flow of the light modulator (m) ~ (p).

solvent and agitated with ultrasonic. The vanadium on the photoresist was removed together with the photoresist and only the metal on the pixel area remained (f).

In the fifth step, the vanadium film was oxidized into VO_2 at 390 °C (g).

The sixth and seventh steps were to pattern the pixel platform. It started with a standard photolithography (h). Then the SiO_2 platform was defined by reactive ion etching (RIE) using etching gas of CHF_3 (i). The SiO_2 etching rate is 40 nm/min.

The eighth step was to define the open area for the pedestals. It also started with a standard photolithography step (k). To open the contact area to the substrate surface, the SiO_2 layer was etched by CHF_3 plasma. The polyimide was etched with O_2 + CF_4 plasma (l). The etch rate for the polyimide was about 200 nm/min.

In the ninth step, the pedestal was formed by aluminum lift-off. It consists a photolithography step (m), followed by an e-beam evaporation of aluminum (n). The aluminum pedestal was lift-off in photoresist strip solvent with ultrasonic agitation (o).

A layer of photoresist was spun on to protect the devices from the contaminations from the dicing process. Then the wafer was diced. The photoresist was removed with acetone. The wafer was broken into single chips and put in an oxygen plasma barrel etcher. The polyimide was sacrificially etched and the whole pixel structure was released (p). The fabrication of the VO_2 light modulator was completed.

Based on above fabrication steps, the VO_2 light modulator was realized in format of 64 × 64 pixel arrays. Figures 5.3 and 5.4 show scanning electron microscope (SEM) pictures of the fabricated light modulator array before and after sacrificial releasing. Figures 5.5 and 5.6 are close view SEM images that illustrate single VO_2 light modulator pixel and the VO_2 film on the silicon dioxide platform, respectively.

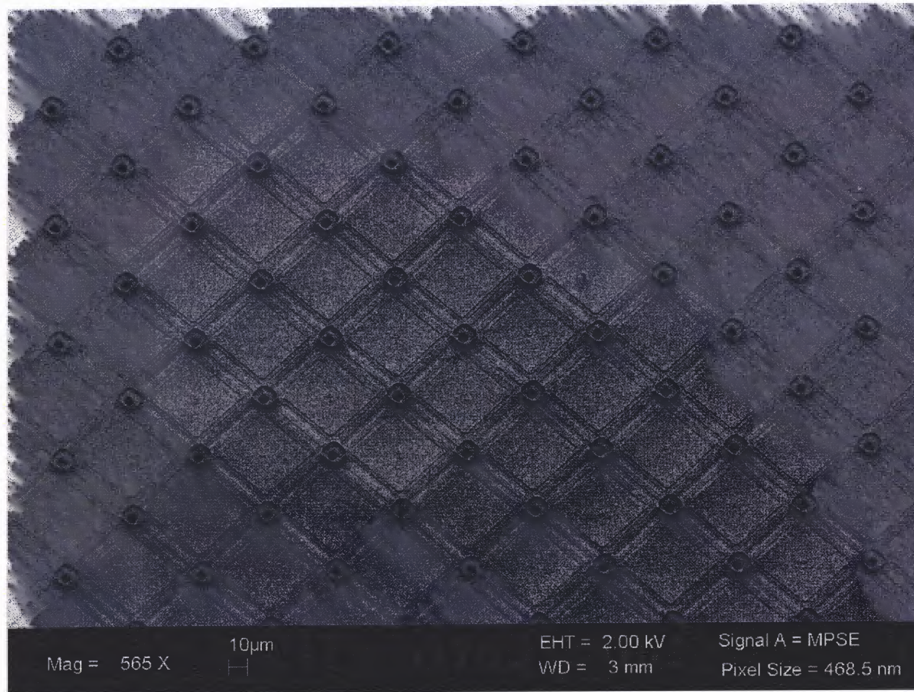

Figure 5.3 SEM micrograph of selected area of the microfabricated VO_2 pixel array before sacrificial releasing.

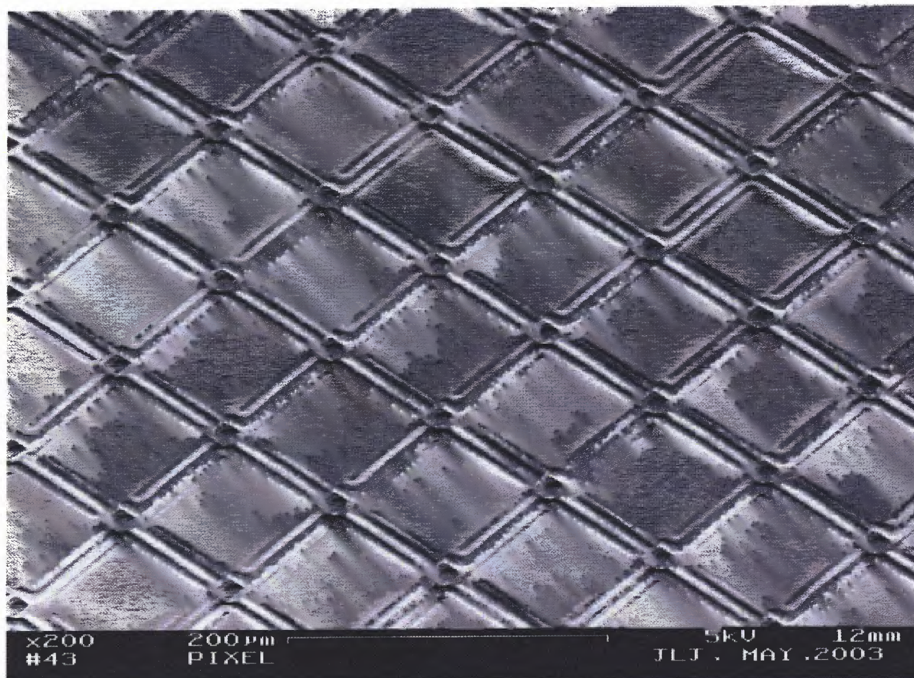

Figure 5.4 SEM micrograph of selected area of the microfabricated VO_2 pixel array after sacrificial releasing.

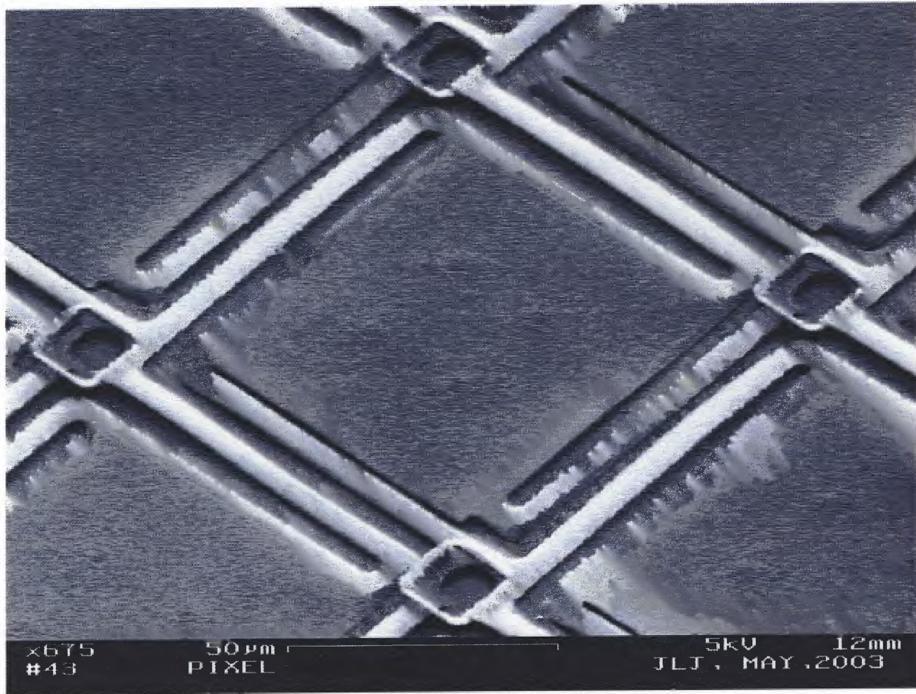

Figure 5.5 SEM image of single VO_2 pixel after sacrificial releasing.

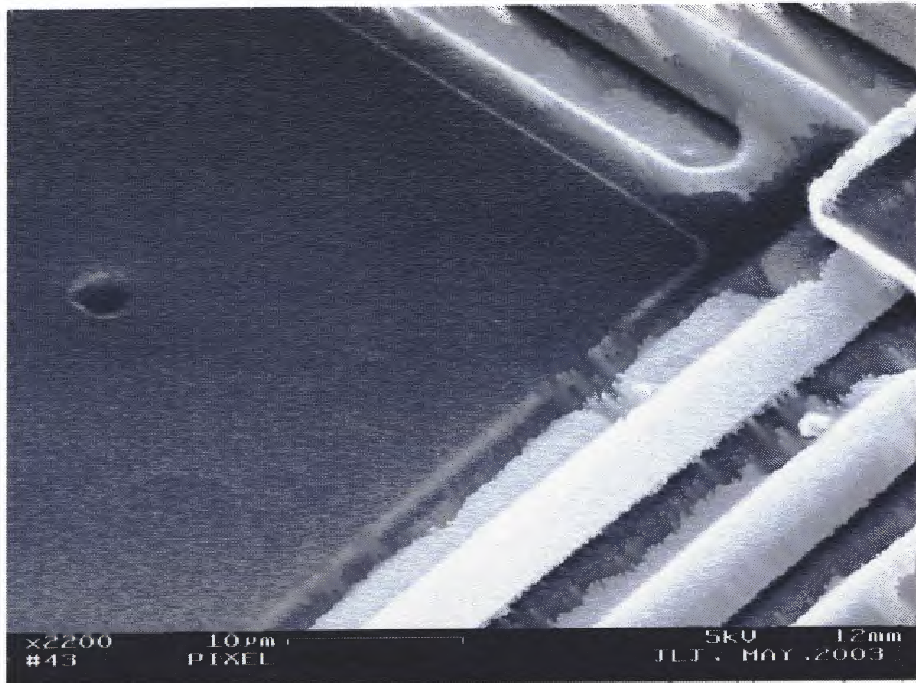

Figure 5.6 SEM image shows the VO_2 thin film on top of the SiO_2 pixel platform.

5.3 Experimental Characterization and Discussions

5.3.1 Surface Planarity

The flatness of the VO_2 light modulator pixel was characterized with a Wyko™ optical profilometer. The profilometer measurement is based on the light interference effect. Figure 5.7 shows the measurement result on a pixel with good surface planarity. It was seen that the flatness is within ± 0.1 um for pixels with good flatness. However, we also observed severe curvatures in pixels on some dies due to the residual stresses in the multiple layer thin film structures (Figure 5.9). Figure 5.8 shows the profilometer measurement result of a curled pixel. In the worst cases, the suspension beams were broken by the stress, as shown in Figure 5.10. To better understand the process, the film stress in the VO_2 pixel was measured.

5.3.2 Stress in VO_2 Thin Film

The residual stress in the thin films comes from several sources, i.e. the thermal stress, the intrinsic stress, and the external applied stress. The total stress is the sum of the three sources. The intrinsic stress reflects the internal structure of the thin film. It depends on the deposition process parameters. The thermal stress develops in high temperature step from the mismatch of thermal coefficients of expansion (TCE) between different materials. The thermal stress can be calculated by [69]:

$$\sigma_{th} = E_f \cdot (\alpha_f - \alpha_s)(T_d - T_r) \quad (5.1)$$

where E_f is the Young's modulus of the thin film, α_f and α_s are the TCE's of the film and substrate respectively, T_d and T_r are the deposition temperature and room temperature respectively.

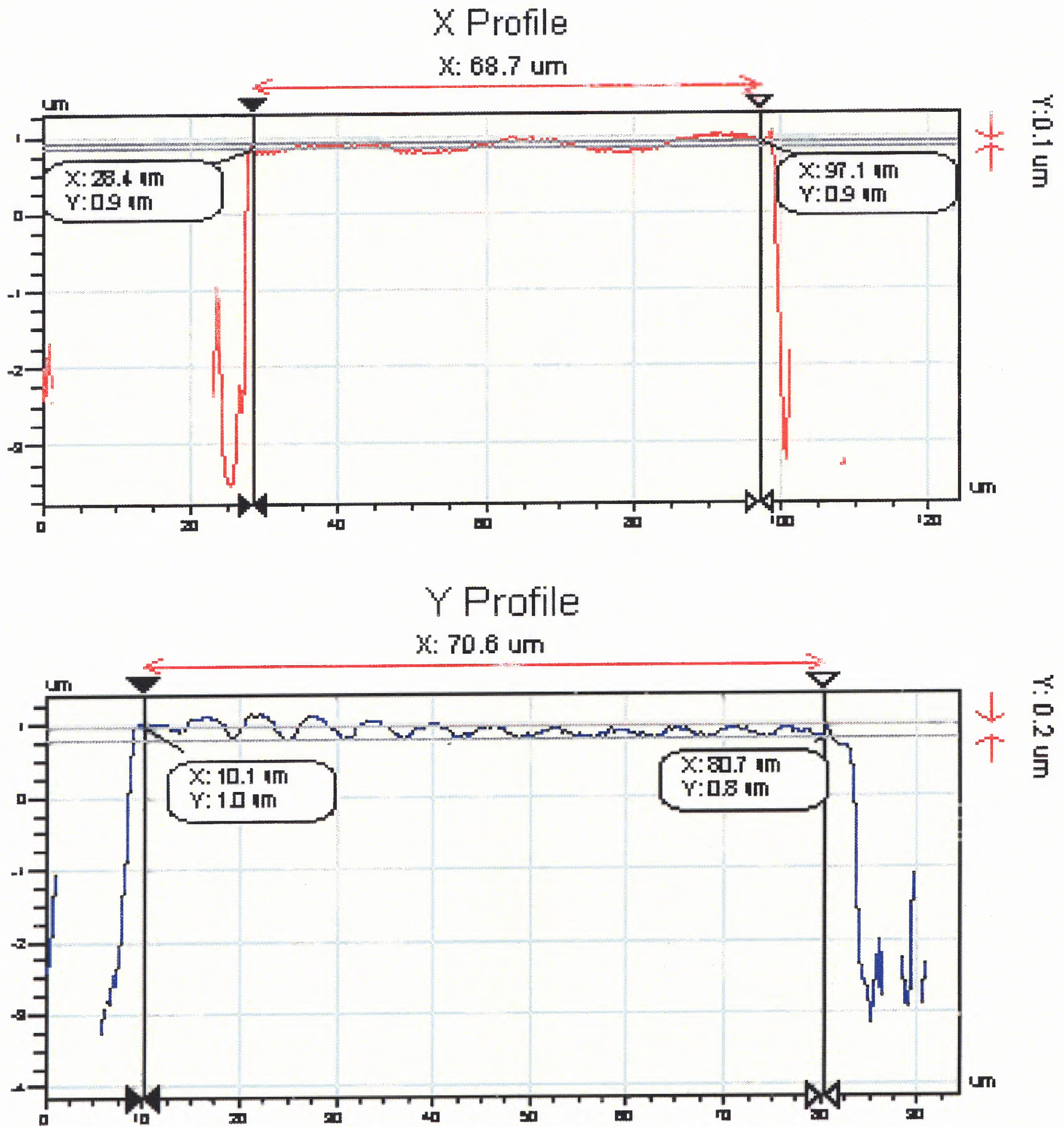

Figure 5.7 Wyko^{TM} optical profilometer measurement result on the pixel with good planarity.

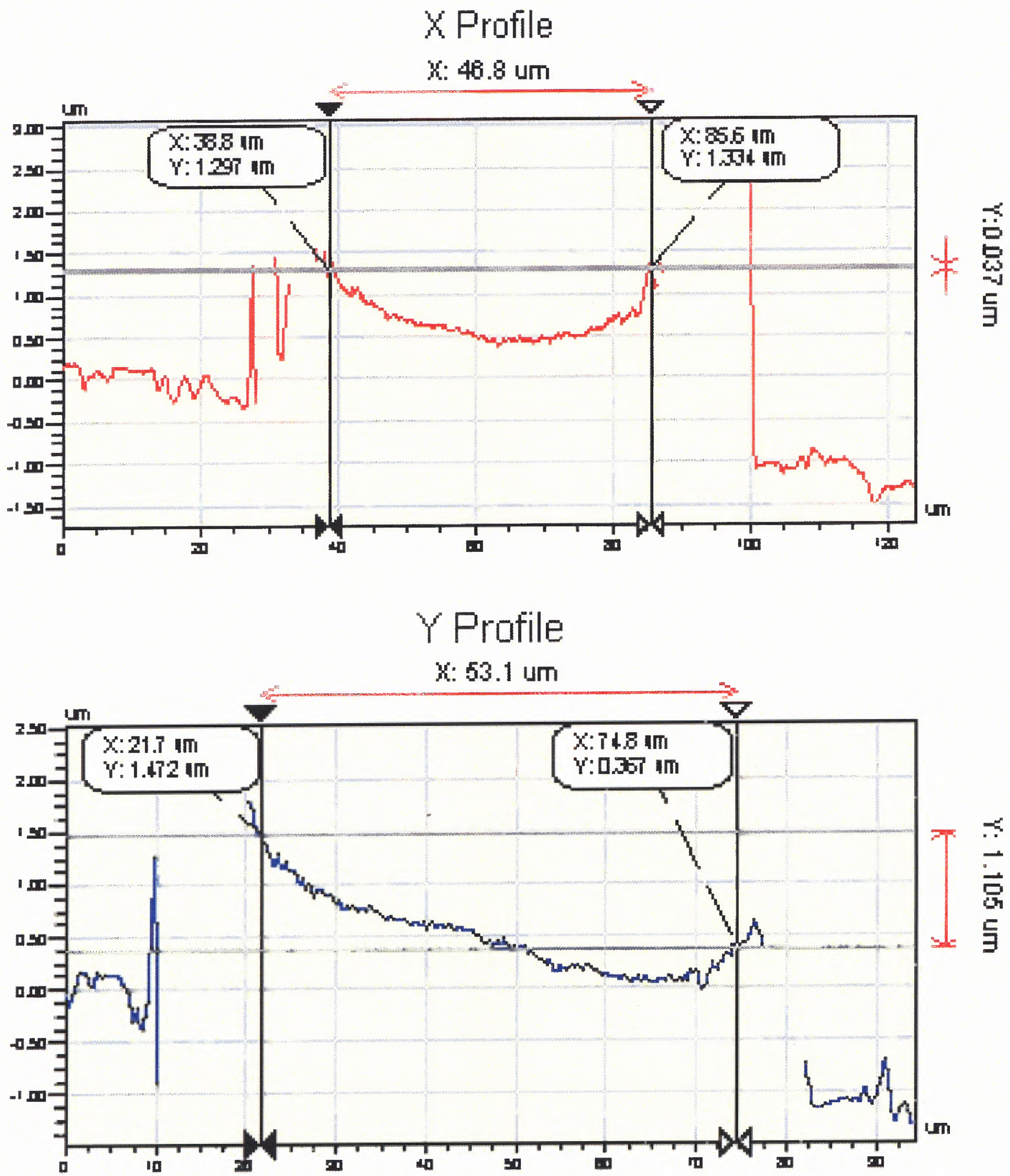

Figure 5.8 Wyko™ optical surface profile measurement result on the undesired curled-up pixel.

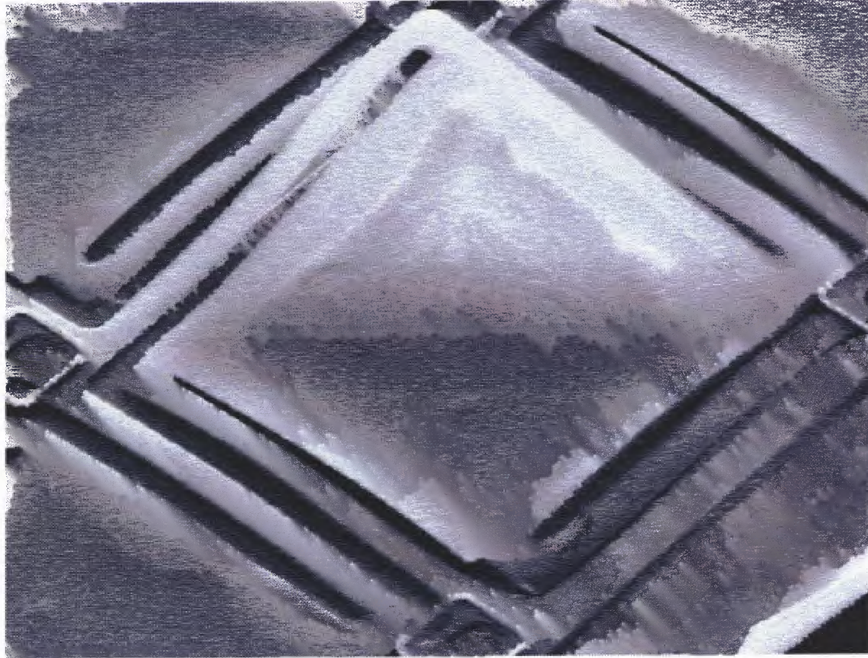

Figure 5.9 SEM image shows the undesired curvature of the VO_2 pixel due to the residual stress.

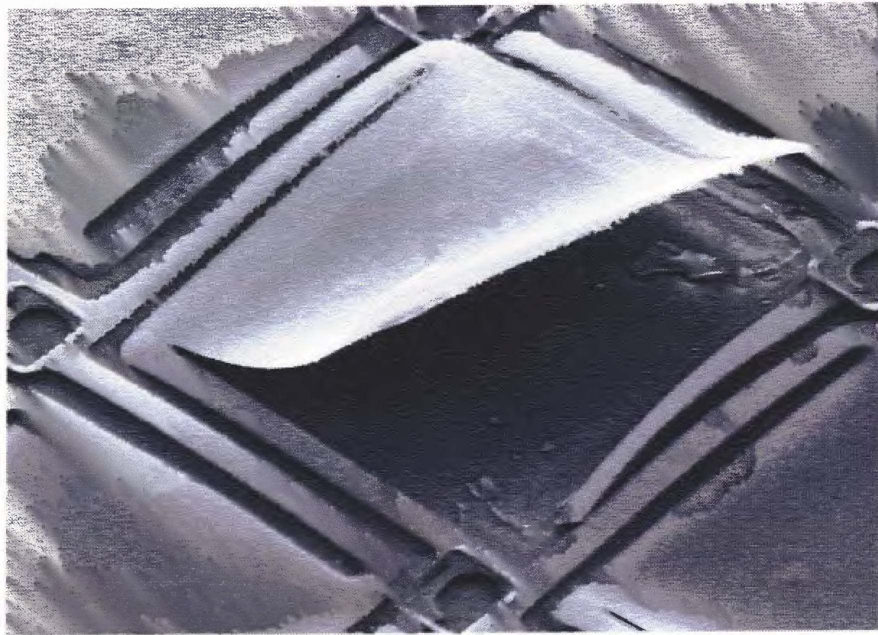

Figure 5.10 SEM image shows that the broken beams by the excess VO_2 stress in the worst case.

In the VO_2 light modulator pixel structure, the major stress should come from the VO_2 layer. There're two steps in the formation of VO_2 film. First step is the e-beam evaporation of the vanadium onto the SiO_2 platform. The second step is the oxidation of vanadium into the VO_2. In the evaporation, the substrate was not heated. However, the actual temperature should be higher than the room temperature. Because the TCE of the vanadium is much higher than the SiO_2, a tensile stress is expected from this step. In the next step of oxidation of vanadium into VO_2, the incorporation of the oxygen atoms into the vanadium film has an effect of expanding the film dimension. As a result, a compressive stress is expected. The net effect will depend on the relative magnitude of the stress from each step.

To confirm above speculation, the residual stresses of the vanadium evaporation and oxidation steps were determined by measuring the wafer bow of the monitor wafers. The wafer bow measurement is made with a Tencor FleXus laser scanning thin film stress measurement system. The stress is calculated from the radius of curvature before and after the film growth with Stoney equation [69]:

$$\sigma_f = \frac{E}{1-v} \cdot \frac{h^2}{6R \cdot t} \tag{5.2}$$

where E/1-v is the biaxial elastic modulus of the substrate (1.805×10^{11} Pa for (100) silicon), h is the substrate thickness, R is the radius of curvature of the substrate after the film deposition, t is the film thickness.

Figure 5.11 shows one of the measurement results for 20 nm vanadium. It was shown that a tensile stress of about 408 MPa resulted from the vanadium evaporation step. After 5 minutes of thermal oxidation at 370 °C, the film thickness increases to 46 nm. The stress measured is 200.8 MPa tensile. It means that a compressive stress results

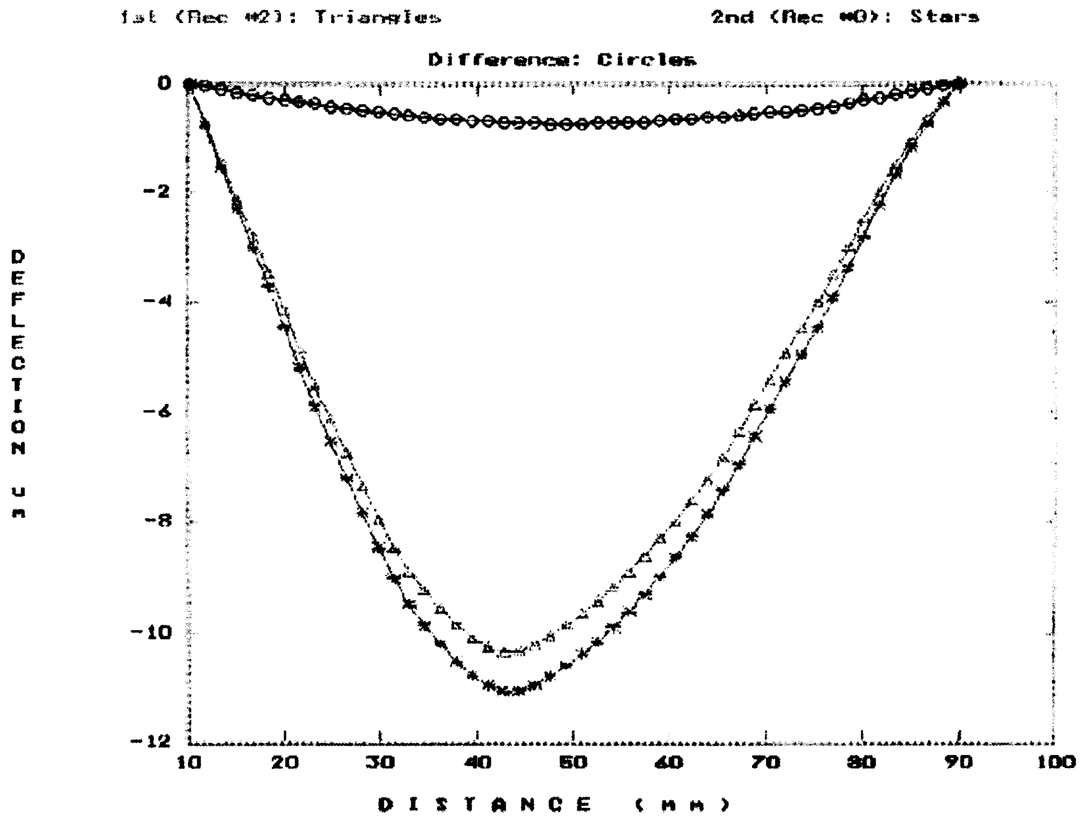

Figure 5.11 Laser scanned wafer bow before and after vanadium evaporation for measurement of the stress.

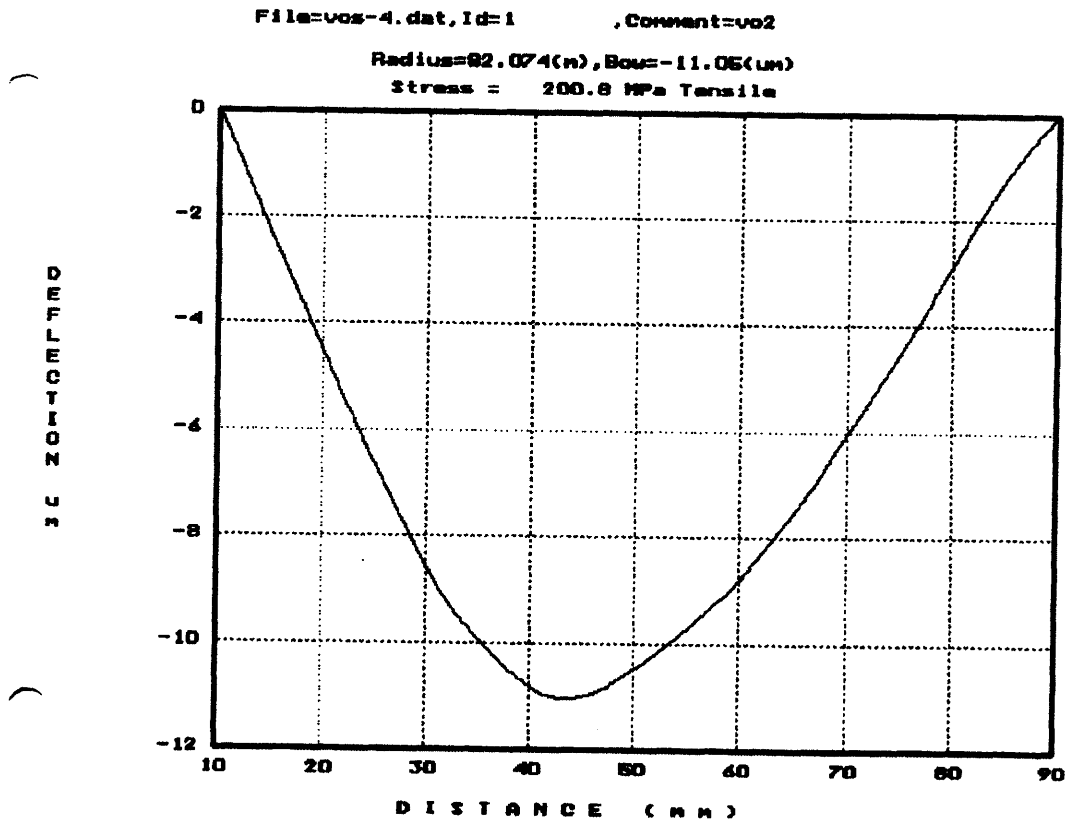

Figure 5.12 Laser scanned wafer bow after VO_2 oxidation for measurement of the stress.

from the oxidation but the magnitude is smaller than the tensile stress from the evaporation. The net stress is still tensile (Figure 5.12). It explains the curl-up of the VO_2 pixels. The stress value in the thermal oxidized VO_2 film is much different from the stress of reactive sputtered VO_2 film. In the reactive sputtering, the reaction of the vanadium with oxygen is expected to mostly happen in the gas phase. The main stress source will be the thermal stress because of the very large thermal coefficient of expansion of VO_2 ($2.1\times10^{-5}/^{o}C$) [70]. It is about 50 times of the TCE of the silicon oxide. However, in the thermal oxidation of the vanadium, the intrinsic stress will dominate due to the incorporation of the oxygen atoms, which expands the volume of the film and results in compressive stress. Table 5.1 summarizes the stress measurement results for VO_2 film with different thickness and oxidation time. The variation of the stress with the temperature was also measured. As shown in Figure 5.13, the stress decreases with the temperature increasing and becomes compressive at about 240 ^{o}C. It comes back to tensile stress after the temperature decreases to room temperature.

Table 5.1 Stress Measurement Result for Vanadium and VO_2 Thin Films

NO.	Wafer	Vanadium			VO_2		
	Radius (m)	Thickness (nm)	Radius (m)	Stress (MPa)	Time (min)	Radius (m)	Stress (MPa)
1	88.68	20	80.90	408.0	5	82.07	200.8
2	22.13	20	21.48	512.2	5	21.69	203.3
3	-40.96	35	-44.56	424.4	10	-41.80	80.4
4	-482.7	20	-1483.0	525.4	7	-965.2	222.5
5	-73.77	35	-86.61	432.0	9	-86.20	319.8
6	-57.84	35	-63.72	342.7	15	-63.66	258.4

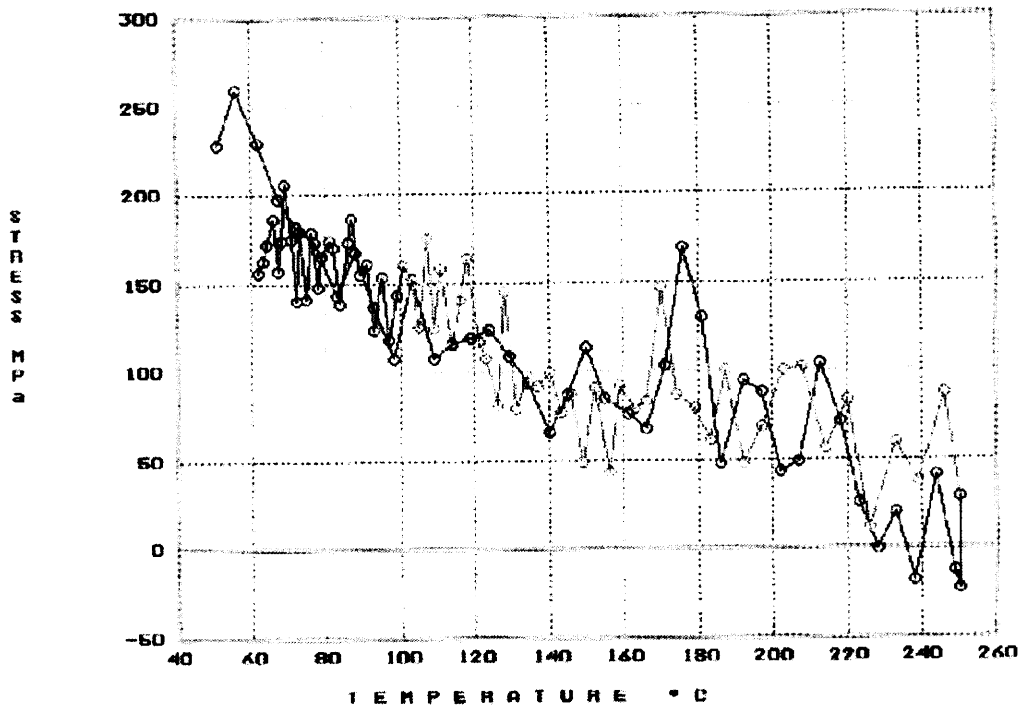

Figure 5.13 Change of the VO_2 thin film stress with the temperature.

5.4 Thermo-Optical Modulation Testing

Two types of testing have been carried out. One was done on the VO_2 thin film testing structures, which was deposited directly on the glass substrate without any releasing. This type of test is to monitor the properties of VO_2 thin film itself during and after the microfabrication processing. Another type of test was done on fully released VO_2 pixel, aiming to demonstrate the thermo-optical switching property of the light modulator array. Figure 5.14 shows the transmittance spectra taken on the VO_2 testing structure before and after its phase transition, with comparison to the simulation results. An optical contrast of ~ 90% to ~ 30% was observed in the near infrared region. The cut-off around 2.5 um comes from the glass substrate. There is very good agreement between the measurement and simulation result, which further proves the optical model.

The thermo-optical switching behavior of the VO_2 pixel array was tested with a LED-CCD setup. The light modulator chip with fully released pixels was mounted on a thermoelectric device. A ring of light emitting diodes (wavelength = 632 nm) was used as light source. The pixel tested here consists of VO_2 on vanadium structure, which has high contrast in visible range. The light of the LED was reflected by the VO_2 array and detected with a CCD camera. The temperature of the VO_2 array was switched between about 30 ^{o}C to 90 ^{o}C by the thermoelectric device. The light was modulated by the changing reflectance of the VO_2 pixels. The CCD camera was focused on the pixel array surface. Both the temperature and the light intensity variations were recorded synchronously with a computer. Figure 5.15 shows the measured intensity variation of the reflected light with the VO_2 temperature. The relatively low switching speed was limited by the temperature-increasing rate of the thermoelectric device.

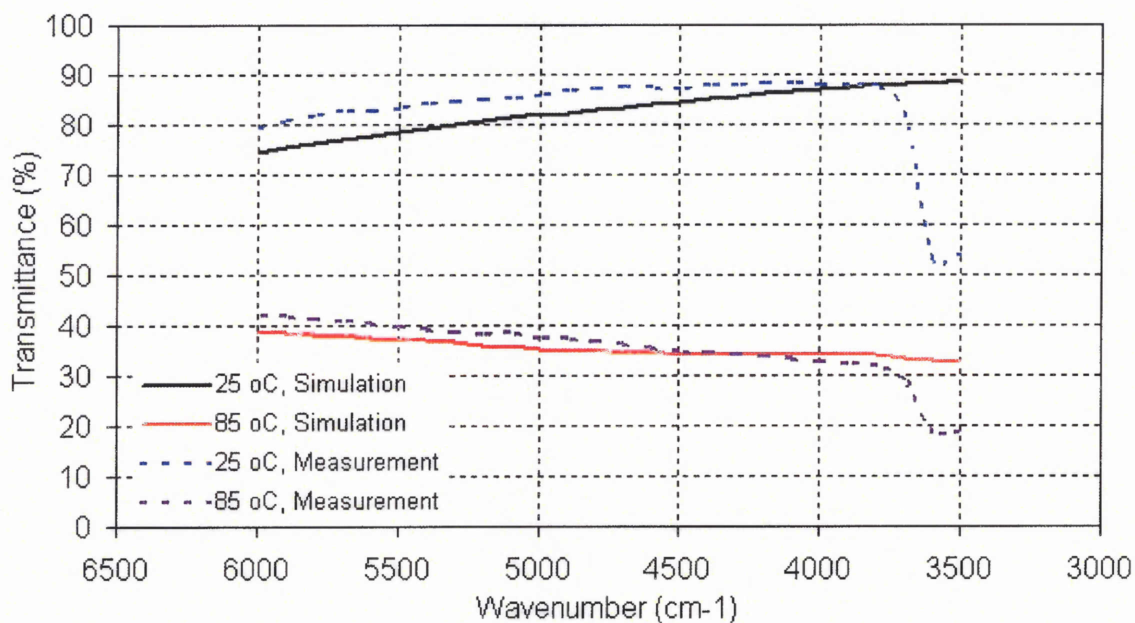

Figure 5.14 Measured and simulated near infrared transmittance spectra of VO_2 thin film (~ 50 nm) on glass before and after its phase transition.

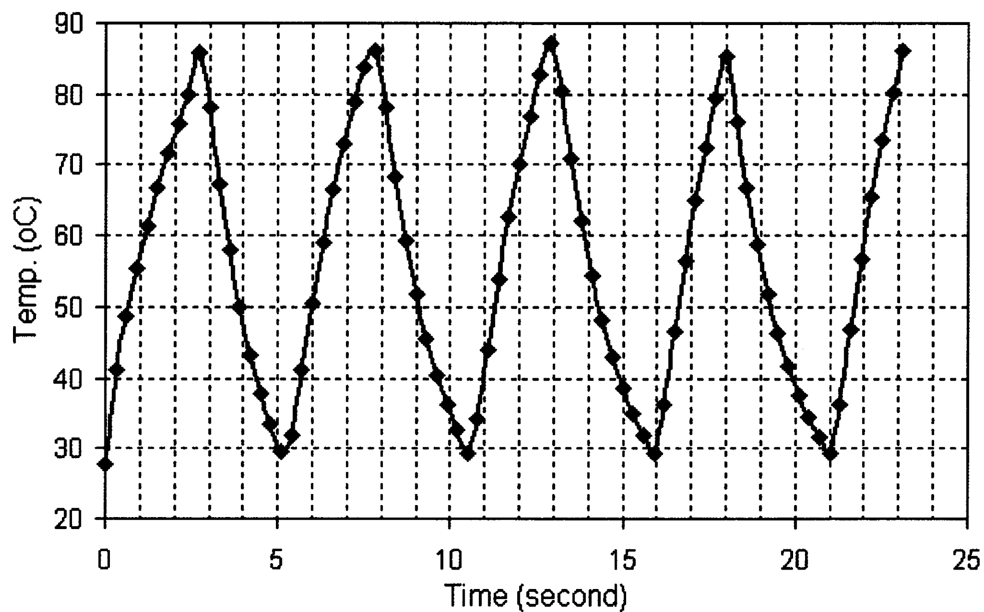

(a)

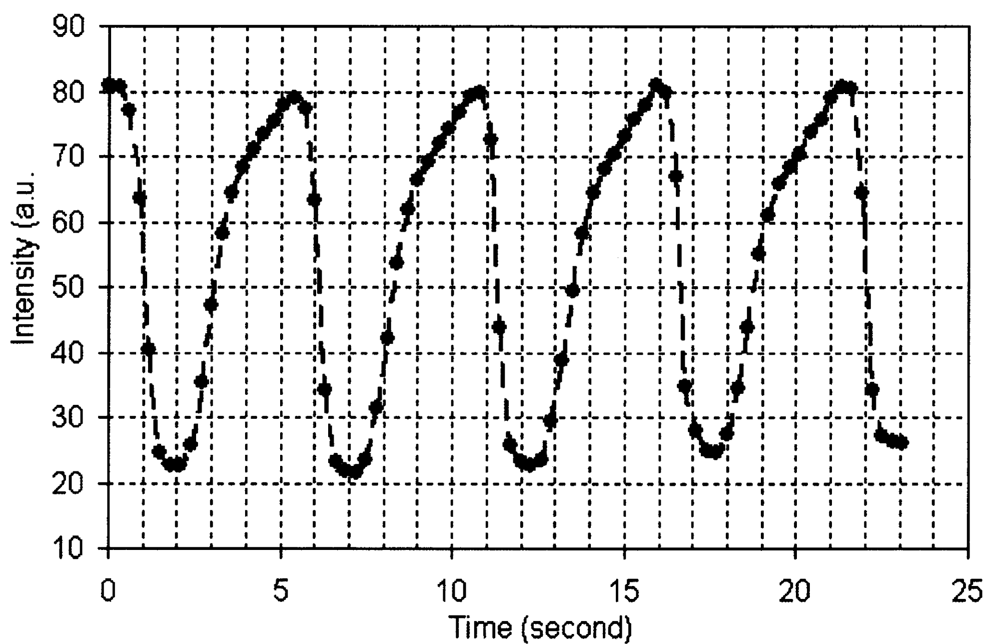

(b)

Figure 5.15 Thermo-optical switching by VO_2 array (a) temperature setup (b) measured variation of reflected LED intensity.

5.5 Effects of Oxygen Plasma

There are potential concerns that the microfabrication processes may change the optical property of the VO_2 thin film. The processing steps after the growth of VO_2 film include the photolithography, the reactive ion etching, and the O_2 plasma for the releasing. In the steps of photolithography and RIE, the VO_2 was covered by photoresist. The photoresist is not likely to alter the optical properties of the VO_2 film. The only step that may affect the VO_2 is the final releasing in the O_2 plasma. The releasing was made in an atmospheric pressure barrel etcher. The high pressure makes the O_2 plasma etching is purely chemical reaction. To test the effect of the O_2 plasma on the VO_2 film, testing films went through the O_2 plasma for different durations and their reflectance switching were measured and compared. Figure 5.16 shows the measurement result for the as-deposited VO_2 film and the VO_2 film after 30 minutes and 60 minutes of O_2 plasma treatment. The power of the plasma is about 600 W and the temperature is maintained at about 240 ^{o}C. There is no obvious changing observed in the optical switching contrast magnitude before and after the plasma treatment. The shift of the phase transition temperature as shown is believed to come from the experimental error instead of the actual effect.

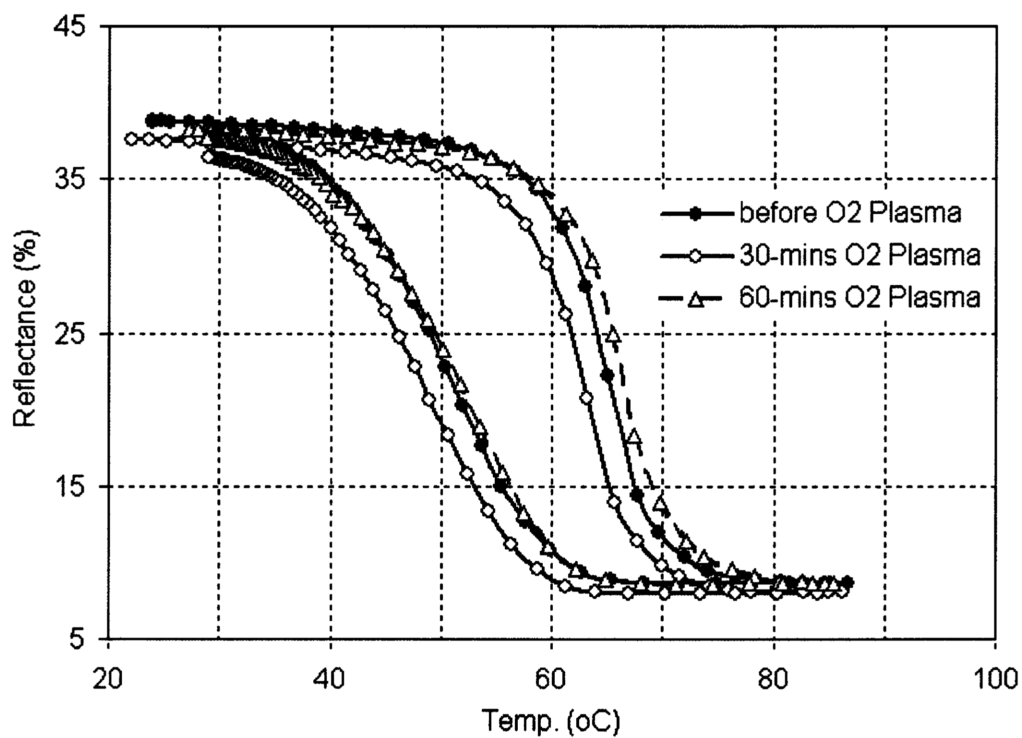

Figure 5.16 Temperature-reflectance curves of VO_2 film before and after O_2 plasma treatment.

CHAPTER 6

SUMMARY AND CONCLUSIONS

This research work concentrates on the development of a micromachined light modulator based on the semiconductor-to-metal phase transition of VO_2 thin film. Two major investigations have been carried out. One is the synthesis and characterization of VO_2 thin film. Another is the development of a microfabrication processing to integrate VO_2 film into MEMS pixels. The main results and key conclusions from the investigation are summarized in this chapter.

First, a deposition process for VO_2 thin films has been developed using e-beam evaporation of vanadium metal film followed by oxidation at elevated temperature. The synthesized VO_2 film undergoes a semiconductor-to-metal phase transition at around 65 ^{o}C, with about 15 ^{o}C hysteresis. The phase transition was signified by the sharp reflectance switching which could be visually detected by a color changing of the thin film. The optical switching was modeled with multiple-layer interference structure incorporating a VO_2 layer with temperature-dependent refractive index. It was found that the amplitude of the optical contrast of VO_2 film strongly depends on the underlying substrate and is a function of the film thickness. Improved visible optical contrast was obtained by growing VO_2 on top of a highly reflective metal layer. The best film in terms of the optical contrast (λ = 635.5 nm) was obtained with VO_2 on vanadium metal by oxidizing ~ 12 minutes at 390 ^{o}C.

The microstructure of the VO_2 film was studied by scanning electron microscope. The SEM results revealed a granular grain structure with sizes of 50 to 100 nm. It was

found that the grain size and local crystalline orientation affect the hysteresis width of optical switching. The effect of the minor loop behavior on the operation of the light modulator was studied. It was suggested that the light modulator should be operated in a bistable manner that the film is restored entirely to its low-temperature semiconductor state each time. The stability of the optical property of the VO_2 was tested and good stability was demonstrated.

A low-thermal-mass (~ 5.5×10^{-9} J/K) pixel with long and thin supporting legs was designed to provide good thermal isolation (~ 1.2×10^{-7} W/K), which prevents the cross talk between the adjacent pixels as well as temperature deviation across the array. Both thermal and optical simulations were done to study the pixel properties.

A surface micromachining process has been developed to fabricate the VO_2 light modulator. The patterning of the VO_2 was made by lift-off. The 64 × 64 modulator array was realized with a four-mask process. The size of the active area of single pixel is 75 × 75 um^2. The whole chip is 7 × 7 mm^2. The device was experimentally characterized and tested. The thermo-optical switching was demonstrated. Further study shows that the microfabrication process doesn't affect the VO_2 property. In the future work, the thermal characteristics of the pixel need to be further tested.

In conclusion, a light modulator was realized with micromachining technology. The thermo-optical switching of VO_2 films from its semiconductor-to-metal phase transition was exploited with miniaturized thermal isolation pixels. The film properties were preserved through the micromachining process. The demonstrated processes for thin film deposition and device fabrication present opportunities for future applications.

REFERENCES

1. G. T. Kovacs, *Micromachined Transducers Sourcebook*, WCB McGraw-Hill, New York, NY, 1999.

2. J. A. Neff, R. A. Athale, and S. H. Lee, "Two-dimensional spatial light modulators: a tutorial," *Proc. IEEE*, Vol. 78 (5), pp. 826-855, May 1990.

3. S. D. Senturia, *Microsystem Design*, Kluwer Academic Publishers, Norwell, MA, 2001.

4. T. Yeow, K. L. Eddie Law, and A. Goldenberg, "MEMS optical switches," *IEEE Communications Magazine*, pp. 158-163, Nov. 2001.

5. F. A. Chudnovskii, "Metal-semiconductor phase transition in vanadium oxides and technical applications," *Sov. Phys. Tech. Phys.*, Vol. 20 (8), pp. 999-1012, 1976.

6. H. W. Verleur, A. S. Barker Jr., and C. N. Berglund, "Optical properties of VO_2 between 0.25 and 5 eV," *Phys. Rev.*, Vol. 172 (3), pp. 788-798, Aug. 1968.

7. J. F. De Natale, P. J. Hood, and A. B. Harker, "Formation and characterization of grain-oriented VO_2 thin films," *J. Appl. Phys.*, 66 (12), pp. 5844-5850, Dec. 1989.

8. R. Lopez Noriega, *Metal semiconductor phase transition in VO_2 nanocrystals*, Ph.D. Dissertation, Vanderbilt University, 2002, and reference there.

9. I. Balberg, and S. Trokman, "High-contrast optical storage in VO_2 films," *J. Appl. Phys.*, Vol. 46 (5), pp. 2111-2119, May 1975.

10. J. A. Coath, and M. A. Richardson, "An infrared reflective optical modulator," *Proc. SPIE,* Vol. 3292, pp. 116-120, Jan. 1998.

11. M. A. Richardson, and J. A. Coath, "Infrared optical modulators for missile testing," *J. Opt. Laser Tech.*, Vol. 30 (2), pp. 137-140, Mar. 1998.

12. J. D. Billingsley, *Dynamic Infrared Scene Projector*, US Patent, 4,530,010, Jul. 1985.

13. D. W. Blodgett, C. H. Lange, and P. J. McNally, "Vanadium-dioxide-based infrared spatial light modulators," *Proc. SPIE*, Vol. 1969, pp. 349-356, Aug. 1993.

14. O. V. Dubrovskaya, M. I. Mikhal'chik, I. A. Khakhaev, and F. A. Chudnovskii, "Vanadium oxide light spatial modulator in an optical real-time correlator," *Proc. SPIE*, Vol. 1978, pp. 312-316, Sept. 1993.

15. E. Mottin, A. Bain, JL. Martin, J. L. Ouvrier-Buffet, S. Bisotto, J. J. Yon, JL. Tissot, "Uncooled amorphous silicon technology enhancement for 25um pixel pitch achievement," *Proc. SPIE*, Vol. 4820, pp. 200-207, Jul. 2002.

16. K. C. Liddiard, J. P. Knauth, S. Balick, B. Xu, N. Robinson, "ICC silicon microbolometer development program," *Proc. SPIE*, Vol. 4369, pp. 305-311, April 2001.

17. M. N. Gurnee, M. Kohin, R. Blackwell, N. Butler, J. Whitwam, B. Backer, A. Leary, and T. Nielson, "Developments in uncooled IR technology at BAE systems," *Proc. SPIE*, Vol. 4369, pp. 287-296, Apr. 2001.

18. F. J. Morin, "Oxides which show metal-to-insulator transition at the Neel temperature," *Phys. Rev. Lett.*, Vol. 3 (34), pp. 34, 1959.

19. A. Zylbersztejn, and N. F. Mott, "Metal-insulator transition in vanadium dioxide," *Phys. Rev. B*, Vol. 11 (11), pp. 4383-4395, 1975.

20. J. B. Goodenough, "The two components of the crystallographic transition in VO_2," *J. Solid State Chem.*, Vol. 3, pp. 490-500, 1971.

21. D. H. Thanh, P. D Long, V. T. Bich, and N. N. Dinh, "Structural formation and Raman scattering spectrum of vanadium oxide thin films made by electron beam deposition," *Communications in Phys.*, Vol. 8 (3), pp. 152-158, 1998.

22. A. Razavi, L. Bobyak, and P. Fallon, "The effects of biasing and annealing on the optical properties of RF sputtered VO_2," *J. Vac. Sci. Tech. A*, Vol. 8, pp. 1391-1394, 1990.

23. E. E. Chain, "Effects of oxygen in ion-beam sputter deposition of vanadium oxide," *J. Vac. Sci. Technol. A*, 5 (4), pp. 1836-1839, 1987.

24. C. H. Griffiths, and H. K. Eastwood, "Influence of Stoichiometry on the Metal-Semiconductor Transition in Vanadium Dioxide," *J. Appl. Phys*. Vol. 45 (5), pp. 2201-2206, May 1974.

25. E. E. Chain, "The Influence of Deposition Temperature on the structure and optical properties of Vanadium Oxide films," *J. Vac. Sci. Tech. A*, Vol. 4, pp. 432-435, 1986.

26. E. Kusano, and J. A. Theil, "Effects of microstructure and nonstoichiometry on electrical properties of vanadium dioxide films," *J. Vac. Sci. Technol. A*, 7 (3), pp. 1314-1317, 1989.

27. G. A. Nyberg, and R. A. Buhrman, "High optical contrast in VO_2 films due to improved stoichiometry," *Thin Solid Films*, Vol. 147, pp. 111-116, 1987.

28. F. C. Case, "Reactive evaporation of anomalous blue VO_2," *Appl. Opt.*, Vol. 26 (8), pp. 1550-1553, 1987.

29. F. C. Case, "The influence of substrate temperature on the optical properties of ion-assisted reactively evaporated vanadium oxide thin films," *J. Vac. Sci. Technol. A*, Vol. 6 (3), pp. 2010-2014, 1988.

30. F. C. Case, "Low temperature deposition of VO_2 thin films," *J. Vac. Sci. Technol. A,* 8 (3), pp. 1395-1398, 1990.

31. F. C. Case, "Improved VO_2 thin films for infrared switching," *Appl. Optics*, Vol. 30 (28), pp. 4119-4123, 1991.

32. T. Maruyama, and Y. Ikuta, "Vanadium dioxide thin films prepared by chemical vapor deposition from vanadium (III) acetylacetonate," *J. Mat. Sci.*, 28, pp. 5073-5078, 1993.

33. H. K. Kim, H. You, R. P. Chiarello, H. L. M. Chang, T. J. Zhang, and D. J. Lam, "Finite-size effect on the first-order metal-insulator transition in VO_2 films grown by metal-organic chemical-vapor deposition," *Phys. Rev. B*, Vol. 47 (19), pp. 12900-12907, May 1993.

34. M. Fukuma, S. Zembutsu, and S. Miyazawa, "Preparation of VO_2 thin film and its direct optical bit recording characteristics," *Appl. Opt.*, Vol. 22 (2), pp. 265-268, Jan. 1983.

35. S.-J. Jiang, C. B. Ye, M. S. R. Khan, and C. G. Granqvist, "Evolution of thermochromism during oxidation of evaporated vanadium films," *Appl. Opt.*, Vol. 30 (7), pp. 847-851, Mar. 1991.

36. A. Z. Moshfegh, and A. Ignatiev, "Formation and characterization of thin film vanadium oxides: Auger electron spectroscopy, X-ray photoelectron spectroscopy, X-ray diffraction scanning electron microscopy, and optical reflectance studies," *Thin Solid Films*, 198, pp. 251-268, 1991.

37. F. Beteille, L. Mazerolles, and J. Livage, "Microstructure and metal-insulator transition of VO_2 thin films," *Mat. Research Belletin*, Vol. 34 (14/15), pp. 2177-2184, 1999.

38. T. J. Hanlon, R. E. Walker, J. A. Coath, and M. A. Richardson, "Comparison between vanadium dioxide coatings on glass produced by sputtering, alkoxide and aqueous sol-gel methods," *Thin Solid Films*, 405, pp. 234-237, 2002.

39. J. Livage, "Optical and electrical properties of vanadium oxides synthesized from alkoxides," *Coordination Chem. Rev.*, Vol. 190-192, pp. 391-403, 1999.

40. D. Yin, N. Xu, J. Zhang, and X. Zheng, "Vanadium dioxide films with good electrical switching property," *J. Phys. D: Appl. Phys.*, Vol. 29, pp. 1051-1057, 1996.

41. G. Guzman, "Vanadium dioxide as infrared active coating," World Wide Internet: http://www.solgel.com/articles/August00/thermo/Guzman.htm, as accessed at May 7th, 2003.

42. Kim D. H., and Kwok H. S., "Pulsed laser deposition of VO_2 thin films," *Appl. Phys. Lett.*, Vol. 65 (25), pp. 3188-3190, 1994.

43. Yuan N. Y., Li J. H., and Lin C. L., "Valence reduction process from sol-gel V_2O_5 to VO_2 thin films," *Appl. Surface Sci.*, 191, pp. 176-180, 2002.

44. M. F. Becker, A. B. Buckman, and R. M. Walser, "Femtosecond laser excitation of the semiconductor-metal phase transition in VO_2," *Appl. Phys. Lett.*, Vol. 65 (12), pp. 1507-1509, Sep. 1994.

45. A. Cavalleri, Cs. Toth, C. W. Siders, and J. A. Squier, "Femtosecond structural dynamics in VO_2 during an ultrafast solid-solid phase transition," *Phys. Rev. Lett.*, Vol. 87 (23), pp. 237401-1 - 237401-4, Dec. 2001.

46. A. S. Oleinik, "Optical data recording with vanadium dioxide-based film reversible media," *Tech. Phys.*, Vol. 47 (8), pp. 1014-1018, 2002.

47. W. Burkhardt, T. Christmann, S. Franke, W. Kriegseis, D. Meister, B. K. Meyer, W. Niessner, D. Schalch, and A. Scharmann, "Tungsten and fluorine co-doping of VO_2 films," *Thin Solid Films*, 402, pp. 226-231, 2002.

48. W. Burkhardt, T. Christmann, B. K. Meyer, W. Niessner, D. Schalch, and A. Scharmann, "W- and F-doped VO_2 films studied by photoelectron spectrometry," *Thin Solid Films*, 345, pp. 229-235, 1999.

49. P. Jin, S. Nakao, S. Tanemura, "Tungsten doping into vanadium dioxide thermochromic films by high-energy ion implantation and thermal annealing," *Thin Solid Films*, 324, pp. 151-158, 1998.

50. P. W. Kruse, and D. D. Skatrud, *Uncooled Infrared Imaging Arrays and Systems*, Semiconductors and Semimetals Series, Vol. 47, Academic Press, 1997.

51. A. Rogalski, "Infrared detectors: an overview," *Infrared Physics & Technology*, 43, pp. 187-210, 2002.

52. P. W. Kruse, *Uncooled Thermal Imaging: Arrays, Systems, and Applications*, SPIE Press, 2001.

53. D. D. Eden, "Vanadium dioxide storage material," *Optical Engineering*, Vol. 20 (3), pp. 377-378, 1981.

54. W. R. Roach, "Holographic storage in VO_2," *Appl. Phys. Lett.*, Vol. 19 (11), pp. 453-455, Dec. 1971.

55. S. A. Pollack, D. B. Chang, F. A. Chudnovskii, and I. A. Khakhaev, "Passive Q switching and mode-locking of Er:glass lasers using VO_2 mirrors," *J. Appl. Phys.*, Vol. 78 (6), pp. 3592-3599, 1995.

56. C. E. Lee, R. A. Atkins, W. N. Gibler, and H. F. Taylor, "Fiber optic application for thermal switching in vanadium dioxide films," *Appl. Opt.*, Vol. 28 (21), pp. 4511-4512, 1989.

57. A. I. Sidorov, "Formation of the reflectance in a controllable mirror based on vanadium dioxide with a thin-film heater," *J. Opt. Technol.*, Vol. 64 (1), pp. 23-25, Jan. 1997.

58. H. A. Macleod, *Thin Film Optical Filters, Institute of Physics Publishing*, 3rd edition, Bristol and Philadelphia, 2001.

59. W. Haidinger, and D. Gross, "Anomalous hysteresis shape of thin VO_2 layers," *Thin Solid Films*, 12, pp. 433-438, 1972.

60. C. Petit, J. M. Frigerio, and M. Goldmann, "Hysteresis of the metal-insulator transition of VO_2: evidence of the influence of microscopic texturation," *J. Phys.: Condens. Matter*, 11, pp. 3259-3264, 1999.

61. V. A. Klimov, I. O. Timofeeva, S. D. Khanin, E. B. Shadrin, A. V. Ilinskii, and F. Silva-Andrade, "Hysteresis loop construction for the metal-semiconductor phase transition in vanadium dioxide films," *Tech. Phys.*, Vol. 47 (9), pp. 1134-1139, 2002.

62. L. A. Luz de Almeida, G. S. Deep, A. M. N. Lima, H. F. Neff, and R. C. S. Freire, "A hysteresis model for a vanadium dioxide transition-edge microbolometer," *IEEE Trans. Instrument. Measurement*, Vol. 50 (4), pp. 1030-1035, Aug. 2001.

63. L. A. L. de Almeida, G. S. Deep, A. M. N. Lima, H. F. Neff, "Thermal dynamics of VO_2 films within the metal-inculator transition: evidence for chaos near percolation threshold," *Appl. Phys. Lett.*, Vol. 77 (26), pp. 4365-4367, Dec. 2000.

64. V. Yu. Zerov, Yu. V. Kulikov, V. N. Leonov, V. G. Malyarov, I. A. khretov, and I. I. Shaganov, "Features of the operation of a bolometer on a vanadium dioxide film in a temperature interval that include a phase transition," *J. Opt. Technol.*, Vol. 66 (5), pp. 387-390, May 1999.

65. P. Eriksson, J. Y. Andersson, and G. Stemme, "Thermal characterization of surface-micromachined silicon nitride membranes for thermal infrared detectors," *IEEE J. MEMS*, Vol. 6 (1), pp. 55-61, 1997.

66. Thin Film Center Inc., 2745 E Via Rotonda, Tucson, AZ 85716, USA.

67. H. Buhay, and K. J. Kogler, "Reactive ion etching of vanadium dioxide thin films," *J. Vac. Sci. Technol. A*, Vol. 4 (3), pp. 440-442, 1986.

68. M. J. Madou, *Fundamentals of Microfabrication: the science of miniaturization*, 2nd edition, CRC Press, 2002.

69. F. C. Case, "Modification in the phase transition properties of predeposited VO_2 films," *J. Vac. Sci. Technol. A*, Vol. 2 (4), pp. 1509-1512, 1984.

70. R. Lopez, L. A. Boatner, T. E. Haynes, R. F. Haglund Jr., and L. C. Feldman, "Enhanced hysteresis in the semiconductor-to-metal phase transition of VO_2 precipitates formed in SiO_2 by ion implantation," *Appl. Phys. Lett.*, Vol. 79 (19), pp. 3161-3163, Nov. 2001.